

FMH606 Master's Thesis 2021
Energy and Environmental Technology

Modeling of evaporation of hydrogen during accidental releases

Mojtaba Afzali

Faculty of Technology, Natural sciences and Maritime Sciences
Campus Porsgrunn

Course: FMH606 Master's Thesis, 2021

Title: Modeling of evaporation of hydrogen during accidental releases

Number of pages: 100 + Appendices

Keywords: Hydrogen, evaporation, cryogenic, pool evaporation, pool spreading, mathematical model

Student: Mojtaba Afzali

Supervisor: André V. Gaathaug, Knut Vågsæther, Per Morten Hansen

External partner: H2Maritime, MoZEES

Summary:

Hopefully, in the near future, liquid hydrogen will be commonly utilized as energy. The cleanest fuel that the primary limit of producing and using it, is safety issues. High possibility safety issues are generated by large amounts of hydrogen, usually stored and transported in the liquid phase. The first phase in developing many accident cycles that end to a significant hazard (e.g., from fire, explosion, and toxic effects) is the discharge of hazardous cryogenic liquids from its container and its evaporation (e.g., liquid hydrogen release), leading to producing dangerous vapor. The main objective of this study is to model this evaporation from the release of liquid hydrogen. The evaporation model is a function of the radius of the spreading pool on the surface. Thus, for modeling the evaporation, the spreading pool on the surface should also be modeled.

Different integral models have been utilized for simulating the spread and vaporization of liquid hydrogen pool, namely Briscoe and Shaw's (B&S), Constant Froude Number (CFN), and a simplified model of Gas Accumulation over Spreading Pool (GASP). The simplified GASP model is suitable for indoor spills, but since the dominant heat transfer in ambient is heat flux by conduction from the ground, this model is also used to model the evaporation of liquid hydrogen for outdoor releases.

For using spreading and evaporation models, basic knowledge about heat transfer and boiling regimes is required. The boiling regime of hydrogen is essential to determine and specify in detail. Knowledge about the characteristics of heat transfer of hydrogen pool boiling alongside assembling consistent correlations to monitor the boiling heat transfer analysis is essential to the utilization of liquid hydrogen (LH₂). Some correlations seeking at various boiling regimes are assessed or adjusted in order to understand the mathematical assessment of hydrogen boiling heat transfer. Several developed correlations for nucleate boiling, critical heat flux (CHF), and minimum heat flux (MHF) suggested by different works are investigated. Comprehensive correlations for hydrogen boiling heat transfer are reviewed, and consequently, a predicted hydrogen boiling curve is formed.

The heat flux from the ground to the pool is determined using two boundary conditions (BCs) at the ground surface. One is specified heat flux, and the other one is specified temperature. The first BC results from suggested correlations for boiling heat transfer regimes (BR-BCs) dependent on the temperature difference between the liquid and the ground surface, while the second is constructed on a hypothesis of perfect thermal contact (PTC-BCs) between the liquid and the ground. The PTC-BCs were found to be in better agreement with the experimental results than the BR-BCs by different works. It was recommended that the PTC-BCs must be applied for a spreading pool while the BR-BCs

must be applied for a non-spreading pool. Thus, the PTC-BC is involved in this study for modeling the evaporation of liquid hydrogen.

The B&S and CFN models, which have the same structures in origin, were applied to model the liquid hydrogen's pool spreading and evaporation in this work. The models were controversial for lower mass flow rates. It was noticed that these models could not be utilized for spills on land. By presenting a minimum edge depth, altering the constant number ε (originally presented Froude number) corresponding to different mass flow rates, and validating against various cryogenic spills, the model demonstrated a roughly accurate result.

The original GASP model could not simulate without a wind speed, and the equations were hard to solve numerically caused by the considerable unpredictability of time scales produced by the many physical phenomena. Thus, a simplified model of the GASP model was probed to model the spreading and evaporation of the liquid hydrogen pool in no wind condition. The ability of the model was extraordinary and effectively justified against the experimental data.

Overall, the GASP model was in superior agreement with experimental data of cryogenic and liquid hydrogen spills than the B&S and CFN models. Although an empirical correlation was suggested determining the Froude number for different mass flowrate releases by this study, more empirical data is required to obtain a more accurate Froude number. So, CFN and B&S models are demanded more investigation.

Preface

This master's thesis ends my two-years study in the Master of Science Energy and Environmental Technology field. A wide range of tasks is conducted during this two-year study to find different solutions to help our planet solve global warming and environmental issues. Among these studies, which shape my ideas to find the best solution, hydrogen as energy was closer to my opinion. A 100% clean energy that the central limit of producing it is safety issues. So, a wide range of studies is needed to make using hydrogen possible and safe. The other primary limit is the economic matter, i.e., producing hydrogen is costly. So, a wide range of research is required to find the best and cheap solution. These challengeable tasks motivate me to enter this area and do something beneficial for being a tiny part of this big deal project.

I want to express my gratitude towards my supervisors Professor André V. Gaathaug, Professor Knut Vågsæther, and Professor Per Morten Hansen, for giving me the opportunity to know more about liquid hydrogen and helped me to have a broad knowledge about evaporation of hydrogen during accidental release.

I am deeply grateful to my parents for always being beside me throughout the twenty-three years of my studies. I would like to appreciate all my family, friends, and teachers supporting me during these years. In the end, I would like to express the most profound appreciation to my wife Nila for make me believe in myself and tolerated the difficulties of this way beside me.

Notodden, 01. May. 2021

Mojtaba Afzali

Contents

Preface	5
Contents.....	6
Nomenclature	8
1 Introduction	13
1.1 Available models review	13
1.2 Models in this study	14
1.3 Report outline.....	15
2 Fundamental physics	16
2.1 Overview of project.....	16
2.2 Heat transfer	16
2.2.1 Conduction	17
2.2.2 Convection.....	17
2.2.3 Radiation	18
2.3 Boiling.....	18
2.4 Pool boiling	19
2.4.1 Free convection boiling.....	19
2.4.2 Nucleate boiling	20
2.4.3 Transition boiling	20
2.4.4 Film boiling	20
2.5 Dimensionless numbers	20
2.5.1 Reynolds number	21
2.5.2 Prandtl number.....	21
2.5.3 Nusselt number	21
2.5.4 Grashof number	22
2.5.5 Galileo number	22
2.5.6 Schmidt number.....	22
2.5.7 Froude number.....	23
3 Hydrogen pool boiling	24
3.1 Process of LH ₂ pool boiling.....	24
3.1.1 Liquid hydrogen natural convection	24
3.1.2 Liquid hydrogen nucleate boiling.....	26
3.1.3 The onset of nucleate boiling	28
3.1.4 Critical heat flux (CHF)	29
3.1.5 Film boiling of liquid hydrogen pool.....	29
3.1.6 Minimum heat flux.....	30
3.1.7 Transition boiling of liquid hydrogen pool.....	30
3.1.8 The boiling curve of hydrogen.....	31
3.2 Boundary conditions (Heat Flux)	33
3.2.1 Boundary conditions selection.....	35
4 Liquid hydrogen spreading and evaporation	36
4.1 Briscoe and Shaw model	36
4.1.1 Production of vapor.....	37
4.1.2 Spreading of liquids.....	37
4.1.3 Vaporization of cryogenic liquids on land.....	39
4.1.4 Result and discussion	41
4.1.5 Instantaneous spill, unbounded.....	42
4.1.6 Instantaneous spill, bounded	43

4.1.7	<i>Continuous spill unbounded</i>	45
4.1.8	<i>Continuous spill, bounded</i>	46
4.1.9	<i>Lower volume spill</i>	48
4.1.10	<i>Validation of B&S model against LNG experimental data</i>	52
4.1.11	<i>Validation of B&S model against liquid nitrogen experimental data</i>	53
4.2	<i>Gas accumulation over spreading pools (GASP) model</i>	55
4.2.1	<i>Some observance of the GASP model</i>	56
4.2.2	<i>The GASP model structure</i>	56
4.2.3	<i>Discharged and vaporization</i>	56
4.2.4	<i>The pool equations</i>	57
4.2.5	<i>Equations for spreading</i>	60
4.2.6	<i>The pool temperature</i>	62
4.2.7	<i>Vapor transport</i>	63
4.2.8	<i>Solutions to GASP model</i>	66
4.2.9	<i>Simplified GASP model</i>	67
4.2.10	<i>Results and discussions (GASP)</i>	67
4.2.11	<i>Continuous Spill (GASP)</i>	68
4.2.12	<i>Continuous spill, bounded</i>	70
4.2.13	<i>Lower spill rates</i>	73
4.3	<i>Constant Froude Number (CFN) model</i>	75
4.3.1	<i>Result</i>	76
5	Liquid hydrogen spill experiments	79
5.1	<i>Literature review</i>	79
5.2	<i>Experiment analysis</i>	79
5.3	<i>Validation Of models against Royle and Willoughby's work experimental data</i>	81
5.3.1	<i>B&S and CFN model</i>	81
5.3.2	<i>GASP model</i>	84
5.3.3	<i>Original GASP model</i>	86
5.4	<i>Validation Of models against work of Takeno et al. experimental data</i>	88
5.4.1	<i>Original GASP model</i>	88
5.4.2	<i>Models in this study</i>	89
6	Discussion	91
7	Conclusion	95
	References	97
	Appendices	101

Nomenclature

Latin Letters

A	Area	(m ²)
B	Antoine coefficients	(-)
C	Antoine coefficients	(-)
C_p	Specific heat capacity	(J/ K ·kg)
D_B	Diffusivity	(m ² /s)
F	Turbulent or viscous resistance term	(-)
F_G	Gravity force	(N)
F_{IL}	Liquid inertia	(N)
F_L	Laminar resistance	(-)
Fr	Froude number	(-)
F_T	Turbulent resistance	(-)
g	Gravity acceleration	(m ² /s)
h_f	Edge depth of the pool	(m)
h_{fg}	Latent heat of vaporization	(J/kg)
h'_{fg}	Effective latent heat of vaporization	(J/kg)
Ga	Galileo number	(-)
Gr	Grashof number	(-)
H	Depth of the spreading pool	(m)
h	Convection heat transfer coefficient	(W/ m ² ·K)
H_0	Minimum depth	(m)
H_e	Dynamic region of mean depth	(m)

		Nomenclature
h_p	Mean depth of the puddle	(m)
h_{st}	Height of storage tank	(m)
J	Mean local vaporization rate	$(\text{kg}/\text{m}^2 \cdot \text{s})$
k	Thermal conductivity	$(\text{W}/\text{m}^2 \cdot \text{K})$
k_v	von Karman constant	(-)
L	Length of fluid or pool	(m)
L_x	Characteristic length	(m)
m	Mass of vaporization	(kg)
Nu	Nusselt number	(-)
n	Wind profile index	(-)
p	Pressure	(pa)
p_v	Vapor pressure above the pool	
Pr	Prandtl number	(-)
q	Heat flux	(W/m^2)
Q	Overall heat transfer	(W)
r	Radius of spreading pool	(m)
R	Universal gas constant	$(\text{kg} \cdot \text{m}^2)/(\text{K} \cdot \text{mol} \cdot \text{s})$
Re	Reynolds number	(-)
S	Discharge rate	(kg/s)
s	Shape factor	(-)
Sc	Schmidt number	(-)
T	Temperature	(K)
t	time	(s)
u	Velocity	(m^2/s)

Nomenclature

u_*	Atmospheric friction velocity above the pool	(m ² /s)
$u_{*,a}$	Atmospheric friction velocity upwind of the pool	(m ² /s)
U10	Wind speed at height of 10m	(m ² /s)
V	Volume of the pool	(m ³)
V_c	Continuous volume metric flow rate	(m ³ /s)
V_i	Instantaneous volume spill	(m ³)
x	Mole fraction of vapor above the pool	(-)
W	Vaporization velocity	(m ³ /m ² ·s)
z_0	Roughness length	(m)
$z_{0,a}$	Roughness length of the surrounding	(m)

Greek Letters

α	Thermal diffusivity	(m ² /s)
$a(s)$	Radial factor	(-)
β	Thermal expansion	(1/K)
Y	Euler's constant	(-)
ε	Constant factor for B&S model Froude number in CFN model	(-)
ϵ	The emissivity of the surface	(-)
Θ	Stefan-Boltzmann constant	(W/ m ² ·K ⁴)
l_c	Characteristic Laplace length	(-)
μ	Dynamic viscosity	(pa·s)
λ	Constant value for minimum depth	(m)

Nomenclature

ρ	Density	(kg/m ³)
σ	Surface tension	(N/m)
σ_s	Turbulent Schmidt number	(-)
τ	Arrival time	(s)
ν	Kinematic viscosity	(m ² /s)
$\phi(s)$	Gravity driving term	(-)
χ	Correction factor of the ground	(-)

Abbreviation

BC	Boundary condition	(-)
BR	Boiling regime	(-)
B&S	Briscoe and Shaw	(-)
CHF	Critical heat flux	(-)
CFN	Constant Froude number	(-)
GASP	Gas accumulation over spreading pool	(-)
ONB	Onset of nucleate boiling	(-)
PTC	Perfect thermal contact	(-)

Subscripts

α	Ambient	(-)
B	Boiling point	(-)
c	critical	(-)
cond	Conduction	(-)

		Nomenclature
conv	Convection	(-)
<i>min</i>	minimum	(-)
L	Leidenfrost	(-)
rad	Radiation	(-)
s	Surface	(-)
sur	Surroundings	(-)
sat	Saturation	(-)
<i>l</i>	Liquid	(-)
∞	Fluid	(-)
<i>v</i>	Vapor	(-)

1 Introduction

The world is suffering from global warming and ecological issues. The origin of global warming is the substantial growth of CO₂ production by the significantly increased use of fossil fuels that also contain other harmful contaminants. By considering global warming and environmental issues, it is a compulsory job for the authorities in the energy sector to find and develop new energy technologies. Hydrogen is a possible carbon-free energy carrier for the near future, which the only by-product of its combustion is water. Thus, applying hydrogen as energy for transportation and industries can significantly reduce greenhouse gas emissions. However, there are many challenges to use hydrogen as energy owing to the characteristic of it.

The hydrogen gas is usually liquified either by raising the pressure on the gas or by lowering the gas temperature to a freezing temperature. These processes are conducted to ease the transport and storage of liquid hydrogen. Therefore, liquid hydrogen is labeled as a cryogenic liquid characterized by a boiling point below the ambient temperature. Meaning that, after spillage of some amount of liquid hydrogen, it will evaporate vigorously. Therefore, a vapor cloud forms immediately and diffuses, which may possibly cause an explosion or a pool fire [1]. Hence, problems arise with the wide use of liquid hydrogen concerning their safe storage, transportation, and application. As an initial step of safety, the evaporation of hydrogen during accidental releases must be understood well, or in other words, a model of evaporation should be available.

This study aims to investigate the available mathematical model to model the evaporation of liquid hydrogen. In order to reach this objective, three main tasks were conducted in this work as below.

- Literature review on the release of cryogenic liquid
- Consideration of possible models for the vaporization of hydrogen and carry out modeling with available mathematical models
- Use different experimental data for model validation and improvements

1.1 Available models review

Accidental spills of cryogenic liquids generate vaporizing pools spreading over the ground or water. Thus, to model the evaporation of the cryogenic liquid, the spreading of the pool should also be considered. The modeling of liquid hydrogen spills is typically conducted in two sections: primarily, the liquid spread and vaporization are modeled, and then the production of this model is utilized as an input, or source term, to a dispersion model of the hydrogen gas/vapor [2]. The initial liquid spread and vaporization phase requires processes happening in more minor time scales than the dispersion phase; consequently, it is challenging for one model to represent both release phases. Thus, numerical models are generally divided into source term models, which account for the release details and gas dispersion models with input from the

former. This methodology depends strongly on the source-term model giving precise input data, so substantial amount of work focuses on this characteristic [2].

Many research has struggled to experimentally and numerically examine the spread and vaporization of cryogenic liquids spilled on both water and solid surfaces. The liquid hydrogen spill models can generally be grouped into integral models, shallow layer models, and computational fluid dynamics (CFD).

The only method that is possibly able to handle modeling the complete process is a CFD model, but although vaporization can be covered in several CFD models, modeling of other complicated processes such as boiling may not yet be satisfactorily developed for this application [2]. However, the CFD models are not the topic of this study; thus, the CFD models are skipped by this research.

The shallow layer models have been utilized widely in one and two-layer forms to model releases of non-volatile fluids and exchange flows [2]. The LAuV (Lachen-Ausbreitung-und-Verdampfung) model, an instance of shallow layer models of Verfondern and Dienhart [3], has been applied to model liquid hydrogen spills. This is a proprietary code created at Forschungszentrum Julich [2]. This model is one of the most comprehensive experimental and numerical findings on spreading cryogenic liquid pools. The model is one-dimensional, axisymmetric, and is able to simulate releases onto the ground or water. The model includes a sub-model for ice formation and validated against LNG and liquid nitrogen spill tests. At present, the LAuV code is no longer in use [2].

The integral models involve the solution of ordinary differential equations, which illustrate the integral properties of the pool [2]. The model considers the pool's depth to be an average value considered over the pool area and presumes the pool is circular [4]. Therefore, one of these models' limitations is not being able to cope with the complex landscape; however, simple geographical characteristics such as surface roughness, puddles, and bunds can be modeled.

1.2 Models in this study

For the reasons mentioned above, the available integral models will be investigated in this study. The available models for modeling the cryogenic spills, such as Briscoe and Shaw (B&S) [5], Constant Froude Number (CFN) [4, 6], and Gas Accumulation over the Spreading Pool (GASP) [7], are chosen by this study. These models are a system of coupled differential equations and must be solved numerically. The B&S and CFN models have been solved using the Forward Euler method, and the GASP model has been solved using the fourth-order Runge–Kutta method. Python version 3.8 is used for implementing the code for solving the models. The python code for these three models can be accessible by request on the Github account [8].

For modeling the spreading and evaporation of cryogenic, some essential mechanisms and physics should be defined and understood. A good understanding of the heat transfer and physical characteristics of cryogenic liquid pool boiling alongside gathering consistent correlations to determine the boiling heat transfer is essential [9]. As a starting point, the heat transfer mechanism should be studied for the pool formed after the spill of a cryogenic release. A set of extensive hydrogen boiling heat transfer correlations must be assembled, and then a predicted hydrogen boiling curve must be constructed to determine the heat flux from the ground in different boiling regimes. Before that, some fundamental physics is necessary to understand well. The Python code for producing the boiling regime curve of hydrogen is attached to Appendix (A-F).

1.3 Report outline

Chapter 2 of this study introduces the fundamental physics of heat transfer, pool boiling, and dimensionless numbers used in different correlations. In chapter 3, the correlations for calculating hydrogen pool boiling are discussed in detail, and then the boiling curve of hydrogen is calculated. Chapter 4 first describes the mentioned models in particularity, then investigates the response of models to different cryogenic release types and validates the models against available experimental data of different cryogenes. In chapter 5, the validity of the models specifically for liquid hydrogen spills is examined. Chapter 6 discusses and compares the models together, and recommendations are introduced. Conclusions are presented in chapter 7.

2 Fundamental physics

This chapter provides essential information about heat transfer, pool boiling, and some essential topics to understand better the physics needed to obtain the project's aim.

2.1 Overview of project

Figure 2.1 gives an overview of the heat transfer to the liquid pool that forms after an instantaneous spill or continuous cryogenic liquid spill. It may cause by a rupture in the pipeline or a failure in a storage tank. After the spillage of cryogenic liquid, the heat is started to transfer to the liquid. This transportation of heat occurs in three major processes such as convection, conduction, and radiation. The dominant heat source to the cryogenic liquid pool is the heat from the ground by conduction [5].

The heat transfer to the pool has been specified in the figure where \dot{q}_{cond} and \dot{q}_{conv} is net conduction and convection heat transfer to the pool, respectively. The \dot{q}_{rad} is heat transfer by radiation, \dot{m}_{evp} is the mass which evaporated from the pool. In the following, each mechanism will describe in detail.

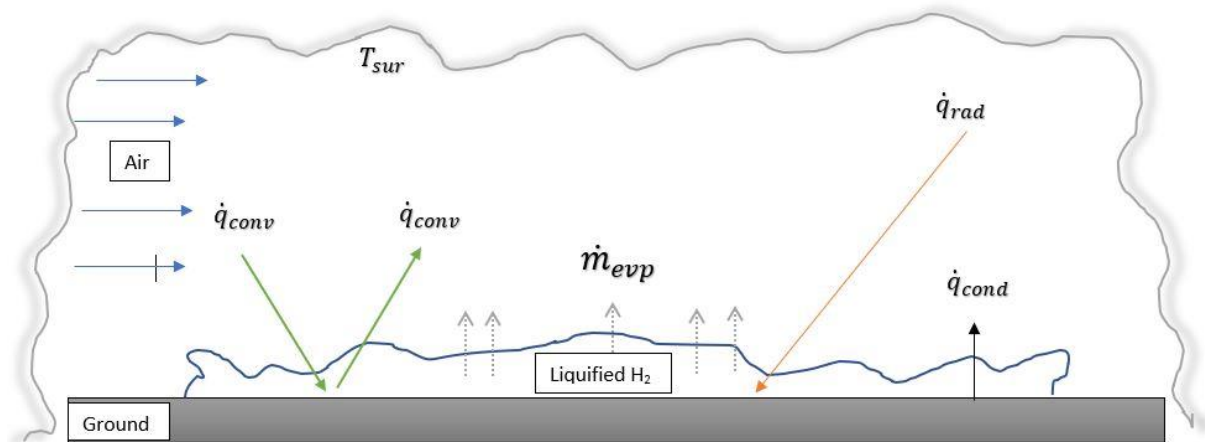


Figure 2.1 Heat transfer mechanism to the pool and mass evaporation

2.2 Heat transfer

Energy as heat can be transported by three main mechanisms, namely convection, conduction, and radiation. These mechanisms are interactions of the pool with its surrounding [10].

2.2.1 Conduction

Heat transfer happens in the presence of the temperature gradient. For conduction, heat transfer appears due to temperature gradient in a solid material or stagnant fluid in the direction of decreasing temperature. The amount of heat being transferred per unit time can be quantified by rate equations. Fourier's law is the rate equation for measuring the heat which being transferred by conduction. For one-dimensional, the Fourier' law can be express as

$$\dot{q}_{cond} = -k \frac{dT}{dy} \quad (2.1)$$

Where \dot{q}_{cond} is the heat flux in the y-direction per unit area, k is the ground's thermal conductivity, and T is temperature. The overall heat transfer by conduction can be described as

$$\dot{Q}_{cond} = -kA \frac{dT}{dy} \quad (2.2)$$

Where A is the area of the pool in contact with the ground. The minus sign is since heat is being transferred in the direction of decreasing temperature [10].

2.2.2 Convection

In convection phenomena, heat transfers due to random molecular motion (diffusion) and bulk motion of macroscopic fluid movements. This fluid motion can be due to density differences (hotter objects have less density than colder ones) or buoyancy. The rate equation for measuring heat transfer by convection is known as Newton's law of cooling. The rate equation has the form below.

$$\dot{q}_{conv} = h(T_s - T_\infty) \quad (2.3)$$

The heat flux \dot{q}_{conv} is the heat transfer rate by convection, T_s and T_∞ are surface and fluid temperature, respectively. The parameter h is labeled as convection heat transfer coefficient. Convection heat transfer coefficient depends on surface geometry, the nature of the fluid motion, fluid thermodynamics, and transport properties [10]. The total heat transfer by convection can be defined as the equation below, where A represents the pool area.

$$\dot{Q}_{conv} = hA(T_s - T_\infty) \quad (2.4)$$

2.2.3 Radiation

Thermal radiation is the energy radiated by a non-zero temperature matter. Electromagnetic waves or photons transport heat in radiation. Although the radiation process is different from convection and conduction, the driving force is still temperature gradient. The term below is used for computing the heat transfer by radiation.

$$\dot{q}_{rad} = \Theta \epsilon (T_s^4 - T_{sur}^4) \quad (2.5)$$

Where T_s is absolute surface temperature, Θ is Stefan-Boltzmann constant $\Theta = 5.67 \times 10^{-8}$ and ϵ is the emissivity of the surface [10]. The overall heat transfer by radiation can be defined as

$$\dot{Q}_{rad} = \Theta \epsilon A (T_s^4 - T_{sur}^4) \quad (2.6)$$

Where A is the area of the surface contributing to radiation.

2.3 Boiling

When some amount of liquid on a solid surface evaporates, it is labeled as boiling. The boiling process occurs when the surface temperature is much more than the liquid's saturation temperature corresponding to the liquid pressure. Transferring of heat occurs from the solid surface to the liquid. For measuring transporting heat of boiling, the suitable form of Newton's law of cooling is

$$\dot{q}_s = h(T_s - T_{sat}) = h\Delta T_e \quad (2.7)$$

Where ΔT_e is called excess temperature. This progression is characterized by the creation of vapor bubbles, which grow and consequently detach from the surface. Bubbles of vapor increasing rely on the excess temperature, nature of the body, and fluid characteristics, e.g., surface tension [10].

2.4 Pool boiling

Understanding the pool boiling depends on fundamental natural processes achieved by analyzing the different forms or regimes. These processes are free convection boiling, nucleate boiling, transition boiling and, film boiling. The boiling curve of water has been illustrated in Figure 2.2 at 1 atm pressure. Similar tendencies characterize other fluid's behavior [10]. In the following, these modes will be described in more detail.

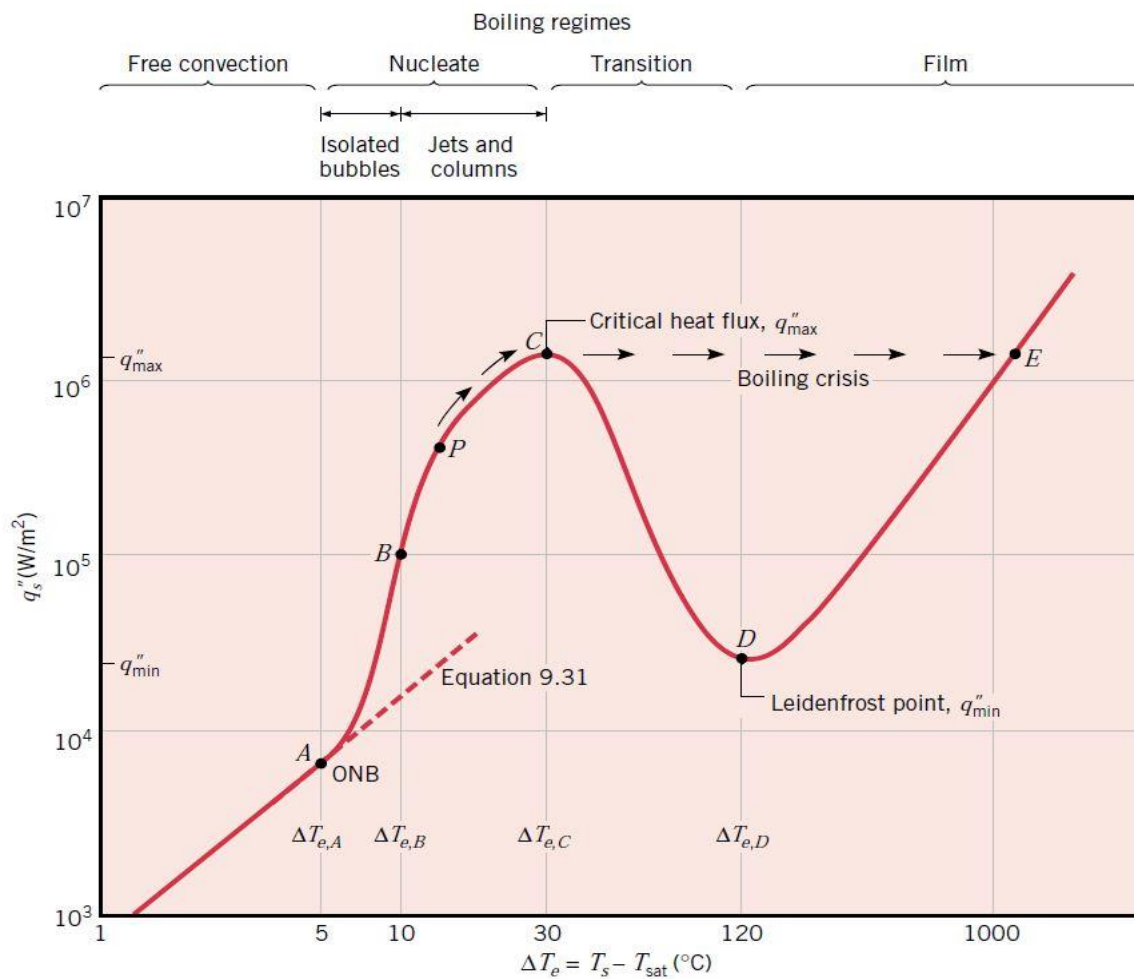


Figure 2.2 Typical boiling curve of water at 1 atm [10].

2.4.1 Free convection boiling

The bubble formation process will start when liquid is heated somewhat beyond saturation temperature. To maintain bubble formation, the temperature of the surface must stay above

2 Fundamental physics

of saturation temperature of liquid ($\Delta T_{eA} \approx 5^\circ\text{C}$ for water), A refers to the onset of nucleate boiling in Figure 2.2. As the excess temperature is boosted, the formation of bubbles will grow further [10].

2.4.2 Nucleate boiling

As mentioned in Figure 2.2, the nucleate boiling splits into two flow regimes. In region A-B, the formation of the isolated bubbles begins at the nucleation site and detaches from the surface. This separation leads the fluid to substantially mix adjacent to the body and significantly increasing convection coefficient and heat transfer rate. After ΔT_e exceeds point B in Figure 2.2, the nucleation site expands and takes the lead to form more bubbles. The bubbles in the region B-C induces enough to escape as jet or columns. Interfering between crowded bubbles prevents liquid from moving close to the surface. The curve's change of behavior occurs in point P of Figure 2.2, and after this point, the curve is not linear anymore. Heat flux rises more gradually after point P as ΔT_e is rose. Between point P and C the heat flux decreased and that leads to a reduction of heat transfer coefficient. Point C is also termed critical heat flux (CHF), the curve's maximum heat flux. At the CHF point, the vapor forms vigorously [10].

2.4.3 Transition boiling

The region from point C to D in Figure 2.2 is called transition boiling, unstable film boiling, or partial boiling. The formation of bubbles in this region is vigorously where a vapor blanket starts to form on the surface, which acts as thermal resistance. The formation of this thermal resistance layer leads to lower heat flux. Surface condition in this region is critical and oscillates between film and nucleate boiling. By increasing the ΔT_e the formation of vapor film becomes faster [10].

2.4.4 Film boiling

As excess temperature ΔT_e is increased and reached point D in Figure 2.2, the film layer formation will get to the maximum of its thickness. Away from point D, the pool boiling will be in the film boiling regime. The film boiling regimes is relevant for every single cryogenic liquid pool due to the very low temperature of the cryogenic liquid and higher ΔT_e i.e., higher temperature differences between surface and liquid.

2.5 Dimensionless numbers

The application of dimensionless numbers is wide. Some of these numbers are described in detail and will be relevant for the following chapters of this work. Dimensionless numbers are really handy in most unsolvable problems.

2.5.1 Reynolds number

The Reynolds number Specifies the flow regimes for being laminar or turbulent. It represents the ratio between viscous forces and inertia [10]. The dimensionless number Reynolds is also used to classify the fluids structures in which the impact of viscosity is the key to control the velocities or the flow model of fluid [11]. The Reynolds number, Re_L , is defined as

$$Re_L = \frac{\rho u_\infty L}{\mu} \quad (2.8)$$

Where ρ , μ , u_∞ are the fluids density, viscosity, and velocity, respectively. The L is the length of fluid or pool on the ground. Accordingly, as can be seen from the equation, if the flow has a high velocity compared to the viscosity, the Reynolds number's value will be tremendous. Hence the flow will be in a turbulent flow regime. Otherwise, the flow is in the laminar regime.

2.5.2 Prandtl number

The Prandtl number is the ratio of the momentum diffusivity to the thermal diffusivity. The equation below is used for determining the Prandtl number [10].

$$Pr = \frac{\nu}{\alpha} = \frac{\mu C_p}{k} \quad (2.9)$$

Where, ν , α , μ , k , and C_p are kinematic viscosity, thermal diffusivity, dynamic viscosity, thermal conductivity, and specific heat capacity, respectively.

2.5.3 Nusselt number

The Nusselt number is fundamentally a function of the Reynolds and Prandtl number, improving the heat exchange rate [12]. Nusselt number is a dimensionless form of the temperature gradient at the surface, and it represents the value of convection heat transfer at the surface [10]. The equation for the Nusselt number has the form of the equation below, where m , n , and C are constants depends on the fluid, which will be described more in chapter 3.

$$Nu = \frac{hL}{k} = C Re^m Pr^n = \frac{\partial T}{\partial y} \quad (2.10)$$

2.5.4 Grashof number

The Grashof number represents the ratio between buoyancy forces and viscous forces in the velocity boundary layers. For calculating the Grashof number, the following equation is used.

$$Gr = \frac{g\beta(T_s - T_\infty)L^3}{\nu^2} \quad (2.11)$$

Where β is the coefficient of thermal expansion and ν is the kinematic viscosity.

2.5.5 Galileo number

Galileo number is characterized as the ratio of forces present in the flow of viscous fluids. Galileo's number can be calculated by the equation as follow

$$Ga = \frac{g\rho_l^2 l_c^3}{\mu_l^2} \quad (2.12)$$

Where, l_c , is the characteristic Laplace reference length. The Laplace reference length can be obtained by the equation below [9].

$$l_c = \left[\frac{\sigma}{g(\rho_l - \rho_v)} \right]^{0.5} \quad (2.13)$$

σ is the surface tension of the fluid.

2.5.6 Schmidt number

The Schmidt number represents the ratio between kinematic air viscosity ν and the diffusivity D_B of particles which is determined as [13]

$$Sc = \frac{\nu}{D_B} \quad (2.14)$$

Fundamentally, Schmidt number characterizes the ratio between the momentum diffusivity and mass diffusivity, which linked to kinematic viscosity ν and diffusivity D_B , respectively. In the case of a low Sc , particles have substantial diffusivity, are tiny, and are barely conditioned by the viscosity of the medium, so that they will effortlessly cross the laminar layer that surrounds smooth surfaces when the turbulence is moderate and will influence the surface. Particles are giant with small diffusivity at high Sc , and this sort of deposition comes to be less applicable [13].

2.5.7 Froude number

Froude number defines the state of flow [14] and characterizes the ratio between gravity and inertia forces inside the hydrodynamic structure [15]. The Froude number can be determined as below [14].

$$Fr = \frac{u}{\sqrt{gD}} \quad (2.15)$$

Where u is velocity, D is the hydraulic depth of flow defines as A/B in non-rectangular sections, where A is the flow area and B is the surface width. The denominator \sqrt{gD} represents the gravity waves propagation speed in an open channel [16]. The equation for discharge rate can be written as below.

$$Fr = \frac{V_c}{\sqrt{g \frac{A^3}{B}}} \quad (2.16)$$

Where V_c is the volumetric discharge rate.

3 Hydrogen pool boiling

The boiling heat transfer of hydrogen must be understood as well as reliable correlations to lead the boiling heat transfer analysis. For liquid hydrogen application, these correlations and characteristics of boiling heat transfer are essential. In this chapter, the heat transfer of liquid hydrogen pool boiling will be investigated, and the main objective of this chapter is to compute the boiling curve of hydrogen. Wang et al. [9] investigated the correlations for calculating heat transfer of hydrogen pool boiling thoroughly. So, the correlation relevant to this study will be investigated and applied to calculate the heat transfer in hydrogen pool boiling.

3.1 Process of LH₂ pool boiling

The pool boiling curve of water has been illustrated in Figure 2.2, which is relatively the same for other liquids. By considering the spill of liquid hydrogen on the ground, the dominant boiling regime is the film boiling regime due to the high-temperature difference between ground temperature and liquid temperature. Because of this high-temperature difference, a layer of vapor would be formed at the surface. By decreasing the surface temperature to the liquid temperature after some moments, the transition boiling and nucleate boiling occur, respectively. During these regimes, a high amount of vapor forms and evaporates. A little after some minutes, the ground (surface) temperature decreases and will be the same as liquid temperature. Thus, there is an insignificant heat transfer due to no temperature gradient in the end [9].

3.1.1 Liquid hydrogen natural convection

As reported in Ref. [9, 17], the behavior of the none-cryogenic liquid is the same as cryogenic liquids; hence, the correlation for none-cryogenic liquids is applicable for cryogenic liquids. McAdams in [17] proposed the famous equation below for calculating heat transfer in liquid natural convection regimes.

$$Nu = C(Gr \cdot Pr)^n \quad (3.1)$$

Where C and n are constants depending on the liquid flow regime. Coeling et al. in [6] proposed the values of 0.14 and 1/3 for C and n respectively for turbulent heat transfer. The relation between Nu and Gr.Pr has been indicated in Figure 3.1. For laminar heat transfer, C and n are 0.79 and 1/4, respectively. By using equation (3.1) and elaborating it, we have

$$\frac{hL_x}{k} = C \left(\frac{g\beta\Delta T_l L_x^3}{\nu_l^2} \cdot Pr \right)^{1/3} \quad (3.2)$$

3 Hydrogen pool boiling

As shown in equation (3.2), now we can easily make heat transfer coefficient independent of length. So, we have

$$h = C \cdot k \left(\frac{g\beta\Delta T_l}{\nu_l^2} \cdot Pr \right)^{1/3} \quad (3.3)$$

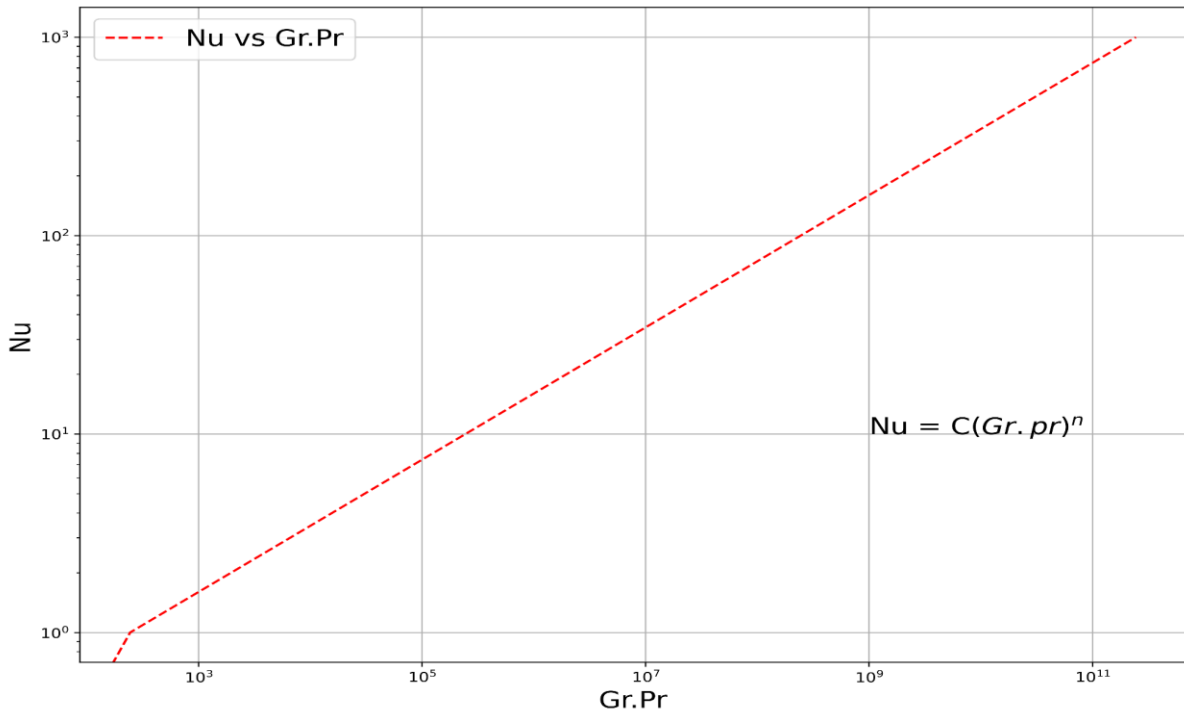


Figure 3.1 Calculated natural convection heat transfer for Nu and Gr.Pr relation.

It must be considered that these equations are relevant for flat plates, i.e., ground or surface. Based on the equation (3.3), Figure 3.2 illustrates the free convection heat transfer of liquid hydrogen spill on the ground.

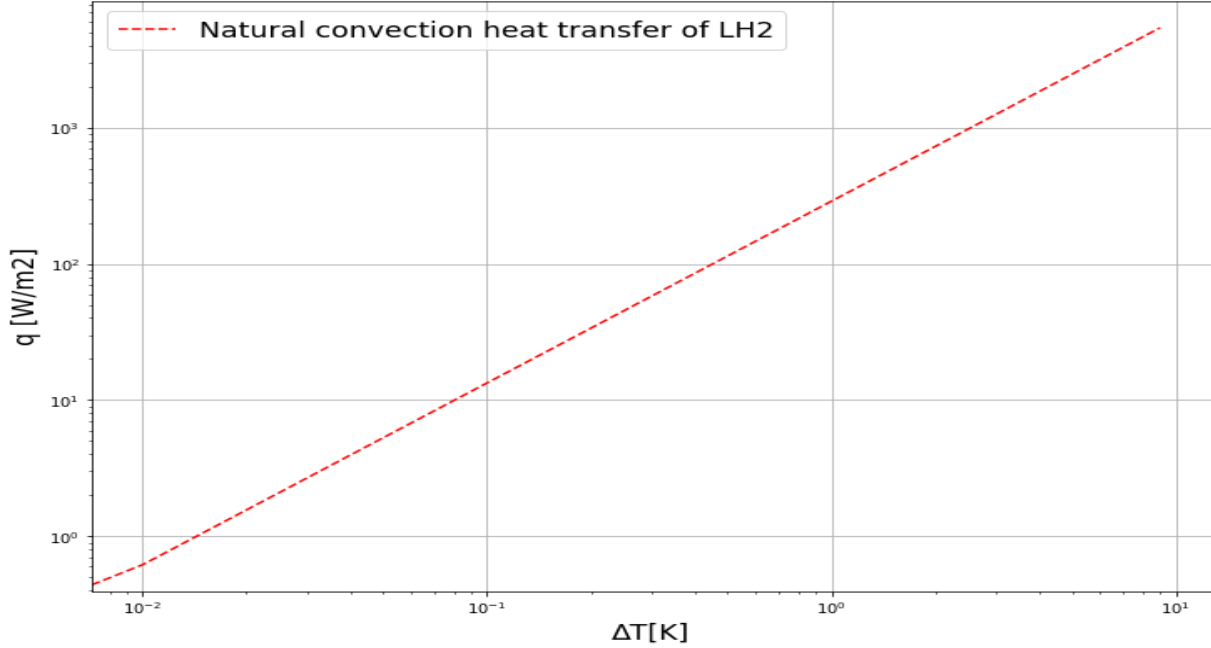


Figure 3.2 Natural convection regime of hydrogen, based on eq (3.1-3.3)

3.1.2 Liquid hydrogen nucleate boiling

For the nucleate boiling regime of fluids, Brentari et al. [9, 18] considered that the correlation suggested by Kutateladze [19] could be applied as follows

$$\frac{h}{k_l} \left(\frac{\sigma}{g\rho_l} \right) = 3.25 \times 10^{-4} \left[\left(\frac{q C_{pl} \rho_l}{h_{fg} \rho_v k_l} \left(\frac{\sigma}{g\rho_l} \right)^{1/2} \right)^{3/5} \times \left[\left[g \left(\frac{\rho_l}{\mu_l} \right)^2 \left(\frac{\sigma}{g\rho_l} \right)^{3/2} \right] \right]^{1/8} \left[\frac{P}{(\sigma g \rho_l)^2} \right]^{7/10} \right] \quad (3.4)$$

Or

$$\frac{h l_c}{k_l} = 3.25 \times 10^{-4} \left[\frac{\rho_l q C_{pl} l_c}{\rho_v h_{fg} k_l} \right]^{3/5} \times G a^{1/8} \left[\frac{P}{\sqrt{\sigma g \rho_l}} \right]^{7/10} \quad (3.5)$$

It can be seen that Kutateladze correlation are consist of dimensionless number. Another correlation as a function of ΔT_l , by considering the Kutateladze correlation proposed in Ref. [20], this equation has the form below.

$$q = 5.66 \times 10^{-10} \cdot \frac{k_l C_{pl}^{1.5} \rho_l^{1.28} P^{1.75}}{\mu_l^{0.625} h_{fg}^{1.5} \rho_v^{1.5} \sigma^{0.9}} \quad (3.6)$$

3 Hydrogen pool boiling

For the nucleate boiling heat transfer of cryogenic liquid Clarke [9, 21] proposed the correlation as a function ΔT_l . The correlation has been indicated below.

$$\frac{q}{\mu_l h_{fg}} \left[\frac{\sigma}{g(\rho_l - \rho_v)} \right]^{0.5} = 3.25 \times 10^5 \cdot \left[\frac{C_{pl}(T_s - T_{sat})}{h_{fg} Pr_l^{1.8}} \left(\frac{T}{T_c} \right)^{1.8} \right]^{2.89} \quad (3.7)$$

An additional pressure effect imposed by $\frac{T}{T_c}$ term. A simple correlation is proposed by Wang et al. [9] to predict the heat transfer in the nucleate site.

$$q = a \cdot \Delta T^b \quad (3.8)$$

Where $b = 2.52$, and $a = 6309$ give a reasonable accuracy for hydrogen pool boiling [9]. Figure 3.3 and Figure 3.4 have been illustrated the result of these correlations in different pressures. It worth mentioning that the pressure in these correlations considers being equal to ambient pressure for the subsequent investigations. In Wang et al.'s work, after comparing the results with experimental data [22], it is concluded that the equation (3.8) is in good agreement with experimental data, as is evident in Figure 3.3 and Figure 3.4.

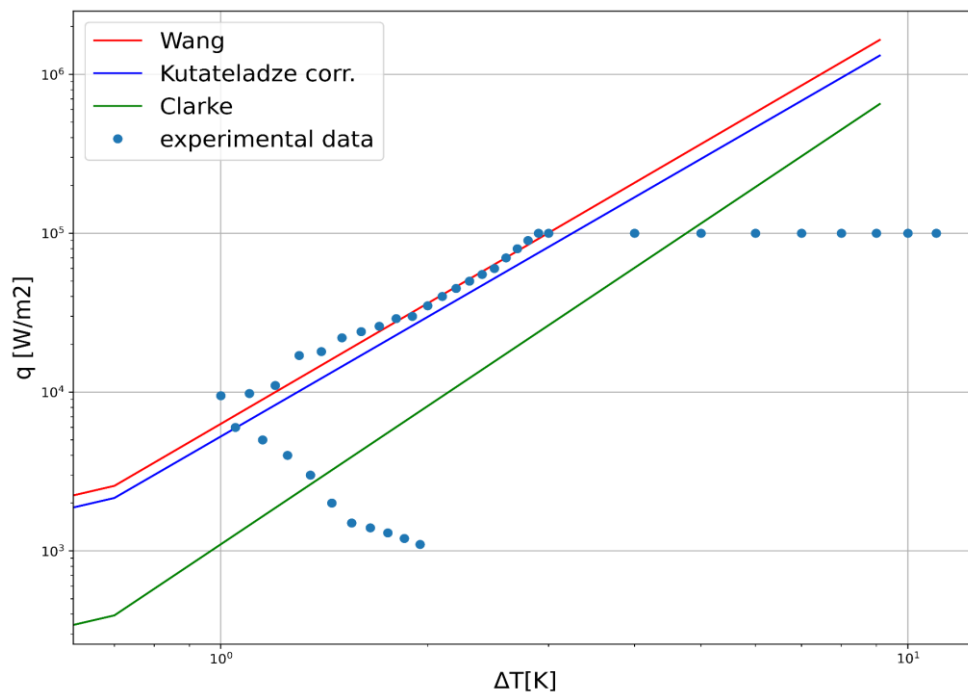


Figure 3.3 Comparison of different correlation with experimental data in nucleate boiling with ambient pressure

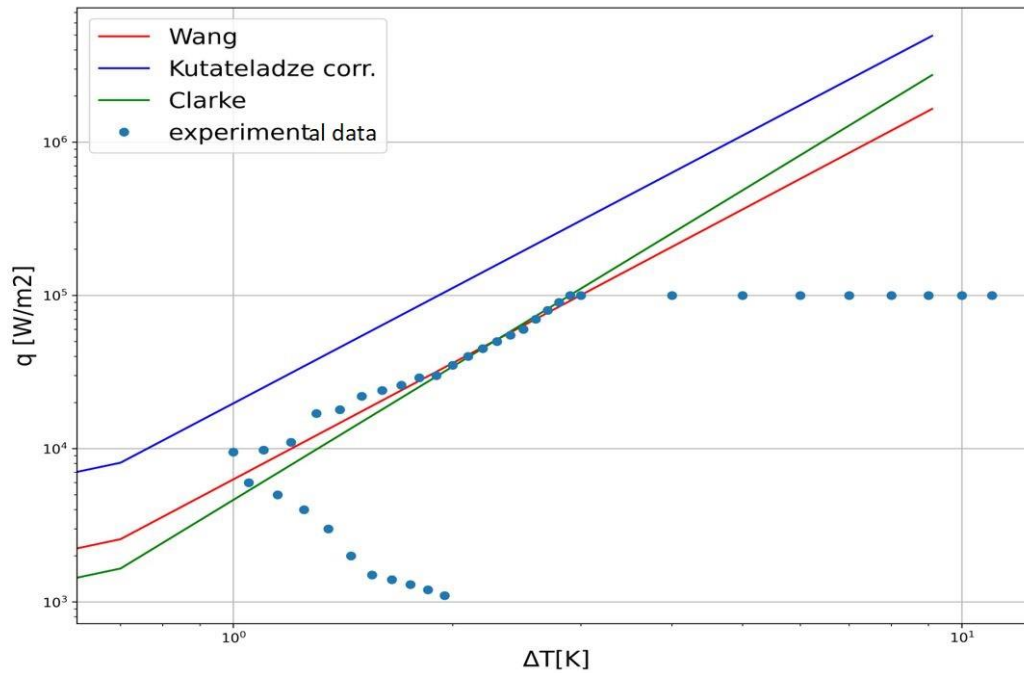


Figure 3.4 Comparison of different correlation with experimental data in nucleate boiling in $(P/P_c) = 0.23$

3.1.3 The onset of nucleate boiling

The onset of nucleate boiling is calculated with the prevalent correlation below [9, 23].

$$q_{ONB} = \frac{k_l h_{fg} \rho_v}{8 \sigma T_{sat}} \Delta T_{ONB}^2 Pr_l^{-2} \quad (3.9)$$

As shown in Figure 2.2, the ONB is a critical point in which both natural convection and nucleate boiling are related to this point. Consequently, the heat flux at ONB must at the same time satisfy the natural convection heat transfer correlation, which measuring with equation (3.1), and for nucleate boiling regime correlation (3.8), the heat flux which calculated at ΔT_{ONB} , thus, the following equation could be suggested [9].

$$q_{ONB} = h \Delta T_l = 6309 \cdot \Delta T_{ONB}^{2.52} \quad (3.10)$$

Then ΔT_{ONB} can be obtained by

$$\Delta T_{ONB} = \left(\frac{h \Delta T_l}{6309} \right)^{\frac{1}{2.52}} \quad (3.11)$$

After iteration of calculating the ΔT_{ONB} by equations (3.8) and (3.10), it can be seen that the deviations are significant. Thus, a large number of experimental data should be achieved. In work of Wang et al. equation (3.11) insisted on calculating ΔT_{ONB} of hydrogen, and the value of $\Delta T_{ONB} = 0.065 \text{ K}$ is obtained.

3.1.4 Critical heat flux (CHF)

For calculating the critical heat flux of hydrogen, the following correlation could be used.

$$q_{CHF,sat} = C_k h_{fg} \rho_v \left[\frac{g \sigma (\rho_l - \rho_v)}{\rho_v^2} \right]^{0.25} \quad (3.12)$$

For liquid hydrogen, the C_k value, based on Brentari et al. [18] and Bewilogua et al. [24] works could be considered 0.16, which gives sufficient accuracy result for hydrogen [9]. The value of 0.16 for C_k based on Shirai et al. [22] work, can be seen that, the pressure has a noticeable impact on C_k [9]. For finding C_k value the following relation proposed [9].

$$C_k = 0.18 - 0.16 \left(\frac{P}{P_c} \right)^{5.68} \quad (3.13)$$

3.1.5 Film boiling of liquid hydrogen pool

As mentioned in previous sections, film boiling heat transfer plays a dominant role in cryogenic liquid spills. A bunch of works has struggled with the problems related to cryogenic film boiling heat transfer. A series of correlations have been suggested to evaluate the heat transfer of film boiling, and these correlations engage with the effects of heater geometry. The spill on the ground has been considered in this work. So, the heater geometry is assumed to be a horizontal surface. Therefore, the correlations for this type of geometry have been investigated. For calculating the heat transfer coefficient for the pool film boiling, Klimenko [25] proposed an approach applicable for horizontal surface geometry. Due to the similarity of natural convection and film boiling, this correlation depended on the Reynolds analogy. Thus, for measuring the heat transfer coefficient, the correlation has the form of [9]

3 Hydrogen pool boiling

$$Nu_{L_x} = \frac{hL_x}{k_v} = C_1 \left[Ra_{L_x} \left(\frac{h'_{fg}}{C_{pv}\Delta T} \right) \right]^m \quad (3.14)$$

The equation (3.14) could be used for all type of heater geometry only with the difference C_1 , h'_{fg} , m , and L_x value. For flat plate, which is our case of the concern, the value of L_x is equal to Laplace reference length l_c [9].

In the work of Berenson [26], the value of C_1 and m for horizontal plate proposed to be 0.425 and (1/4) respectively. The modified heat of vaporization h'_{fg} for pool film boiling in Berenson work suggested to calculate from equation below.

$$h'_{fg} = h_{fg} + 0.4c_{pv}\Delta T \quad (3.15)$$

3.1.6 Minimum heat flux

To calculate the Leidenfrost temperature, which is a critical value between film boiling and transition boiling regimes, the value of minimum heat flux is needed. The following relation is proposed for calculating the minimum heat flux (MHF).

$$q_L = C_L h_{fg} \rho_v \left[\frac{g\sigma(\rho_l - \rho_v)}{(\rho_l - \rho_v)^2} \right]^{0.25} \quad (3.16)$$

Brentari et al. [18] proposed the value of 0.16 for C_L for heat transfer of hydrogen. The value of 0.031 for C_L proposed on the purpose of high-pressure case. Since our case is in ambient pressure the value of C_L considered to be 0.16 which is more accurate based on experiment data [9, 27] for ΔT_L , but because of overestimating of heat transfer in MHF point, the value of C_L considered to be an average of this two value in this work which is approximately 0.09 for ambient pressure.

3.1.7 Transition boiling of liquid hydrogen pool

Previously, there is no empirical correlation for calculating the heat transfer rate in the transition boiling regime. Thus, the measuring of heat transfer rate in transition boiling regime is obtained by interpolation between critical heat flux (CHF) and minimum heat flux (MHF) [9].

$$q = q_{CHF} - \frac{\Delta T - \Delta T_{CHF}}{\Delta T_L - \Delta T_{CHF}} (q_{CHF} - q_L) \quad (3.17)$$

3.1.8 The boiling curve of hydrogen

Based on previous correlations, the values in Table 3.1 have been obtained. Thus, after calculating these values, the boiling curve of hydrogen built on mentioned correlations has been shown in Figure 3.5. The comparison of different correlations on the nucleate boiling regime has also been plotted in the figure.

Table 3.1 The critical values of hydrogen boiling curve.

Parameters	Values	Equation
Q_{ONB}	9.03 [W.m ²]	(3.1) and (3.9) (iteration)
ΔT_{ONB}	0.061 [K]	(3.1),(3.10) and (3.11) (iteration)
Q_{CHF}	89627 [W.m ²]	(3.12) and (3.13)
ΔT_{CHF}	2.86 [K]	(3.8) and (3.12)
Q_L	1596[W.m ²]	(3.16) and $C_L = 0.09$
ΔT_L	5.27 [K]	(3.14),(3.15) and (3.16)

For making the graph more relevant for the case of this work, the boiling curve of hydrogen proposed by this work has been shown in Figure 3.6. The reason behind this suggestion is that Figure 3.6 is in more agreement for spills on the ground, i.e., ambient pressure is the case of study for this work.

3 Hydrogen pool boiling

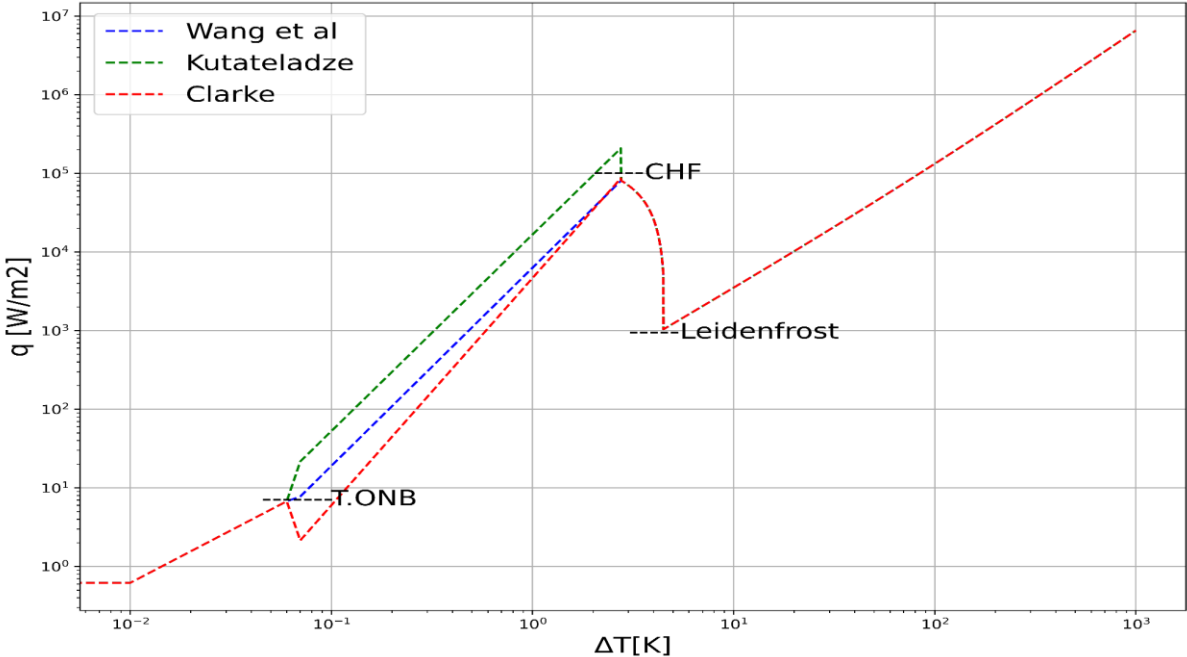


Figure 3.5 The boiling curve of hydrogen with the comparison of different correlations for the nucleate regime.

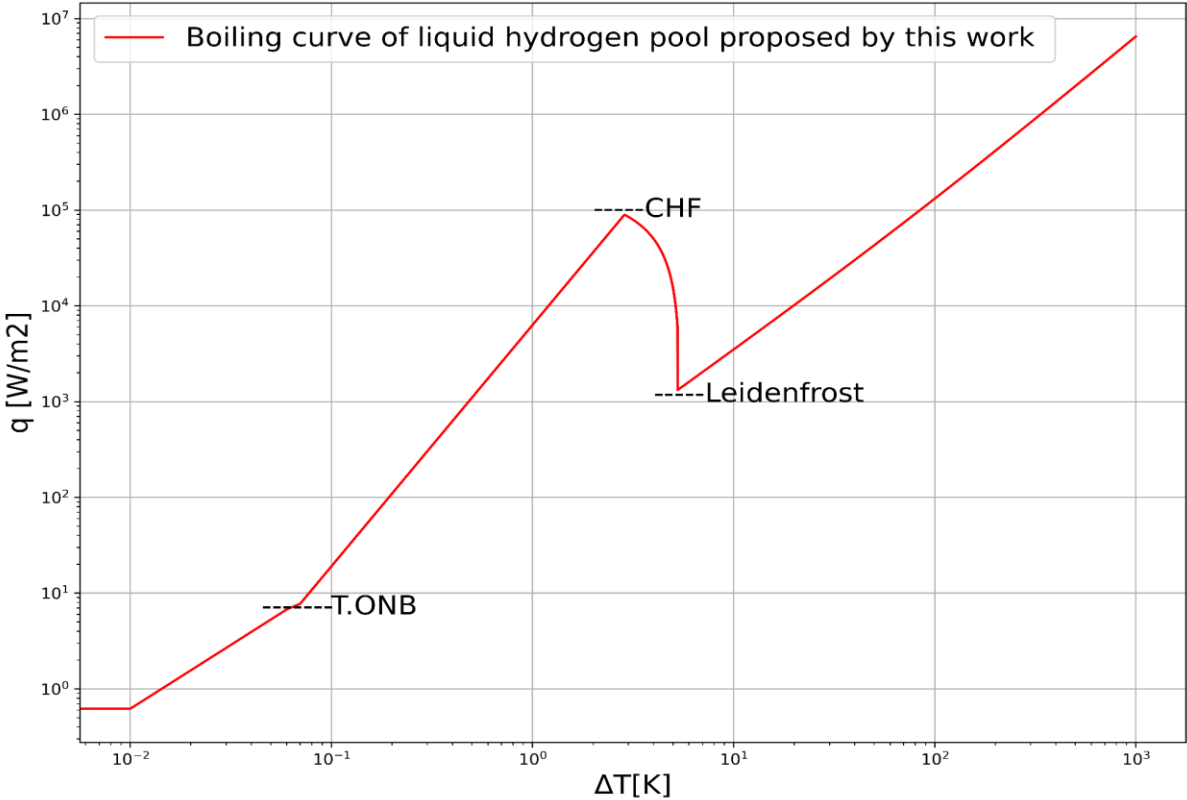


Figure 3.6 The boiling curve of hydrogen proposed by this work $C_L = 0.09$.

3.2 Boundary conditions (Heat Flux)

As will be discussed in the next chapter, a coupled differential equation system should be solved numerically for modeling the spreading and vaporization of cryogenic liquids. Thus, boundary conditions should be considered for heat transfer to the cryogenic liquid pool to model the spreading and vaporization of cryogenic liquid due to accidental release on solid ground. Two boundary conditions commonly have been taken for determining the heat flux from the ground to the pool: (I) specified heat flux and (II) specified temperature [28]. The boundary condition is developed from the predictive correlation boiling heat transfer regimes (BR-BCs) for specified heat flux, which has been done in this chapter. The boiling regimes BC is dependent on the excess temperature, i.e., the temperature difference between liquid and surface.

The assumption for the specified temperature BCs is perfect thermal contact (PTC) between the surface and liquid. The perfect thermal contact boundary conditions (PTC-BCs) implementation in a computer code is more straightforward than the boiling regime boundary condition (BR-BC) [28]. This is because the boiling regime correlations give out the heat flux adjusting with the temperature difference between the ground surface and liquid, and for finding the heat flux as a function of time, the boiling regime correlations must be solved numerically, while the PTC-BR gives the heat flux as a function of time achieved by the analytical solution.

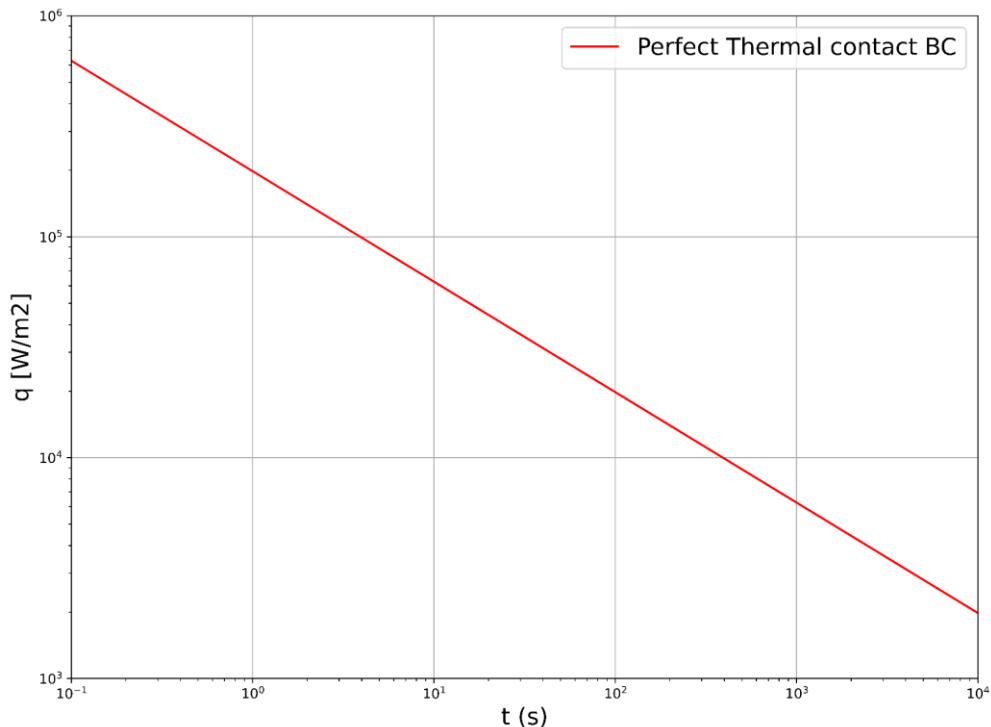


Figure 3.7 Heat flux versus time (PTC-BR).

3 Hydrogen pool boiling

By assuming a perfect thermal contact between liquid and ground surface, i.e., the ground surface temperature being equal to the liquid's boiling point, and the equation (3.18) for determining the one-dimensional unsteady-state heat conduction from the annular ground into the pool, Figure 3.7 can be obtained.

$$q = \frac{k(T_a - T_B)}{\sqrt{\pi\alpha(t - \tau)}} \quad (3.18)$$

As shown in Figure 3.7, it is evident that the heat flux from the PTC-BC declines smoothly. In contrast, BR-BC's heat flux curve encounters a spike during the boiling regime transition from film to nucleate regime. As shown in Figure 3.8, Nguyen et al. utilized the BR-BCs to simulate the pool spreading for liquid oxygen and liquid nitrogen on land.

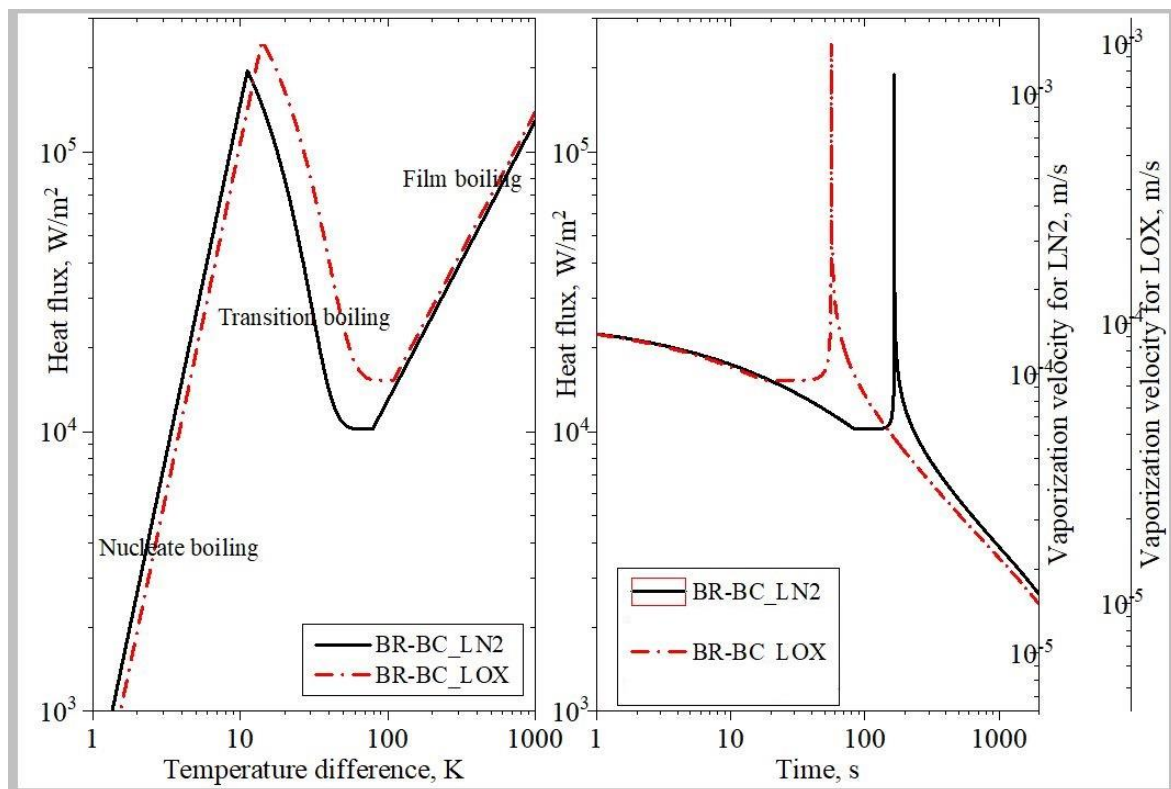


Figure 3.8 The heat flux versus temperature difference and time BR-BC [28].

3.2.1 Boundary conditions selection

Nguyen et al. [28] and Basha et al. [29] used the BR-BC to simulate the pool spreading of LN₂, LO_x, and LNG on land, while the Refs [3-5, 28, 30] applied the PTC-BCs. As it is clear, the PTC-BCs are more common to use in different studies.

Nguyen et al. [28] compared the BR-BCs and PTC-BCs in their research and realized the PTC-BCs are in better agreement with the experimental results. They discovered that the BR-BC underestimates the vaporization velocity and over-estimates the pool radius. These behaviors are because of the ignorance of boiling regimes correlations for the radial flow's effect [28]. Nguyen et al. concluded that the PTC-BCs must be utilized for a spreading pool, and BR-BC must be utilized for a non-spreading pool. Thus, in this work, the PTC-BCs will be applied to liquid hydrogen spreading and evaporation models.

4 Liquid hydrogen spreading and evaporation

Liquefied natural gas (LNG) and in the near future liquid hydrogen and such cryogenic liquids are commonly utilized as energy or other applications in industries. As a consequence of this wide range of usage, the probability of accidents rises significantly. The casualties could be a rupture in pipelines, fragile strength of the storage tanks, or a wrong design due to human error, leading to the continuous or instantaneous spill. When one of these accidents happened, a liquid pool of cryogenic will be formed. Due to the high difference temperature of liquid and surface, the liquid starts to evaporate vigorously, and a vapor cloud is created. Most of these cryogenics are flammable, or for some others, they are toxic for humans, animals, and the environment. Therefore, it is vital to understand the spreading and evaporation of these cryogenic liquids comprehensively.

A few numerical and analytical models are proposed for studying the spread and evaporation of cryogenic liquid on water or land. However, in this work, the spread and evaporation of liquid hydrogen will be investigated on the ground. In previous different works, which will be discussed next, the spread and evaporation of LNG, LN₂, and LO_x were investigated. However, there is still a shortage of suitable models for spreading liquid hydrogen. There is also a shortage of appropriate experimental data for validating the models for hydrogen. Thyer [31] reviewed the experimental data's accessibility and utility on spreading and vaporizing cryogenic liquid spills for validating computer software [4].

4.1 Briscoe and Shaw model

The first model that has been investigated for modeling the spread and evaporation of liquid hydrogen is the model proposed by Briscoe and Shaw [5]. A system of coupled differential equations is presented in this model to determine the pool's spreading length, height, volume, and mass evaporation rate. In Briscoe and Shaw work, foremost, a relation for defining the volumetric flowrate has been proposed, which has the form of

$$\dot{V}_c = AC_d \left\{ 2gh_{st} + \frac{2}{\rho}(p - p_a) \right\}^{0.5} \quad (4.1)$$

Where A is the cross-sectional area of the hole which has been created due to control failure, e.g., a rupture of pipeline, C_d is the discharge coefficient, which is 0.5 for a circular hole, p is the storage tank pressure, p_a is ambient pressure, and h_{st} is the height of the storage tank above the hole. It is obvious that with reducing the h_{st} by the time the \dot{V}_c will also decline. Thus, the maximum volume release rate arises for a hole at the bottom of the control vessel.

4 Liquid hydrogen spreading and evaporation

4.1.1 Production of vapor

The released liquid will form a pool of cryogenic liquid. This release can be occurred on the ground or water, i.e., spillage on the floor or water. Since the study's case is for spillage of land, the part for water will not be investigated in this work. For determining the evaporation rate at time t after the beginning of spillage, the pool's area, the spread rate of the pool, and heat supplied to the pool by ground must be specified. The dominant heat transfer to the pool is from the ground for cryogenic liquid with extremely low boiling temperature (e.g., for hydrogen, the boiling temperature is $-253\text{ }^{\circ}\text{C}$) [5].

4.1.2 Spreading of liquids

The spreading of liquid on the flat surface, i.e., land, is dominated by the conservation equations of incompressible fluid flow, and gravity is the main driving force for pool spread. The gravity force generates an uneven pressure allocation in the pool; even if this force performs downwards, it triggers the pool to spread sideways [5]. The gravity force declines as the pool spread and become thinner. This decline happens because of acting the force in the shrinking pool's direction, reducing with pool thickness. The dominant force for spreading the liquid on the ground is gravity, but this is until the pool thickness becomes very thin. In this step, the prevalent driving force is the imbalance between surface tension forces at the liquid-air-ground interface. Nevertheless, for reaching the final surface tension-driven regime, a smooth surface such as concrete is needed [5]. If it is assumed that the spreading pool is a circular cylinder with a radius r and height of H , then,

$$V = V_i + \dot{V}_c t - \left(\frac{m}{\rho}\right) \quad (4.2)$$

and,

$$H = \frac{V}{\pi r^2} \quad (4.3)$$

Where V represents the volume of liquid in the pool, V_i is an instantaneous spill, \dot{V}_c is a continuous spill, m is the mass of liquid that has been evaporated, and H is the depth of the pool at the edge.

The relation between gravity and liquid inertia drives the cryogenic liquid pool to spread. Thus, the radius equation of the pool at time t can be obtained by the energy balance of

$$F_G = F_{LL}$$

4 Liquid hydrogen spreading and evaporation

Where F_G is gravity force and F_{iL} represent the liquid inertia. So, we have

$$\rho\pi r^2 H g \frac{\Delta H}{r} = -\frac{1}{\varepsilon} \rho\pi r^2 H \frac{d^2 r}{dt^2}$$

Thus,

$$\frac{d^2 r}{dt^2} = -\varepsilon g \frac{\Delta H}{r}$$

After integration,

$$\frac{dr}{dt} = \sqrt{\varepsilon g \Delta H} \quad (4.4)$$

Where $r_0 = 0$, $\Delta = 1$ for spills on the ground and $(1 - \rho/\rho_w)$ for spills on water. The factor ε presents the liquid inertia, and the value in Ref. [32] is derived theoretically ($\varepsilon = 1.34$), and Briscoe and Shaw suggested $\varepsilon = 2$ for being more conservative in perspective of safety reasons. However, the values of 1.34 and 2 do not response well to low volumetric flow rate, and it is only applicable for the significant volume of the spill, as Briscoe and Shaw solved the model for a continuous spill of $10 \text{ m}^3/\text{s}$ and instantaneous spill of 1000 m^3 in their work. In the following, the value of ε will be investigated for a lower volumetric flow rate.

There is also an analytical solution for determining the radius of pool in Briscoe and Shaw's work, with neglecting the term (m/ρ) in equation (4-2) for a continuous spill and an instantaneous spill. For instantaneous spill, the proposed equation has the form of

$$r = \left\{ r_0^2 + \left(\frac{8g\Delta V_i}{\pi} \right)^{1/2} t \right\}^{1/2} \quad (4.5)$$

Where r_0 is the initial radius, and for a continuous spill, the equation is,

$$r = \left(\frac{32g\Delta V_c}{9\pi} \right)^{1/4} t^{3/4} \quad (4.6)$$

Briscoe and Shaw considered symmetric pool spreading on a flat surface including most concern circumstances, i.e., unbounded spills or spills bounded by a circular bound on the land, while there can be other possible situations concerning, e.g., asymmetric confinement (e.g., a

4 Liquid hydrogen spreading and evaporation

long straight wall) or spills on sloping ground. In these circumstances, pool spread will be asymmetric, and the rate of vaporization will vary from that estimated by the asymmetric pool-spread model since the liquid will be uncovered to diverse areas of ground or water surface and, in the situation of spills on sloping ground, the liquid will be crashed to the other uncooled ground surface as the pool flows bodily over the ground. It is typically probable to consider these impacts, although often in an estimated manner, by modifying the estimates of the asymmetric pool spread model [5].

4.1.3 Vaporization of cryogenic liquids on land

Briscoe and Shaw first considered a pool of steady area so that the focus was on heat transfer instead of pool spread. As mentioned before, for cryogenic liquids spills on land, the leading supplier of latent heat to vaporize the spill is heat contained in the ground. Primarily, the heat flux into the pool may be restricted by the heat transfer rate throughout a vapor blanket between the land and the liquid (i.e., film boiling situation). Nevertheless, as the surface temperature of the ground falls, the vapor blanket dissipates and lets improved thermal contact and quicker heat transfer in the nucleate boiling situation [5]. The heat flux rate into the pool is then dominated by the rate of heat conduction throughout the land. These phases have been reviewed thoroughly in chapter 3.

The B&S model is based on several assumptions, and there are: 1) the pool is thin, 2) the temperature is uniform all over the pool equal to boiling temperature of the liquid, 3) perfect thermal contact with the ground, 4) the heat conduction is the dominant heat source for cryogenic liquids, and it is one dimensional. The governing equation is

$$\frac{\partial T}{\partial t} = \alpha \frac{\partial^2 T}{\partial z^2} \quad (4.7)$$

and the boundary conditions are

$$\begin{aligned} T &= T_a \quad \text{for } 0 \leq z \leq \infty \\ T &= T_B \quad \text{at } z = 0 \\ T &= T_a \quad \text{at } z = \infty \end{aligned} \quad (4.8)$$

Where z is the distance measured downwards from the surface and T is ground temperature. The analytical solution for equation (4.7) and (4.8) is [5, 33]

4 Liquid hydrogen spreading and evaporation

$$T = T_a - (T_a - T_B) \operatorname{erfc} \left(\frac{z}{2\sqrt{\alpha t}} \right) \quad (4.9)$$

So that the heat flux into the pool, same as equation (3.18), is

$$q = k \left. \frac{\partial T}{\partial z} \right|_{z=0} = k \frac{(T_a - T_B)}{(\sqrt{\pi\alpha t})} \quad (4.10)$$

And the mass of vaporization is given by

$$\dot{m} = \frac{q}{h_{fg}} = k \frac{(T_a - T_B)}{h_{fg}(\sqrt{\pi\alpha t})} \quad (4.11)$$

h_{fg} is the latent heat of vaporization.

By combining and elaborating the equations discussed and the equations (4.2) with (4.4), we have

$$\frac{dm}{dt} = \frac{q}{h_{fg}} = \chi k \frac{(T_a - T_B)}{h_{fg}(\sqrt{\pi\alpha t})} \int_0^{r(t)} \frac{2\pi r'}{\sqrt{(t - t')}} \quad (4.12)$$

Where t' is the arrival time of spreading pool and r' is also the corresponded radius to arrival time, and χ is the correction of the ground equal to 3 for compensating the ground's uncertainties [5]. There is also an analytical solution with neglecting the m/ρ in equation (4.2) for vaporization mass. By considering equation (4.5) and (4.6) for spreading radius, for an instantaneous spill, the vaporization mass is

$$m = \chi k \frac{(T_a - T_B)}{h_{fg}(\sqrt{\pi\alpha t})} \times \frac{8}{3} (2\pi g V_i)^{1/2} t^{3/4} \quad (4.13)$$

And for continuous spills,

$$m = \chi k \frac{(T_a - T_B)}{h_{fg}(\sqrt{\pi\alpha t})} \times \left(\frac{\pi^3 g V_c}{2} \right)^{1/2} t^2 \quad (4.14)$$

4 Liquid hydrogen spreading and evaporation

Finally, Briscoe and Shaw recommended using equations (4.2), (4.4), and (4.12) for cryogenic liquids spreading and evaporation and solving them numerically, which this work follows the same procedure.

4.1.4 Result and discussion

Briscoe and Shaw have modeled a large amount of LNG spill. Since the model validation is not investigated in their work, it can only be said that the model response seems to be realistic or not. However, the validation of the model will be studied in this work in the following. The simulation stopped when the pool completely vaporized.

The heat transfer by conduction from the ground (concrete) has been plotted using equation (4.10) in Figure 4.1. As can be seen from the figure, the heat transfer decreasing with time. Thus, the evaporation rate should be reduced with time as well.

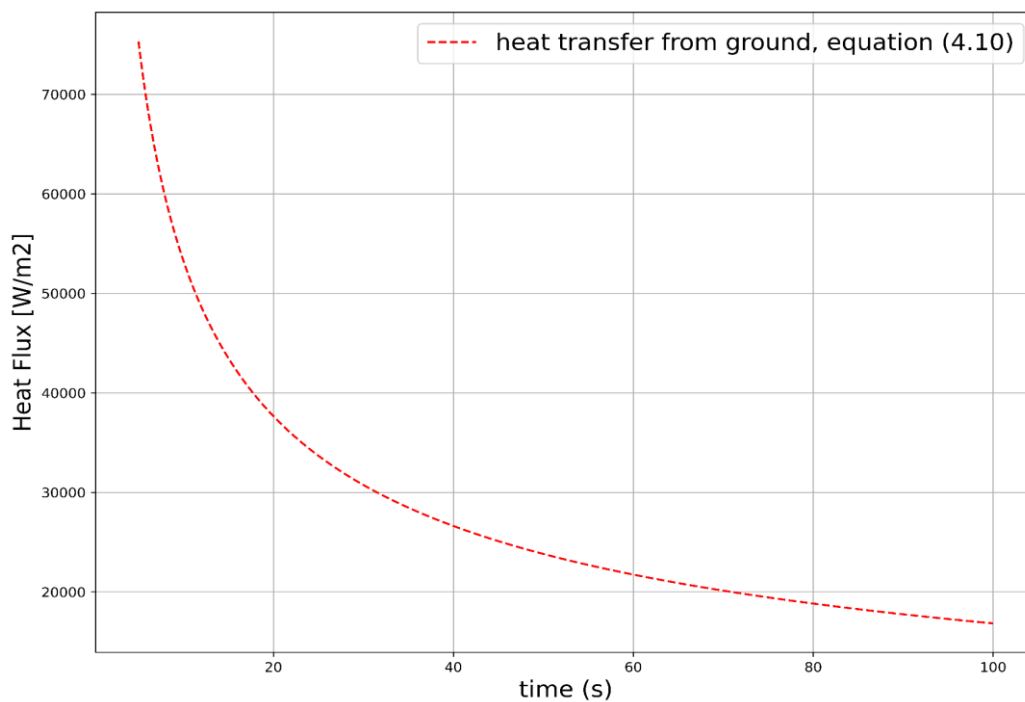


Figure 4.1 The heat transfer by conduction from the ground (concrete).

4 Liquid hydrogen spreading and evaporation

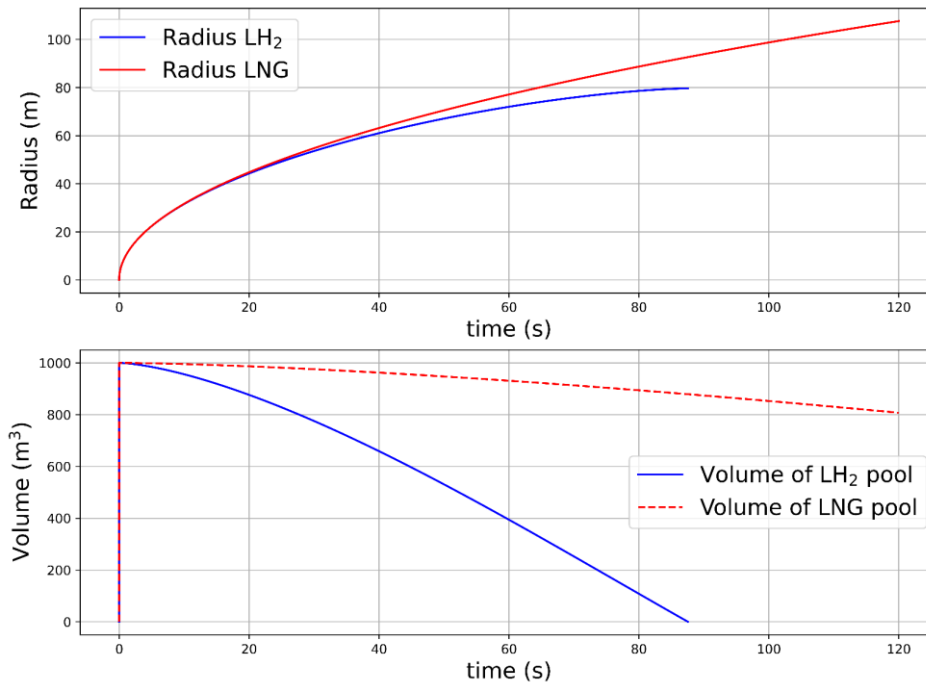


Figure 4.2 The spreading radius and the pool volume of LNG and liquid hydrogen pool by 1000 m³ of an instantaneous spill (B&S).

4.1.5 Instantaneous spill, unbounded

As a first step, the pool's spreading and vaporization mass by an instantaneous spill of 1000 m³ of liquefied natural gas (LNG) have been calculated by Briscoe and Shaw's work.

In this work, the same amount of hydrogen has been investigated and plotted in Figure 4.2. As can be noticed from the figure, the hydrogen pool stops spreading at approximately $r = 80\text{m}$ at $t=90\text{s}$, but the LNG pool extends continuously. For discovering the cause for this phenomenon, both components' pool volume has been plotted in Figure 4.2. As expected, the hydrogen pool evaporates vigorously, and the entire pool of the liquid hydrogen volume has been vaporized in just nearly 90 seconds. This vigorous evaporation of hydrogen may occur due to having a lower density and boiling temperature than LNG. However, the validation of the model is needed to find out the result is realistic or not.

Figure 4.3 illustrates the mass evaporation of LNG and liquid hydrogen of 1000 m³ instantaneous spill. The evaporation rate of liquid hydrogen is extraordinarily intense. The entire pool of hydrogen is predicted to evaporate after approximately 90 (s), so the evaporation process is also stopped in 90 (s). As can be seen from the figures, the model predictions for hydrogen can be realistic due to lower density and extremely lower boiling point of hydrogen than LNG (the difference is approximately 91 °C for temperature and 344 kg/m³ for density).

4 Liquid hydrogen spreading and evaporation

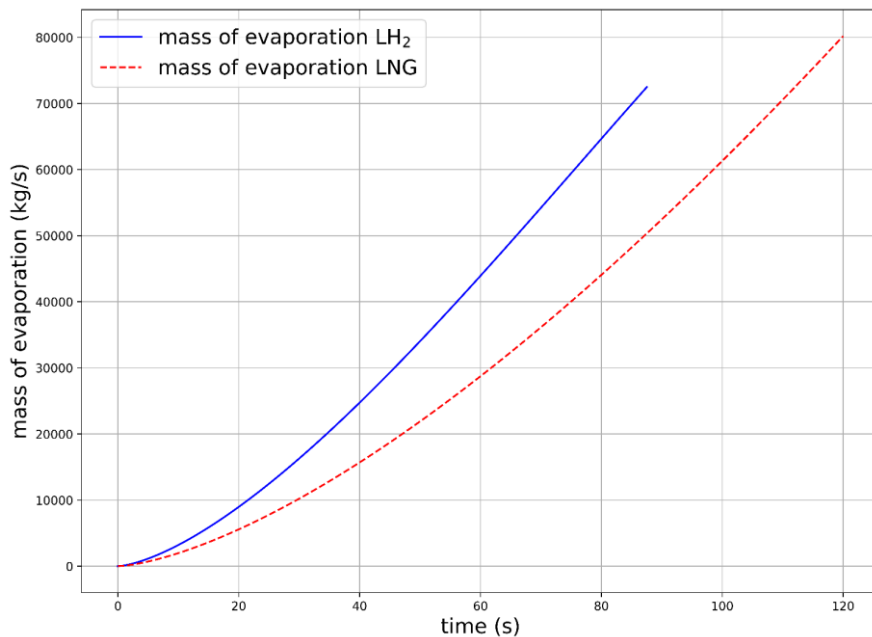


Figure 4.3 Mass evaporation of 1000 m³ instantaneous spill of LNG and Hydrogen (B&S).

4.1.6 Instantaneous spill, bounded

For bounded area, the radius can only spread until reaching a specified point. LNG and liquid hydrogen behavior in this subchapter will be examined for an instantaneous spill of 1000 m³ at the fixed point of $r = 50\text{m}$.

As shown in Figure 4.4, the LNG and liquid hydrogen radius spread roughly the same tendency because of the large spill in a confined space. The liquid hydrogen pool volume evaporates as expected vigorously and reaches nearly 200 m³ after 120s (slightly less vigorous than instantaneous spills in unbounded space). The entire pool of liquid hydrogen disappears approximately after 170 seconds. It takes nearly double the time of unbounded space to evaporate the pool entirely.

As anticipated and shown in Figure 4.5, the mass vaporization of hydrogen is also more extreme than LNG in bounded space. Compared with the instantaneous spill in free space, the mass vaporization is slightly lower in confined space due to less contact area with an ambient temperature surface, while in unbounded space, the pool spreads continuously and reaches the uncooled spots. In other words, the area that contacts the pool in the bounded area is limit to a finite size, and that limited size of ground becomes cold, while in free space, the pool always reaches the ground's uncooled point, and the contact area is infinite. Thus, the mass vaporization is more intense in the unbounded setting.

4 Liquid hydrogen spreading and evaporation

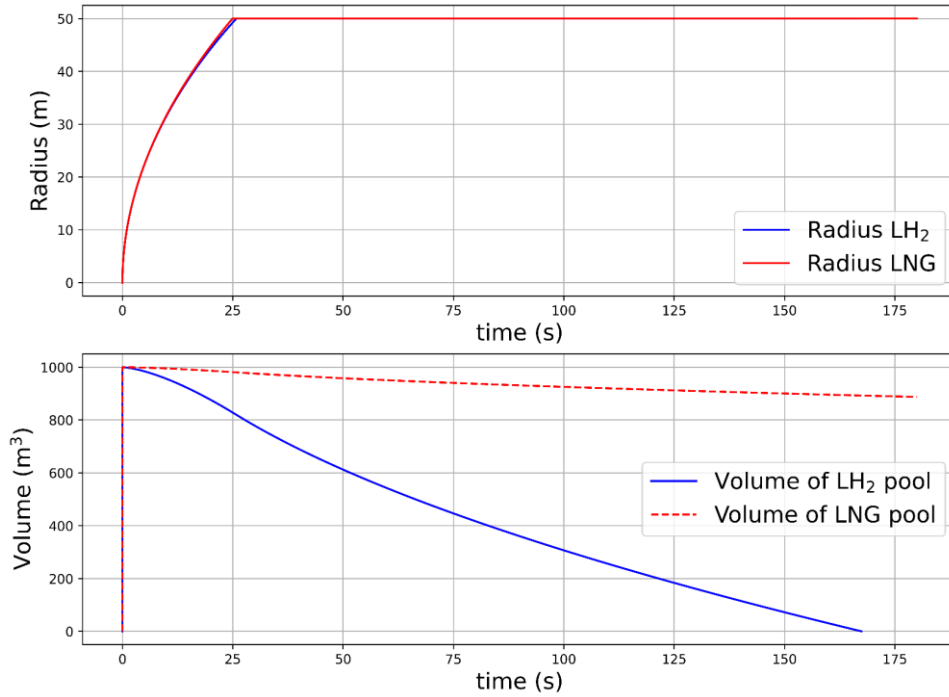


Figure 4.4 The spreading radius and the pool volume of LNG and liquid hydrogen pool by 1000 m³ of an instantaneous spill bounded at $r = 50\text{m}$ (B&S)

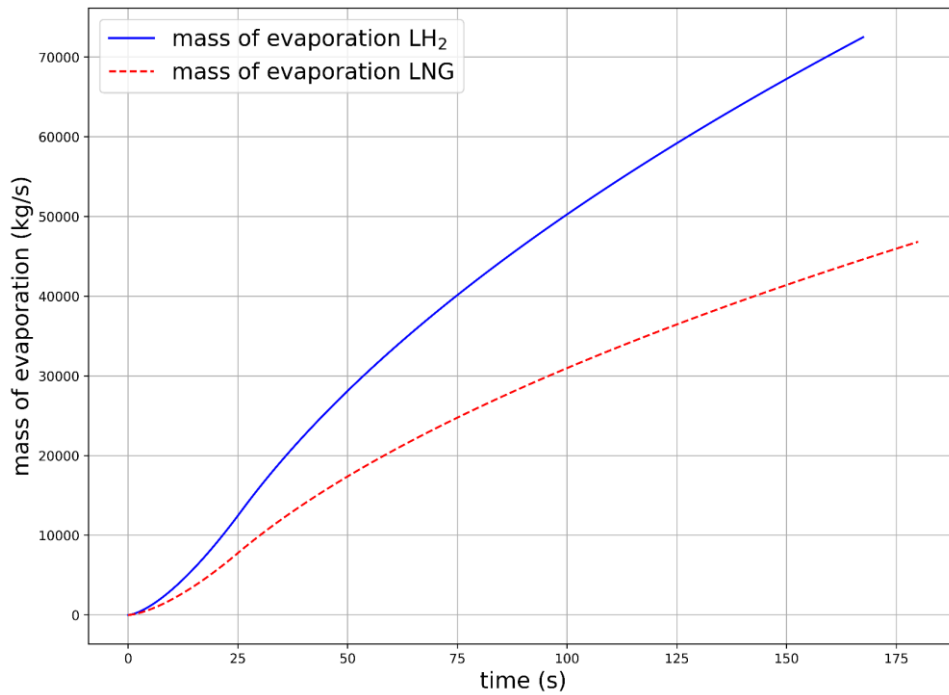


Figure 4.5 Mass evaporation of 1000 m³ instantaneous spill of LNG and Hydrogen bounded at $r = 50\text{m}$ (B&S).

4 Liquid hydrogen spreading and evaporation

4.1.7 Continuous spill unbounded

The next step is to model the continuous spill of hydrogen and LNG. The amount of $10 \text{ m}^3/\text{s}$ same as the work of Briscoe and Shaw selected for the simulation.

Figure 4.6 has been plotted for investigating the radius and pool volume of liquid hydrogen and LNG during the continuous spill. The pool of liquid hydrogen is predicted to evaporate energetically same as the instantaneous spill in the continuous spill, and the volume of the pool will constantly increase until reaching a maximum point. The maximum volume that the pool of hydrogen reaches is 400 m^3 at $t = 85\text{s}$ and after that decreases with time. In contrast, the LNG pool is predicted to maintain and increase almost intensely, and its vaporization will be less intense than hydrogen. It can be seen from Figure 4.6 that the spreading speed of the LNG is more than hydrogen. It can be a result of being heavier than liquid hydrogen since gravity controls the spreading in this model.

In Figure 4.7, the mass evaporation of the LNG and liquid hydrogen during continuous spill has been plotted. As expected, in continuous spills, same as an instantaneous spill, liquid hydrogen's vaporization is more intense than LNG. It can be said that the nearly entire pool during the continuous spill is evaporated.

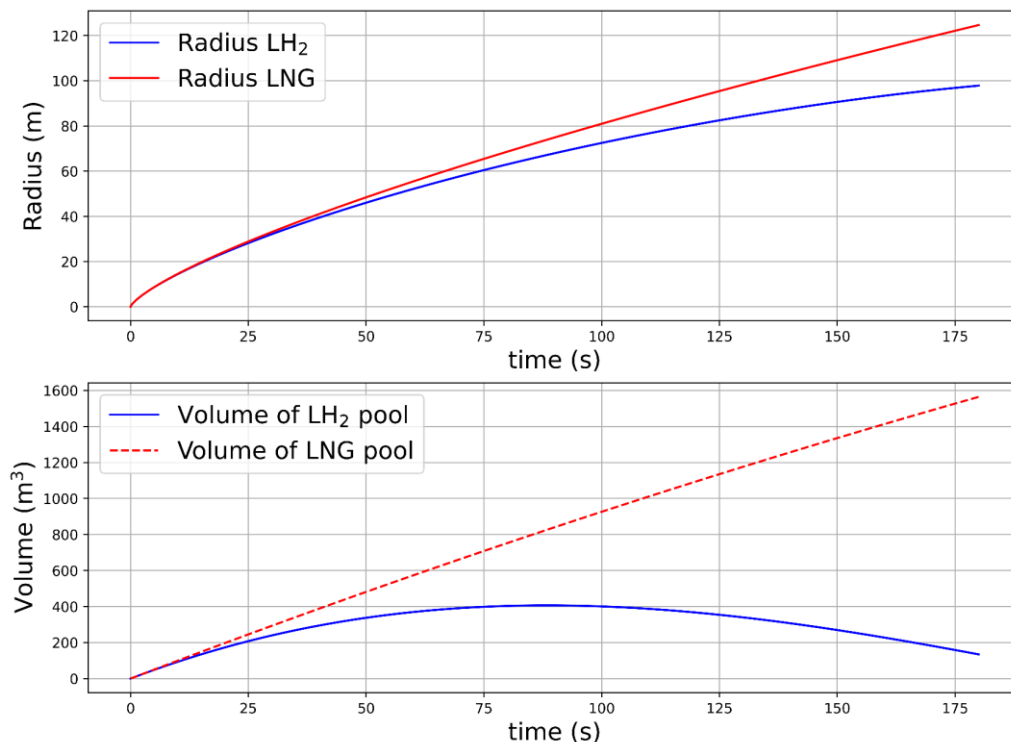


Figure 4.6 The spreading radius and the pool volume of LNG and liquid hydrogen by a continuous spill of $10 \text{ m}^3/\text{s}$ (B&S).

4 Liquid hydrogen spreading and evaporation

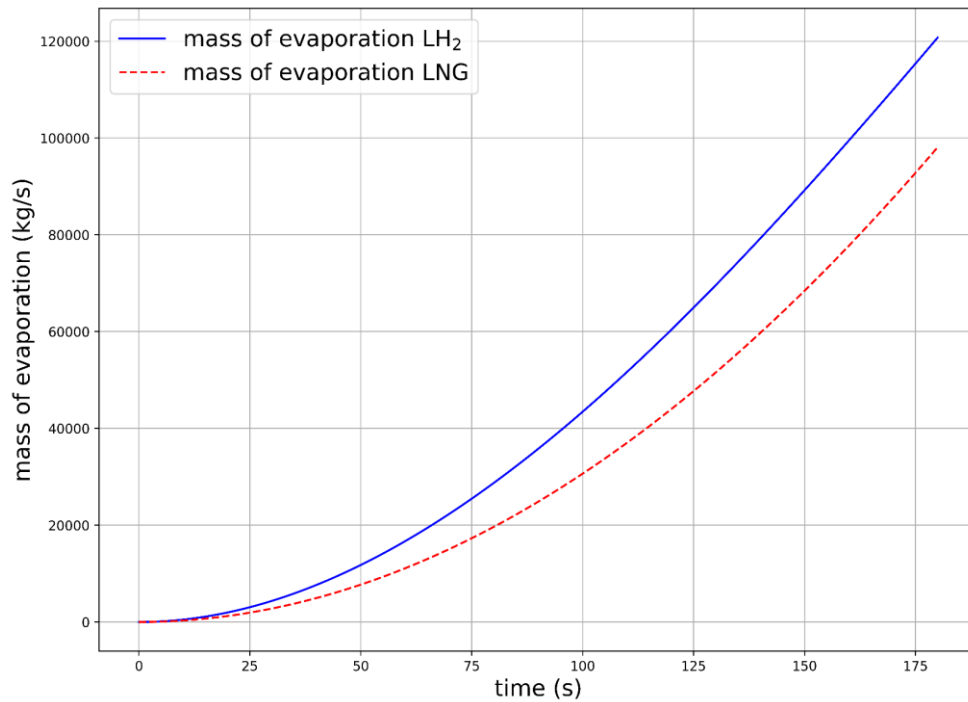


Figure 4.7 Mass evaporation by 10 m³/s continuous spills of LNG and Hydrogen (B&S).

4.1.8 Continuous spill, bounded

In this subchapter, the continuous spill of 10 m³/s of LNG and liquid hydrogen will investigate at the bounded area. The assumption for fixed distance is $r = 50\text{m}$.

Figure 4.8 demonstrates the volume and radius of liquid hydrogen and LNG spreading at a continuous spill. As shown in Figure 4.8, in contrast with the unbounded area Figure 4.6, the hydrogen pool will maintain at the bounded area due to mentioned reasons in 4.1.6, but it is still robust evaporation for hydrogen than LNG even at the fixed site.

Figure 4.9 indicates the mass vaporization of liquid hydrogen and LNG at the bounded area. Compared with the unbounded area, the evaporation mass will be lower at the bounded area, as shown in Figure 4.7 and Figure 4.9. This phenomenon occurs because the pool is in less contact with the ground than the unbounded site. Therefore, the area connected with the pool becomes cold faster, leading to less mass vaporization.

4 Liquid hydrogen spreading and evaporation

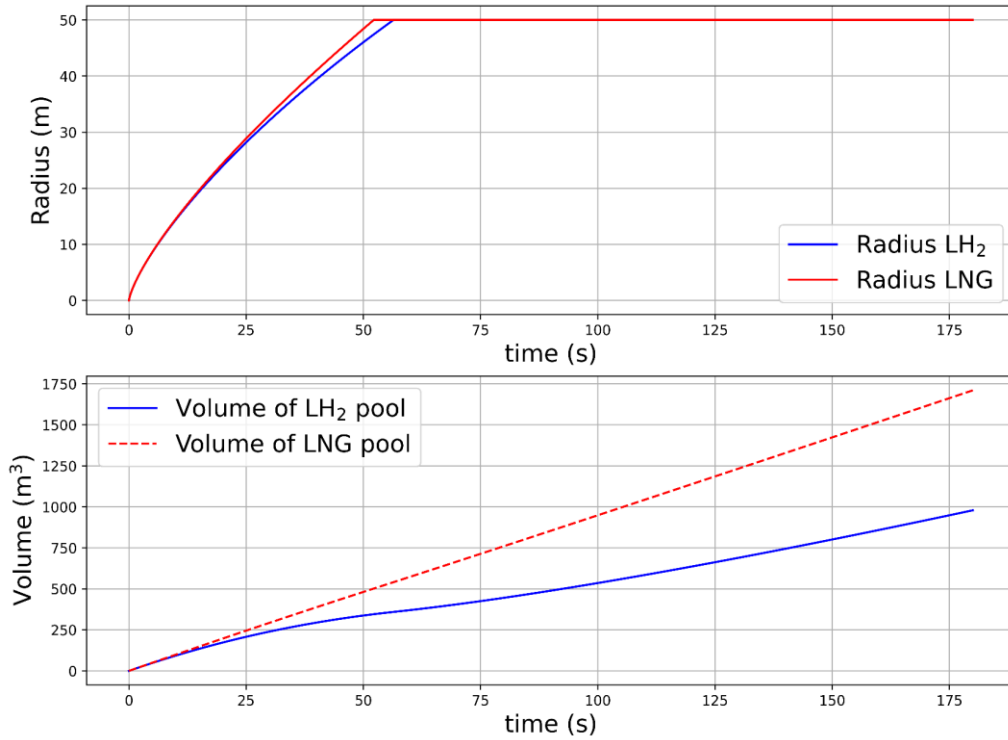


Figure 4.8 The spreading radius and the pool volume of LNG and liquid hydrogen pool by 10 m³ /s of a continuous spill bounded at r =50m (B&S)

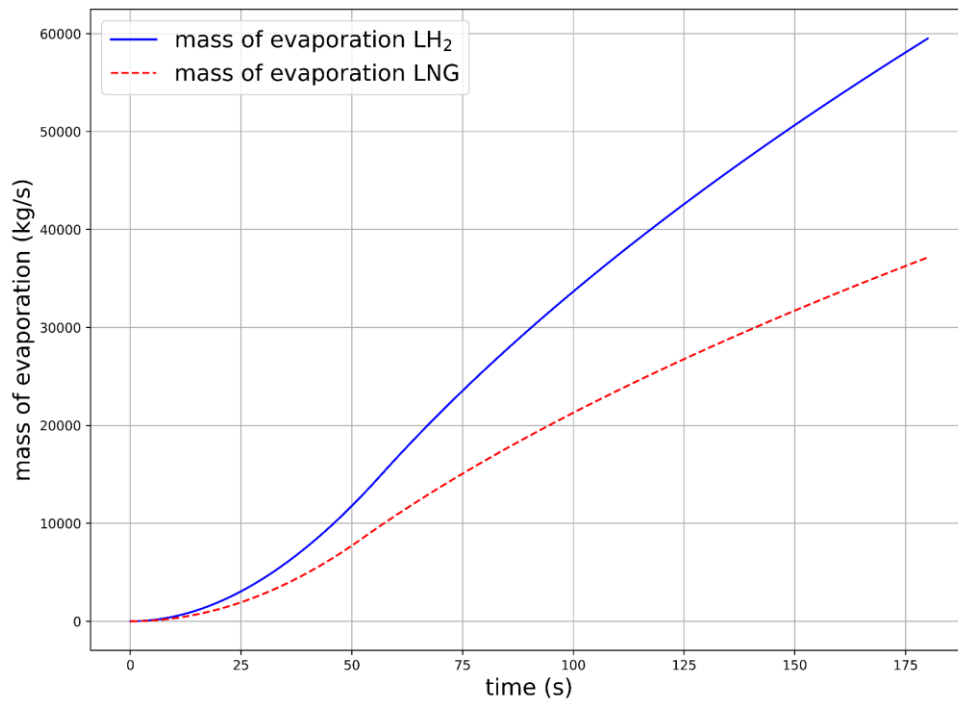


Figure 4.9 Mass evaporation of 10 m³ /s continuous spill of LNG and Hydrogen bounded at r = 50m (B&S).

4 Liquid hydrogen spreading and evaporation

4.1.9 Lower volume spill

So far, the model response is convincing, but as was mentioned in previous subchapter 4.1.2, this model is only applicable for the large volume of the spill. The shortcoming of this model, such as the value of constant number ε for lower amount of spills, (ε is Froude number in origin, but it does not mention directly in Briscoe and Shaw's work, it will be reviewed more later) and the pool's minimum depth, are not discussed in Briscoe and Shaw's work.

Figure 4.10 shows the radius and volume of the pool for a spill rate of 0.07 kg/s. As it is evident from the figure, the graph becomes unstable and collapses at $t=0.001$ s or, in other words, the entire mass of the vaporize in 0.001s, as illustrated in Figure 4.11. So, the model is not applicable for lower spill rates without modifications.

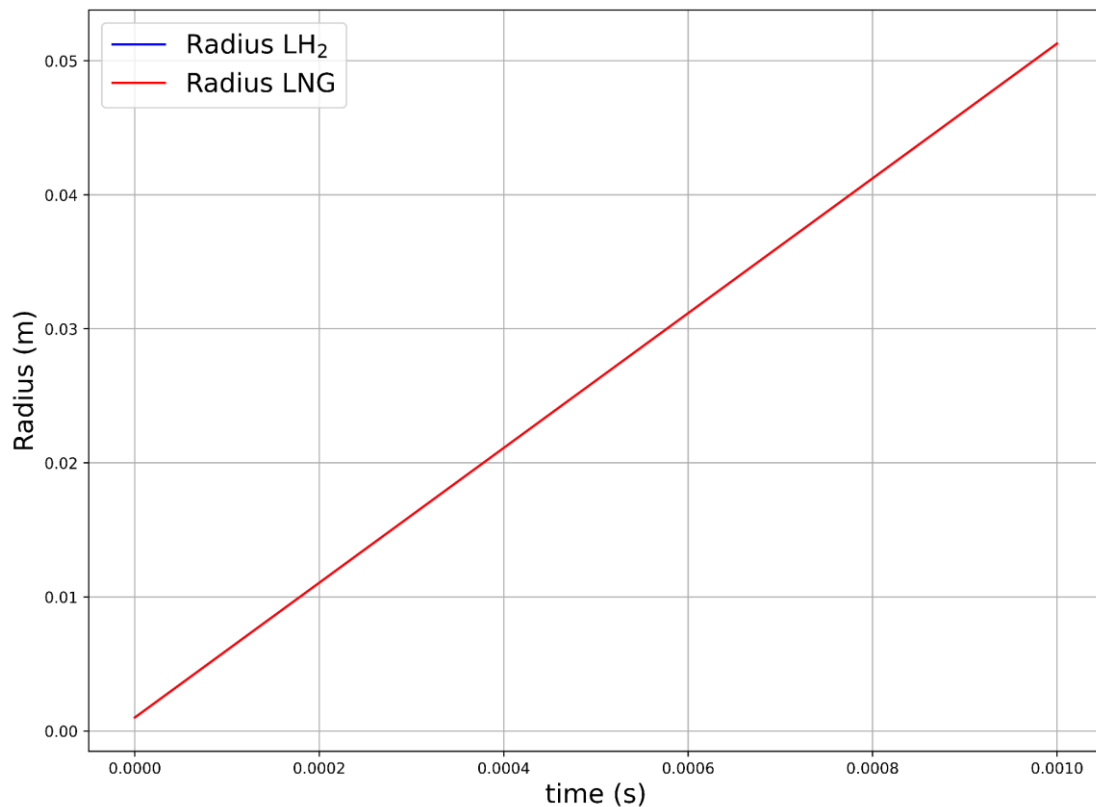


Figure 4.10 The spreading radius and the pool volume of LNG and liquid hydrogen pool by 0.07 kg /s of a continuous spill (B&S)

4 Liquid hydrogen spreading and evaporation

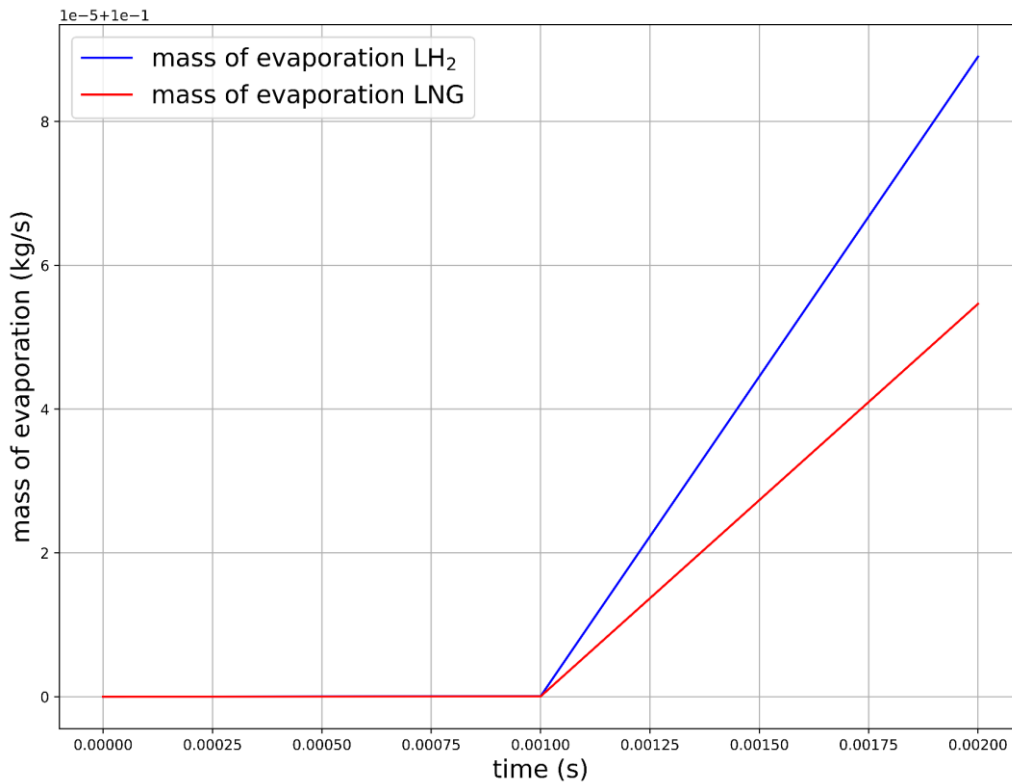


Figure 4.11 Mass evaporation of 0.07 kg /s continuous spill of LNG and Hydrogen (B&S).

Nguyen et al. [4] suggested that a minimum depth for the model should be considered to prevent the model from stopping spreading. The minimum depth can be defined as

$$H_{min} = \left(\frac{6vV_c}{\pi g} \right)^{0.25} \quad (4.15)$$

Figure 4.12 has been plotted after utilizing the equation (4.15). The response still is not applicable for this model. As shown in Figure 4.12, the pool radius for LNG and liquid hydrogen spreads to 35m and 23m at t=120, respectively. The result is not realistic for a low spill rate of 0.07 kg /s, equal to 0.001 m³/s for hydrogen and 0.0002 m³/s for LNG. As mentioned in Webber's work [34], this model must not use for the spills on land, and the value of the Froude number for spreading on the ground is not specified and must be determined empirically. Thus, the model should be examined more next.

4 Liquid hydrogen spreading and evaporation

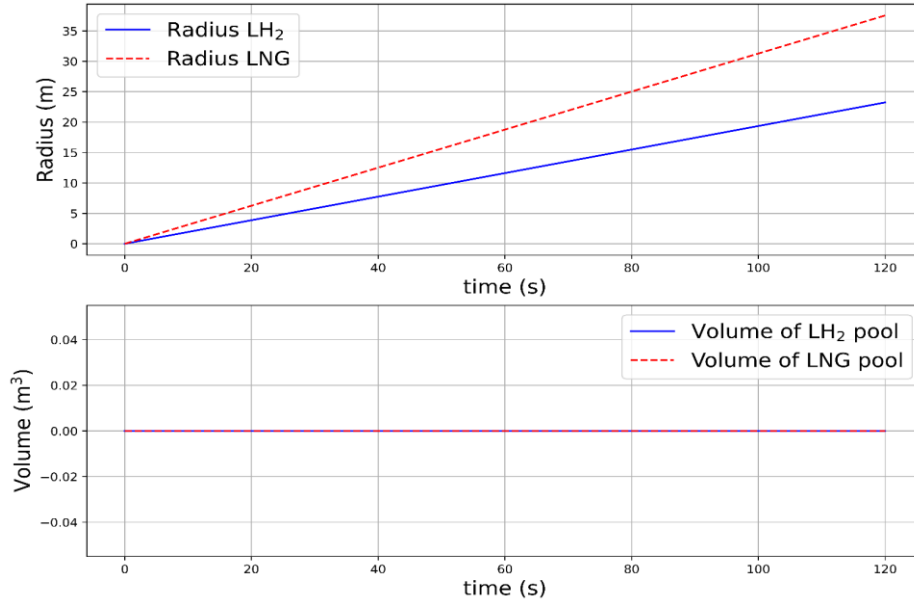


Figure 4.12 The spreading radius and the pool volume of LNG and liquid hydrogen pool by 0.07 kg /s of a continuous spill with $\varepsilon = 1.34$ and applying equation (4.15) (B&S).

In this work, for keeping the pool spread and model the resistance corresponding to mass flow rate, the value of Froude is modified together with using H_{min} . Since the value of 1.34 and $\sqrt{2}$ are in good agreement with the model for significant spills, so another value must be specified for a low spill rate. Thus, after trial and error, in this work, and validating the model with gas accumulation over spreading pool GASP model, which will be discussed in 4.2, the value of, ε , should be $10^{-3} \leq \varepsilon \leq 15 \times 10^{-3}$ for lower spill rates. Overall, the Froude number has to be determined empirically [34], or it is suggested by this work to use the rule of thumb, which can be defined for the Froude number as follow. However, comprehensive experimental data is needed for the validation of this suggestion. It should be considered that the spill rate is in mass flow rate, not volumetric flow rate, since gravity control the spreading in this model.

$$\begin{aligned}
 10^{-3} &\leq \varepsilon \leq 15 \times 10^{-3} && \text{for } S < 1 \\
 15 \times 10^{-3} &< \varepsilon \leq 1.34 && \text{for } 1 \leq S \leq 100 \\
 \varepsilon &= \sqrt{2} && \text{for } S > 100
 \end{aligned} \tag{4.16}$$

Figure 4.13 and Figure 4.14 have been plotted after applying the equation (4.15) and rule of thumb (4.16). The model becomes stable and realistic, as seen in the figure. Thus, more experimental data are needed for validation of the model and determining the Froude number. The value of 0.015 for the Froude number seems to respond well. But, experimental data is required for validation.

4 Liquid hydrogen spreading and evaporation

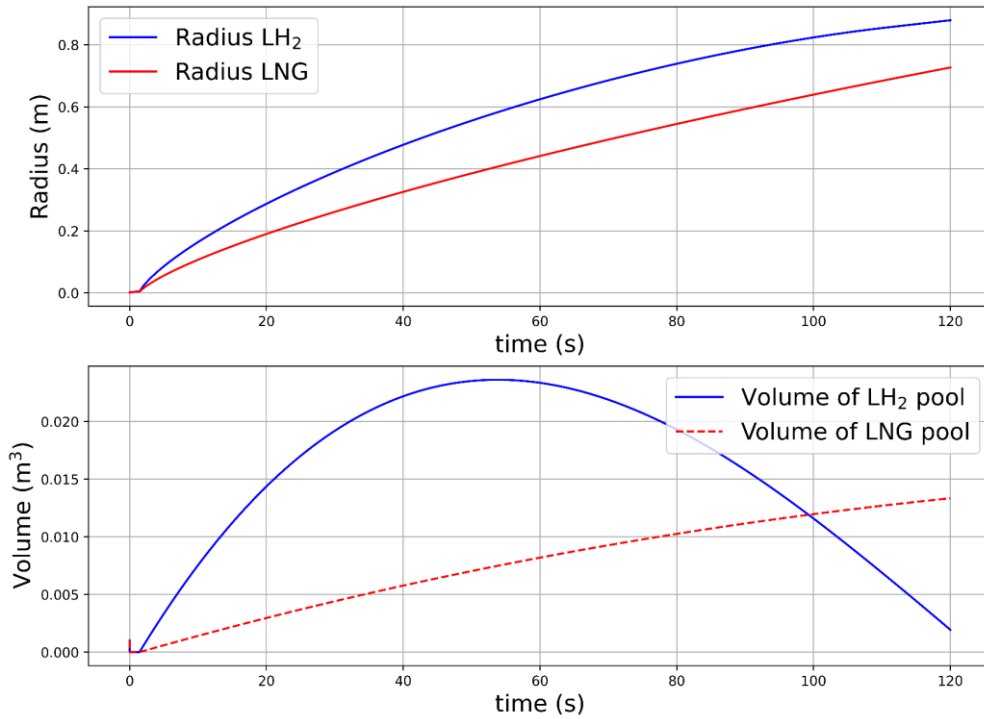


Figure 4.13 The spreading radius and the pool volume of LNG and liquid hydrogen pool by 0.07 kg /s of a continuous spill with $\varepsilon = 0.015$ (B&S)

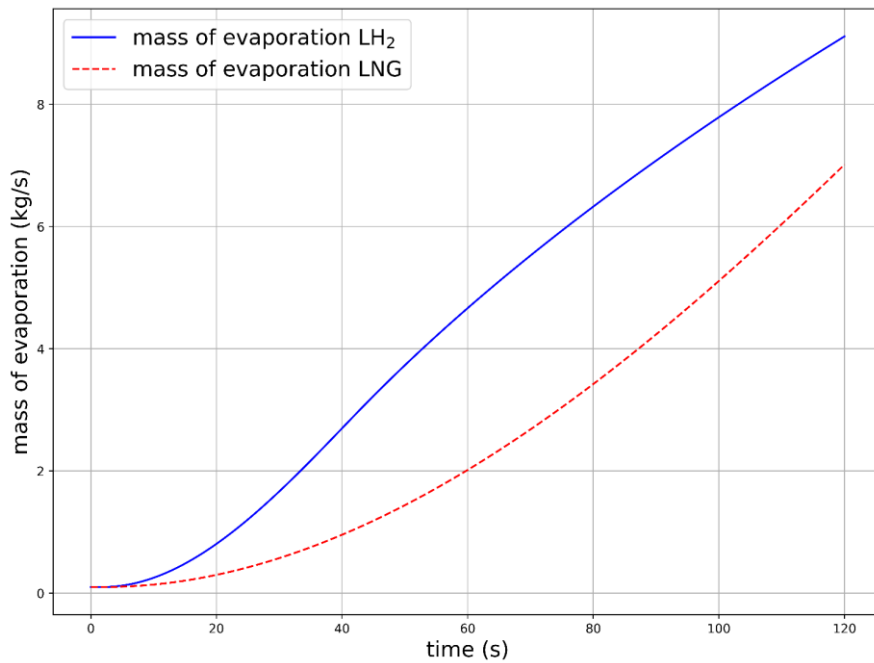


Figure 4.14 Mass evaporation of 0.07 kg /s continuous spill of LNG and Hydrogen with $\varepsilon = 0.015$ (B&S).

4 Liquid hydrogen spreading and evaporation

4.1.10 Validation of B&S model against LNG experimental data

In Moorhouse and Carpenter's work [35], two continuous spills of 14 tons/h and 17 tons/h were tested on concrete and soil, respectively. The description of the experiment is not available, So it is assumed that the spill occurs on a flat surface. The experimental data of Moorhouse and Carpenter has been taken from Basha et al. [29]. The thermal properties of the concrete and the soil are tabulated in Table 4.1.

Table 4.1 Thermal properties of concrete and soil [5].

Material	Density $\rho(\text{kg/m}^3)$	Specific heat $C_p(\text{J/kg-K})$	Thermal conductivity $k(\text{W/m-K})$	Thermal diffusivity $\alpha(\text{m}^2/\text{sec})$
Concrete	2300	961.4	0.92	4.16×10^{-7}
Soil (average)	2500	836.0	0.96	4.59×10^{-7}
Soil (sandy, dry)	1650	794.2	0.26	1.98×10^{-7}
Soil (moist, 8% water, sandy)	1750	1003.2	0.59	3.36×10^{-7}

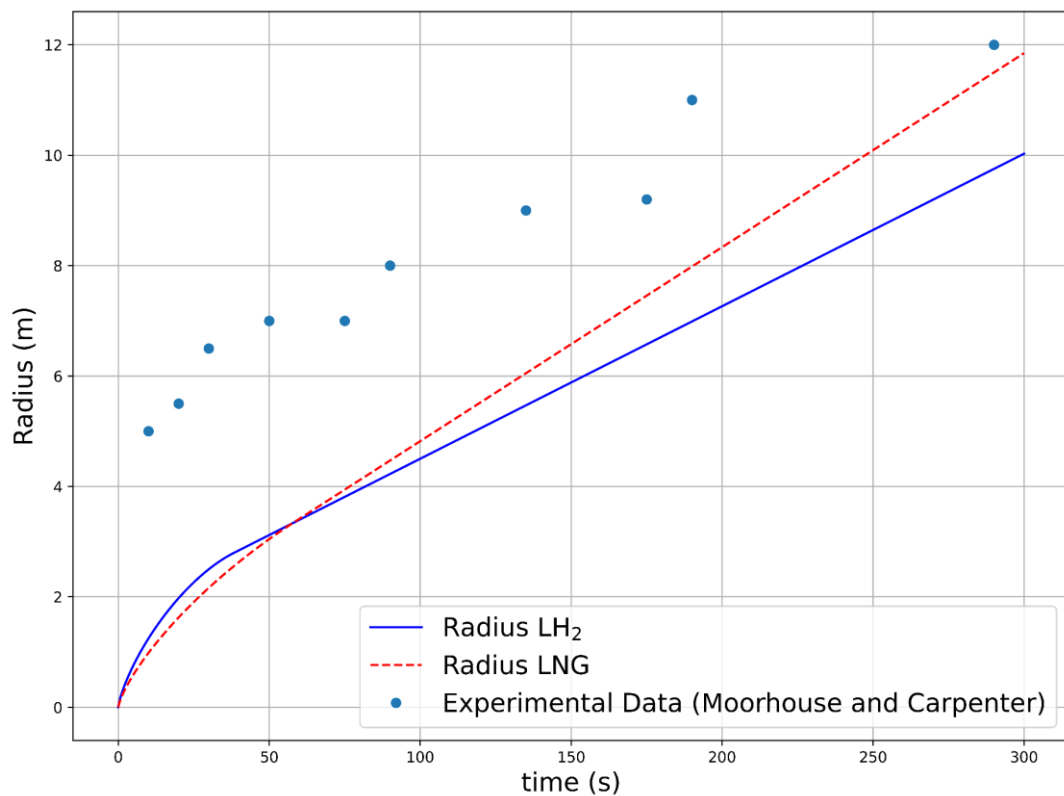


Figure 4.15 The spreading pool's radius versus time (Concrete) (B&S).

Figure 4.15 and Figure 4.16 show that the model is nearly in good agreement with experiment data. The Froude numbers are taken to be $\varepsilon = 0.12, 0.15$ for 14 tons/h and 17 tons/h,

4 Liquid hydrogen spreading and evaporation

respectively. For vaporization mass and pool mass or volume, there is no experimental data. Thus in this section, the figures for vaporization mass and pool volume have not been plotted.

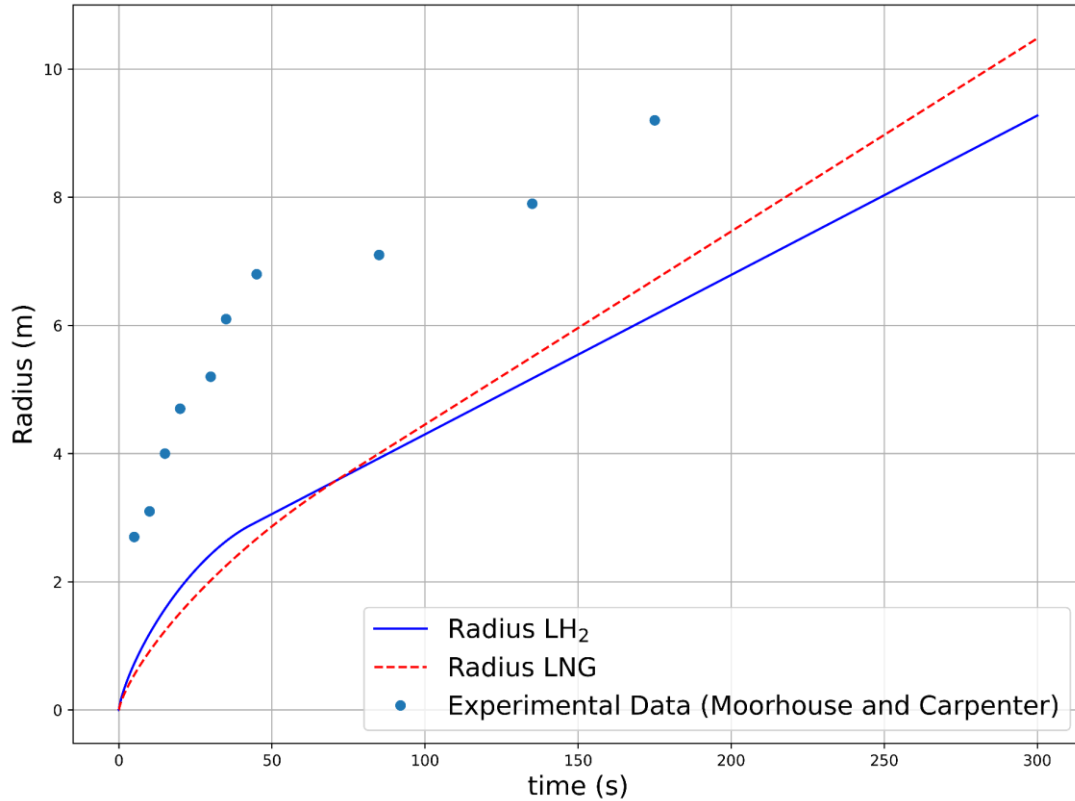


Figure 4.16 The spreading pool's radius versus time (Soil) (B&S).

4.1.11 Validation of B&S model against liquid nitrogen experimental data

In the work of Nguyen et al. [1], a series of experimental investigations have been conducted to measure the evaporation rate of cryogenic liquids for the radially spreading pool. For safety reasons, liquid nitrogen was selected as a working fluid by the work. The liquid was constantly spilled onto a concrete plate to simulate an accidental leak of cryogenic liquid. Seven cases were selected for nominal spill rates, which are tabulated in Table 4.2.

Table 4.2 Nominal spill rates of liquid nitrogen [1].

Case	Discharge time, s	Nominal mass spill rate, kg/s
1	198	0.0402
2	135	0.0546
3	87	0.0739
4	67	0.0877
5	51	0.1050
6	37	0.1319
7	27	0.1629

4 Liquid hydrogen spreading and evaporation

Cases 1 and 7 are selected for simulation in this work. The simulation's result was validated against liquid nitrogen experimental data and compared with liquid hydrogen and LNG behavior. It is worth mentioning that after trial and error, the Froude number for these two cases is taken to be 0.003 and 0.06 for cases 1 and 7, respectively.

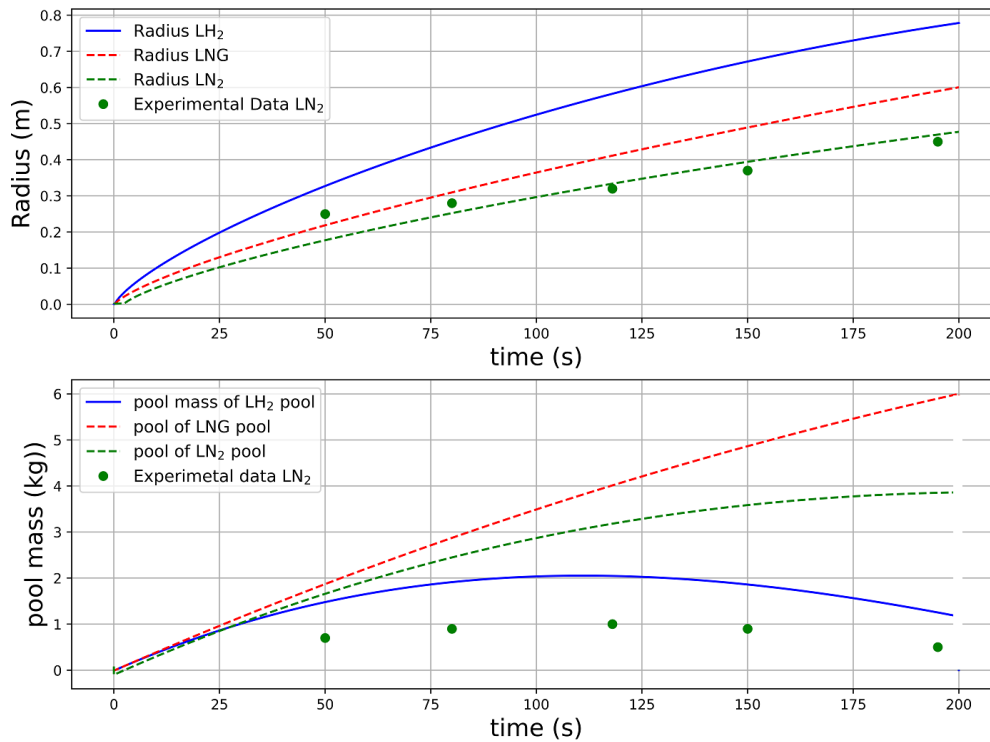


Figure 4.17 Predicted spreading pool radius and mass of LN₂ and LH₂ and LNG with time versus experimental data of LN₂ (case 1) (B&S).

As shown in Figure 4.17 and Figure 4.18, the model anticipates the liquid nitrogen spreading pool radius nearly accurate, and it is in good agreement with experimental data for both cases 1 and 7.

The model overestimates the pool mass of liquid nitrogen. The model's tendency is not consistent with the experimental data. For case 1, the pool in the experiment tends to evaporate the entire pool, while the model underestimates the evaporation for liquid nitrogen. For case 7, the pool mass of experimental data is rising and maintains for a longer time than case 1, but still, the prediction by the model is higher. Overall, it can be determined that Briscoe and Shaw's model underestimates the vaporization of cryogenic liquid for all time while the spreading radius by the pool is predicted well.

As exhibited in Figure 4.17 and Figure 4.18, and as discussed in the previous simulations, liquid hydrogen's behavior tends to go to zero, i.e., evaporated vigorously. It makes sense due

4 Liquid hydrogen spreading and evaporation

to the characteristic of liquid hydrogen, as we know. Nevertheless, the experimental data for liquid hydrogen is required for validating the model. The liquid hydrogen spreads faster than two other liquified gas. It is due to the lower density of hydrogen than two other liquified gas and more volume of liquid hydrogen spills per mass. Thus, the volume of hydrogen spilled on the surface is more than two other liquids. There is a lack of experimental data for validating the model against the vaporization mass; however, there are experimental data for vaporization velocity, i.e., the vaporized volume per unit area, which the model is incapable of predicting. So, the model should be modified to make it capable of predicting the vaporization velocity. The Constant Froude Number (CFN) model is a modified version of the Briscoe and Shaw model, which will be discussed more in section 4.3.

Overall, the model prediction is roughly in good agreement with experimental data, but it can be an excellent idea to determine the Froude number by an empirical equation. Thus, comprehensive experimental data is needed.

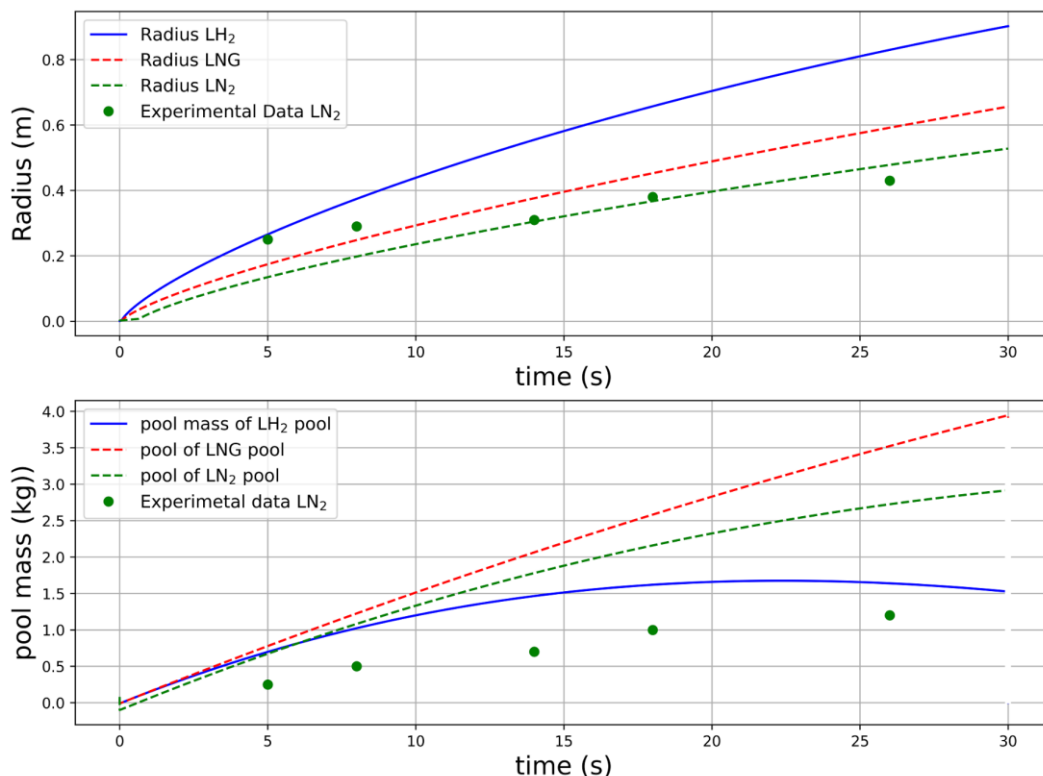


Figure 4.18 Predicted spreading pool radius and mass of LN₂ and LH₂ and LNG with time versus experimental data of LN₂ (case 7) (B&S).

4.2 Gas accumulation over spreading pools (GASP) model.

The GASP model provides a circular axisymmetric pool of liquid on land or water, which can model the pool's vaporization rate and spread. The GASP model assessed the vaporization rate as a function of wind condition, pool temperature, pool size, properties of the studied liquids,

4 Liquid hydrogen spreading and evaporation

and the environment's thermal properties. In the following, the original GASP model will be examined thoroughly. In this work, the Gas Accumulation over Spreading Pool model has been taken from the work of Webber [7].

4.2.1 Some observance of the GASP model

It must be considered that the surface on which the liquid is spilled is flat, horizontal, and statistically uniform. The spill can occur in confined or free space. The release of liquid could be instantaneously or continuously. The atmospheric dispersion of the vapor and heat transfer to the pool control the vaporization rate. The mass vaporization is given by

$$\frac{dm}{dt} = JA \quad (4.17)$$

Where J is the mean local vaporization rate, and A is the surface area of the pool. Thus, the spreading of the pool is as essential as mass vaporization. For spreading the liquid on the confined space, measuring the area is not difficult to calculate, but it is not always the case, e.g., for transport accidents [7].

4.2.2 The GASP model structure

The structure of the model consists of a couple of differential equations same as the B&S model. Firstly, It will be convenient to categorize the variables as primary and secondary. The differential equations should be written for radius, velocity, volume, and temperature of the pool. The discharge volume of the liquid to the pool and the vaporized volume should also be considered in the model. These are the primary variables. The right-hand side of the model must be defined in terms of secondary variables, e.g., the pool's depth, area, and mean temperature. In general, the secondary variables are an algebraic function of primary variables. For solving these coupled differential equations, the appropriate initial value is needed [7].

4.2.3 Discharged and vaporization

For simplicity, three primary volume variables must be considered including the volume of the pool V , the discharge volume of liquid into the pool V_d , and the vaporized volume of liquid from the pool V_E . For discharge volume, we have

$$\frac{dV_d}{dt} = \dot{V}_c \quad (4.18)$$

4 Liquid hydrogen spreading and evaporation

Where \dot{V}_C is the volumetric flow rate, and for instant release, \dot{V}_C may be zero, and the V must initially be non-zero. The vaporized volume of liquid from the pool is

$$\frac{dV_E}{dt} = WA' \quad (4.19)$$

Where A' is the top area of the pool, and W is the regression rate. The regression rate W is related to evaporation mass flux density J and the liquid density by the equation below

$$J = \rho W \quad (4.20)$$

And V_E is related to the mass which has vaporized and given by

$$m = \rho V_E \quad (4.21)$$

Thus, the differential equation for the volume of the mass may be written as

$$\frac{dV}{dt} = \dot{V}_C - WA' - D \quad (4.22)$$

The term D is for loss of the volume other than by vaporization, e.g., leaking into permeable ground or moving into sewers.

4.2.4 The pool equations

The GASP model considers three possible surface areas for spreading, i.e., on smooth land, rough enough land to retain in puddles, and water [7]. Our case of study is spreading the liquid hydrogen on the ground. So, the equations and terms for water will not be investigated in this work.

For rough and smooth lands, the reduced acceleration due to gravity is

$$g' = g \quad (4.23)$$

For the area of the pool, both for rough and smooth land, we have

4 Liquid hydrogen spreading and evaporation

$$A = \pi r^2 \quad (4.24)$$

The mean depth for smooth land may be written as

$$H = \frac{V}{A} \quad (4.25)$$

For spreading the pool on rough lands, the puddle forming must be considered. Thus, there will be two layers of liquid. One layer of the dynamic pool, which spread over a stagnant region. Therefore, the depth will be

$$H_e = \frac{V}{A} - h_p \quad (4.26)$$

Where H_e and h_p is the dynamic region of mean depth and mean depth of the puddle, respectively. Hence, the volume of the pool will be

$$V_e = V - h_p \cdot A \quad (4.27)$$

The edge depth of the pool, h_f , is not equal to mean depth at all times [7]. It is essential to maintain some measures of the depth profile in the pool [36]. Therefore, a dimensionless shape factor, s , is defined as follows.

$$s = \frac{h_f}{H} \quad (4.28)$$

The shape factor s will influence gravity spreading. If $s < 1$, the pool spread outward on average, and if $s > 1$, the spread will be inward. On smooth land, the shape factor will be equal to zero ($s=0$). The shape factor as well depends on the factors related to the frontal depth. Thus, surface tension σ must be included in the model by setting the frontal depth to a constant value λ which is defined with the equation below.

4 Liquid hydrogen spreading and evaporation

$$\lambda = \left(\frac{\sigma}{g\rho} \right)^{1/2} \quad (4.29)$$

The surface tension act against gravitational spread [7]. The viscous effect provide improvement to minimum depth so that the minimum depth same as equation (4.15), based on viscous impact, will be

$$H_0 = \left(\frac{6\nu S}{\pi g} \right)^{1/4} \quad (4.30)$$

Where ν is the dynamic viscosity of the liquid. Thus, the minimum depth will be the more significant effect of viscous and surface, and we have

$$H_{min} = \max\{\lambda, H_0\} \quad (4.31)$$

After the above discussion, the shape factor can be now set to

$$s = \frac{H_{min}}{H} \quad (4.32)$$

If the roughness of the ground dominates, the shape factor will be

$$s = \frac{\Phi_1(\omega)a}{2H} \quad (4.33)$$

Where a is the roughness scale, and ε is

$$\varepsilon = \frac{8U^2}{ga} \quad (4.34)$$

4 Liquid hydrogen spreading and evaporation

Where U is the radial velocity of the pool at edge, and $\Phi_1(\varepsilon)$ is defined as

$$\Phi_1(\omega) = (1 + \varepsilon)^{0.5} - 1 \quad (4.35)$$

The functions of (ω) take into account the removal of mass and momentum from the pool's dynamic portion as it spreads over depressions in the rough ground model. Thus, for future references

$$\Phi_2(\omega) = 1 - \frac{2}{\omega} \Phi_1(\omega) \quad (4.36)$$

Moreover, if the pool is confined to a band, the shape factor will equal one ($s = 1$).

4.2.5 Equations for spreading

For the radius of the liquid pool spreading on smooth land, it can be considered as

$$\frac{dr}{dt} = U \quad (4.37)$$

For rough land, it can be defined as

$$\frac{dr}{dt} = \Phi_2(\omega) \cdot U \quad (4.38)$$

And the frontal velocity of the pool, U , can be expressed as

$$\frac{dU}{dt} = \phi(s) \frac{4g'H}{r} e - F \quad (4.39)$$

Where F is turbulent or viscous resistance term. $\phi(s)$ is the gravity driving term expressed as

$$\phi(s) = 1 - s; \quad s < 2 \quad (4.40)$$

4 Liquid hydrogen spreading and evaporation

$$\phi(s) = \frac{-s^2}{4}; \quad s > 2$$

The resistance term F depends on the flow regime. For the laminar flow regime, we have

$$F_L = \beta(s) \frac{cvU}{H_e^2} (1 - f) \quad (4.41)$$

Where $c = 3$ for smooth and rough land. The vertical velocity profile can specify the c factor in the pool. The factor β is a factor determined by radial profiles and defined as

$$\beta(s) = 2.53 j(s)^2 \quad (4.42)$$

Where $j(s)$ can be defined as

$$\begin{aligned} j(s) &= 1; & s < 2 \\ j(s) &= \frac{2}{s}; & s > 2 \end{aligned} \quad (4.43)$$

Factor (f) allows for the radial motion of water under the pool. Therefore, it equals zero ($f = 0$) for smooth and rough land [7].

For turbulent resistance, we have

$$F_T = \frac{a(s)CU^2}{H_e} \quad (4.44)$$

Where C is a turbulent friction coefficient, and the optimum value of C is 1.5×10^{-3} . The radial factor, $a(s)$, can be defined as

$$a(s) = 4.49 j(s) \quad (4.45)$$

4 Liquid hydrogen spreading and evaporation

Finally, the value of F can be determined by

$$F = \text{sign}(U) \cdot \max(|F_T|, |F_L|) \quad (4.46)$$

The shift from turbulent to laminar flow is controlled by Reynolds number, which is [36]

$$Re = \frac{UH}{\nu} = \frac{1.69}{C} \quad (4.47)$$

4.2.6 The pool temperature

The average liquid temperature T is taken to perform along with the heat balance below

$$\frac{dT}{dt} = \left(\frac{A_{top}}{C_p \rho V} \right) (Q - \rho WL) + (S/V)(T_s - T) \quad (4.48)$$

Where Q is the heat flux density, C_p is the specific heat capacity of the liquid, and T_s is the liquid source temperature. This equation's solutions showed clumsy performance, especially in $dT/dt = 0$, where for $\exp(Q/\rho WL) \gg 1$, the solutions reveal an almost instantaneous transition from a regime [7]. This obstacle can be overcome by specifying

$$Y = \ln \left(\frac{T_A}{T_B - T} \right) \quad (4.49)$$

T_A is an arbitrary temperature scale, taken to be 1K. Now the equation may be changed with

$$\frac{dY}{dt} = [\Lambda e^Y (\Lambda^2 + e^{2Y})^{-0.5}] \cdot \left[\frac{1}{T_A} \right] \cdot \left[\left(\frac{A_{top}}{C_p \rho V} \right) (Q - \rho WL) + (S/V)(T_s - T) \right] \quad (4.50)$$

Λ is the temperature smoothing factor. This equation is corresponding to the original in the limit $\Lambda \rightarrow \infty$. For finite Λ , the shift from boiling to non-boiling is smoothed appropriately for numerical computation without disturbing the outcome. Therefore, the equation (4.50) is a basic temperature equation of the model. In practice, to avoid numerical problems, Λ needs to

4 Liquid hydrogen spreading and evaporation

be selected small enough that the problem's stiffness to be suitably mitigated but large enough, so it does not smooth the solution excessively [37]. A value of about 1000 will satisfy both cases.

4.2.7 Vapor transport

The equation (4.50) couples to the spreading equations already discussed in section 4.2.5, and it also involves an atmospheric mass transport model for $W(T)$ and heat flux for $Q(T,t)$. Brighton [38, 39] improved Sutton's model [40] for $W(T)$, and the result of their work is as below.

$$W(T) = \left[\frac{Mp_v}{RT} \right] \left[\frac{u_*}{\rho} \right] \left[\frac{k_v}{\sigma_s} \right] [1 + n] G(e^\lambda) x^{-1} \ln((1-x)^{-1}) \quad (4.51)$$

Where:

M is the molecular weight of the liquid;

R is the universal gas constant;

$p_v(T)$ is the vapor pressure above the pool;

u_* is the atmospheric friction velocity above the pool;

k_v is the von Karman constant (equal to 0.4);

σ_s is turbulent Schmidt number (equal to 0.85);

n is the wind profile index;

x is the mole fraction of vapor above the pool surface;

The argument λ in $G(e^\lambda)$ function which will be discussed next is defined as below

$$\lambda = n^{-1} + 2 + \ln(2(1+n)^2) - \gamma + \frac{k_v}{\sigma_s} (1+n) \cdot \beta(Sc) \quad (4.52)$$

Where γ is Euler's constant taken to be 0.577, and Sc is the laminar Schmidt number of the air's vapor. The function of $\beta(Sc)$ is given by

$$\beta(Sc) = 7.3 R_{e_0}^{1/4} Sc^{1/2} - 5\sigma_s \quad (4.53)$$

Or

4 Liquid hydrogen spreading and evaporation

$$\beta(Sc) = (3.85 Sc^{1/3} - 1.3)^2 + \left[\frac{k_v}{\sigma_s} \right] \ln(0.13Sc) \quad (4.54)$$

Depending on the pool, whether it is aerodynamically rough or not, R_{e_0} is the roughness Reynolds number can be defined as below.

$$R_{e_0} = \frac{u_* z_0}{\nu} \quad (4.55)$$

Where z_0 is the roughness length. The function $G(e^\lambda)$ can be determined by the equation below.

$$G(e^\lambda) = \frac{1}{2} - \left[\frac{g_0}{\pi} \right] \arctan\left(\frac{\lambda}{\pi}\right) + \left(\frac{g_1}{\lambda^2 + \pi^2} \right) + \frac{g_2 \lambda}{(\lambda^2 + \pi^2)^2} + \frac{g_3 (\lambda^2 - \frac{\pi^2}{3})}{(\lambda^2 + \pi^2)^3} \quad (4.56)$$

$$g_0 = 1$$

$$g_1 = 1 - \Upsilon = 0.42278$$

$$g_2 = 1 + (1 - \Upsilon)^2 + \frac{\pi^2}{6} = 2.824$$

$$g_3 = (1 - \Upsilon)^3 + \left(3 + \frac{\pi^2}{2} \right) (1 - \Upsilon) - 2\zeta(3) = 1.024$$

Where ζ is the Riemann zeta function.

The vapor pressure p_v can be obtained by Antoine correlation as follow

$$x = \exp\left(\frac{B(T - T_B)}{(T + C)(T_B + C)}\right) \quad (4.57)$$

Thus, the p_v can be defined as

$$p_v = x \cdot p_a \quad (4.58)$$

4 Liquid hydrogen spreading and evaporation

Where p_a is atmospheric pressure. B and C are Antoine coefficients, and in support of the boiling point, the Antoine coefficient A has been removed.

The W(T) model is in contact with removing vapor from the surface. The atmosphere state is specified in terms of friction velocity u_* and wind speed index n. The wind speed index has been taken from Brighton's approximation of the wind profile by a power law. The index n which most significant estimates of logarithmic profile over the pool is determined as

$$\frac{1}{n} = N \left[\frac{A^{0.5}}{z_0} \right] \left[\frac{k_v^2}{\sigma_s} \right] e^{-(1+\gamma)} \quad (4.59)$$

Where N (X) is a function given implicitly by

$$N e^N = X \quad (4.60)$$

Where X can be defined as

$$X = N \left(\frac{k_v^2 A^{0.5}}{z_{0,a}} \right) \quad (4.61)$$

It should be noted that n weakly depends on the pool size.

The friction velocity u_* depends on the roughness of the pool and surrounding. Thus, If the pool roughness length z_0 is different from that, z_{0a} of the surrounding, u_* above the pool will be different from u_{*a} , well upwind of the pool. In this case, an inner boundary layer develops over the pool and can be determined as

$$u_* = u_{*a} \left\{ \frac{X}{\left[X + \ln\left(\frac{z_{0a}}{z_0}\right) \right]} \right\} \quad (4.62)$$

According to the X term in equation (4.61), which is a function of area, the friction velocity changes weakly with the pool size for most situations. The ambient friction velocity can be defined from 10-meters wind speed, U_{10} , and the roughness length z_{0a} by assuming a neutral boundary layer. Hence

4 Liquid hydrogen spreading and evaporation

$$u_{*a} = \left\{ \frac{k_v U_{10}}{\left[\ln\left(\frac{z_{10}}{z_{0a}}\right) \right]} \right\} \quad (4.63)$$

with $z_{10} = 10\text{m}$ (characterized in order to maintain noticeable dimensionless stability). On The Other Hand, for the smooth surface assumption the z_{0a} can be found by taking

$$Re_{0a} = \frac{u_{*a} z_{0a}}{v_a} = 0.13 \quad (4.64)$$

So,

$$u_{*a} = \left[\frac{0.13 v_a}{z_{10}} \right] N\left(\frac{k_v U_{10} z_{10}}{0.13 v_a}\right) \quad (4.65)$$

And

$$z_{0a} = \left[\frac{z_{10}}{N\left(\frac{k_v U_{10} z_{10}}{0.13 v_a}\right)} \right] \quad (4.66)$$

Correspondingly for equation (4.62) with the smooth surface assumption, it can solve by considering $u_{*a} z_{0a} = 0.13 v_a$ and in terms of the function N defined above.

4.2.8 Solutions to GASP model

In the GASP model, the vaporization rate is anticipated as a function of wind conditions, pool temperature, pool size, properties of the examined liquid, and the environment's thermal properties. The complexity was separated into two cases: vaporization because of the pool boiling process and vaporization caused by evaporation. In the pool boiling process, the vaporization rate is entirely dominated by the heat flux into the pool, while in the latter atmospheric flow over the pool surface controlled the vaporization rate [4, 36]. The equations are not simple to solve numerically due to the enormous range of time scale created by the multiple physical phenomena [37]. Besides, the model is not capable of modeling boiling pools in no wind situation [2]. Thus, a simplified GASP model is required to solve the model.

4 Liquid hydrogen spreading and evaporation

4.2.9 Simplified GASP model

Nguyen et al. [4] simplified the model for indoor spills of cryogenic liquids on solid ground (since the conduction heat is dominant and the gravity drives the pool to spread [5], it can also be applied for outdoor spills). Nguyen's study assumes that wind is not existing, and vaporization is governed by the pool boiling process powered by conductive heat flux from the ground. Furthermore, the pool is assumed to be a uniform temperature equal to its boiling point. Consequently, the equation (4.48) for the pool temperature could be eliminated, and the upper limit for vaporization is achieved since heat is not needed to boost the pool temperature to its boiling point. Thus, the complicated equations are substituted by simpler ones. So, the vaporization velocity equation (4.51) may be simplified as follow.

$$W = \frac{T_a - T_B}{\rho h_{fg}} \left[\frac{1}{\pi r^2} \frac{k}{(\pi \alpha)^{0.5}} \int_0^{r(t)} \frac{2\pi r' dr'}{(t - t')^{0.5}} + h \right] \quad (4.67)$$

The heat transfer coefficient h is evaluated to be equal to $3.81 \text{ W}/(\text{m}^2 \cdot \text{K})$ [4].

On the other hand, the vaporization velocity can be obtained as a function of spill rate and time empirically. In Nguyen et al. study [1], this empirical equation is achieved as below.

$$W_{empirical} = 0.021 \left(\frac{S}{\rho} \right)^{0.296} t^{-0.478} \quad (4.68)$$

Where $W_{empirical}$ is empirical vaporization velocity, S is mass spill rate, and t is time (it is only applicable for spills on concrete).

4.2.10 Results and discussions (GASP)

In this step, due to the lack of experimental data for liquid hydrogen, the LNG and liquid nitrogen spreading and evaporation are modeled for release on land with GASP code. If experimental data is available, the model is validated against experimental data. The LNG and liquid nitrogen spill results compared with liquid hydrogen behavior with the same amount of release.

4 Liquid hydrogen spreading and evaporation

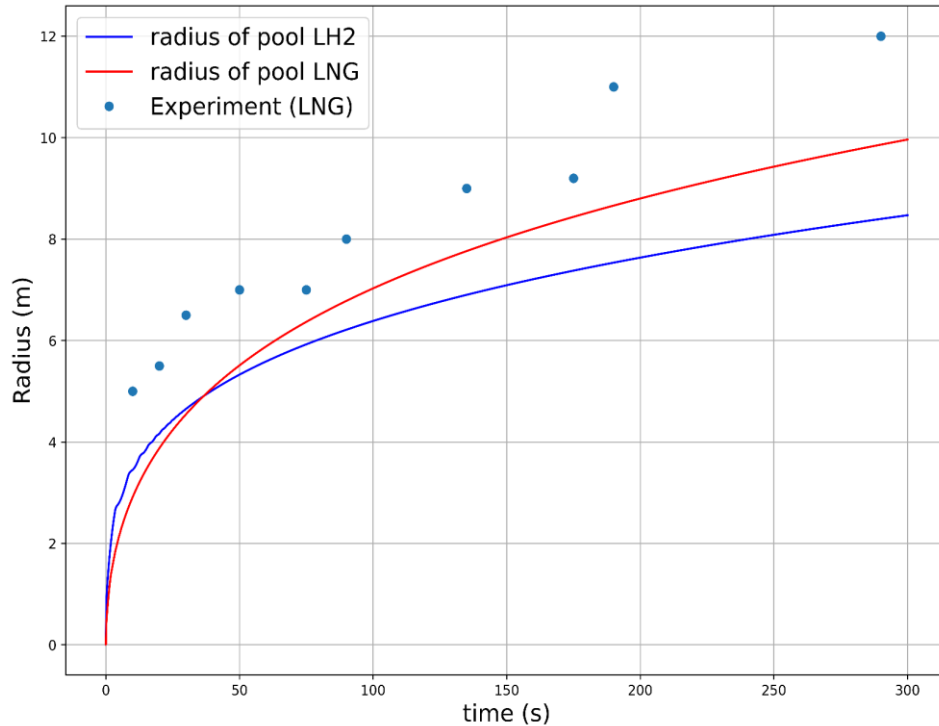


Figure 4.19 The spreading pool's radius versus time (Concrete).

4.2.11 Continuous Spill (GASP)

As mentioned in section 4.1.10, two continuous spills of 14 tons/h and 17 tons/h were tested on concrete and soil in Moorhouse and Carpenter's work [35]. As shown in Figure 4.19, the GASP model is in convincingly good agreement with experimental data for concrete as surface, while for the soil, as shown in Figure 4.20, the result is in better agreement with the model.

There is no experimental data for vaporization mass and pool mass or volume for Moorhouse and Carpenter's work to the extent of our knowledge. Nevertheless, in this work, the vaporization mass and pool mass of the same amount has been plotted in Figure 4.21 and Figure 4.22. As seen from the figures, the liquid hydrogen vaporization is more vigorous than LNG as expected in both cases, i.e., concrete and soil. This is owing to lower boiling temperature and density of liquid hydrogen than LNG, as mentioned before. The significant difference between the pool mass of liquid hydrogen and LNG is that LNG is much heavier per volume, i.e., higher density than liquid hydrogen, and liquid hydrogen vaporization is much faster than LNG. It can be seen from Figure 4.21 and Figure 4.22 that nearly the entire pool of hydrogen is vaporized, the same result as obtained by the B&S model. Overall, the model's response is acceptable due to the characteristic of hydrogen, and it can be said that the result is realistic.

4 Liquid hydrogen spreading and evaporation

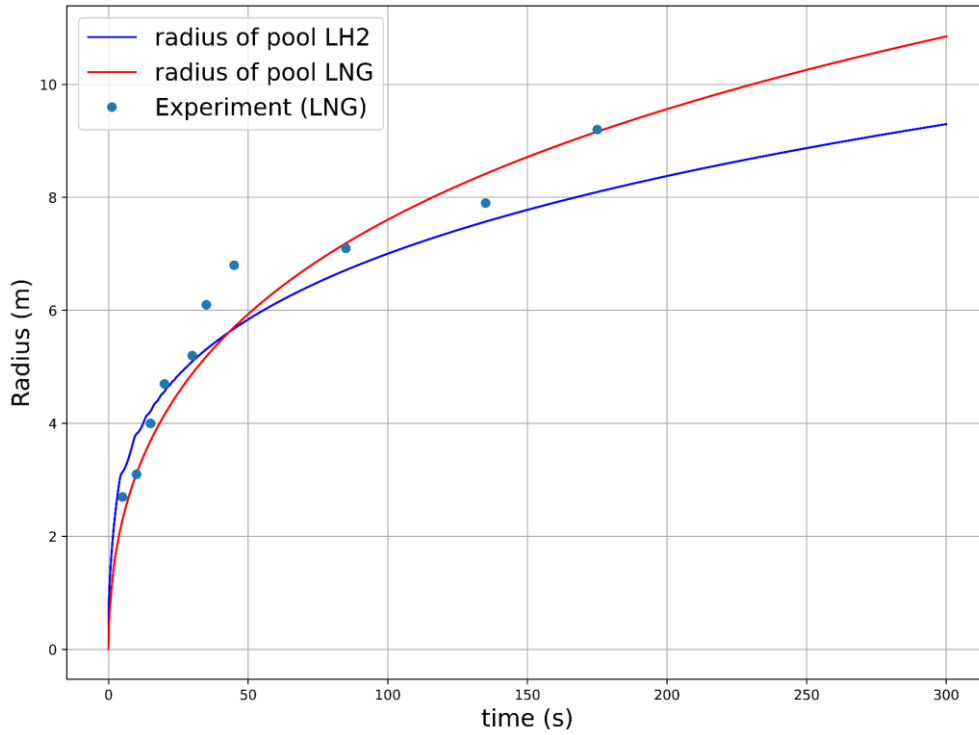


Figure 4.20 The spreading pool's radius versus time (Soil).

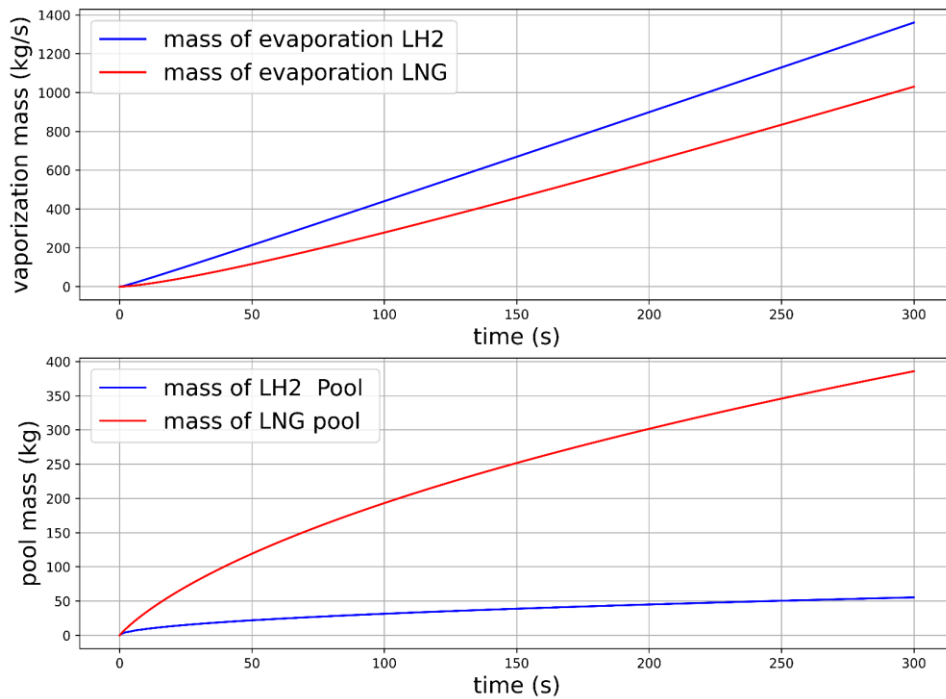


Figure 4.21 The vaporization and pool mass (soil).

4 Liquid hydrogen spreading and evaporation

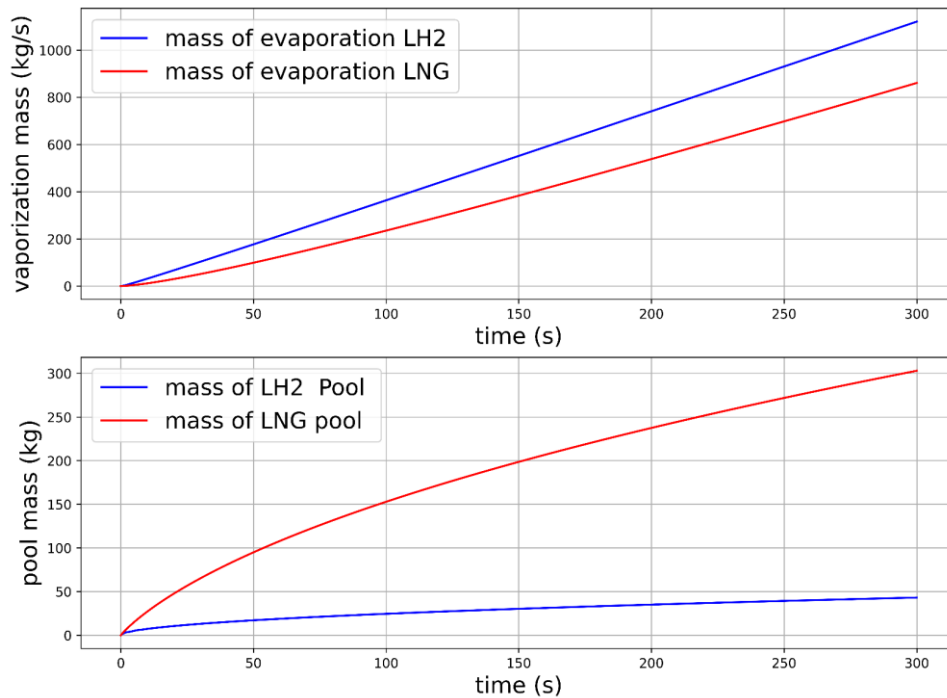


Figure 4.22 The vaporization and pool mass (concrete).

4.2.12 Continuous spill, bounded

In this section, although the experimental data is not available for bounded area spills, the same spill rate on soil and concrete has been modeled as Moorhouse and Carpenter's work with the assumption that the area is bounded at $r = 5\text{m}$. As shown in Figure 4.23, the pool stops spreading at $r = 5\text{m}$. Thus, the spill's effect on confined space on vaporization can be seen in Figure 4.24 and compare with Figure 4.22. As evident, the vaporization rate is smoother in confined space, and as mentioned before, the result is realistic due to less contact area with the warmer ground, and as a consequence of that, the pool mass tends to maintain in confined space in the unbounded area. The same result is also obtained for the higher spill rate and lower spill rate in the B&S model.

As illustrated in Figure 4.25 and Figure 4.26 same behavior has been achieved for the spill on the soil. The less contact area with the ground is the main reason mass vaporization becomes smoother than an unbounded area since the conduction heat flux is dominant. As the pool spreads on the unbounded area, the pool connects with the fresh ground that is in ambient temperature. Overall, it can be concluded that the GASP model is more accurate than the B&S model by comparing Figure 4.15 and Figure 4.16 with Figure 4.19 and Figure 4.20.

The comparison between soil and concrete spills could not give beneficial results because of different spill rates. Thus, in the next, more data for validation will be investigated.

4 Liquid hydrogen spreading and evaporation

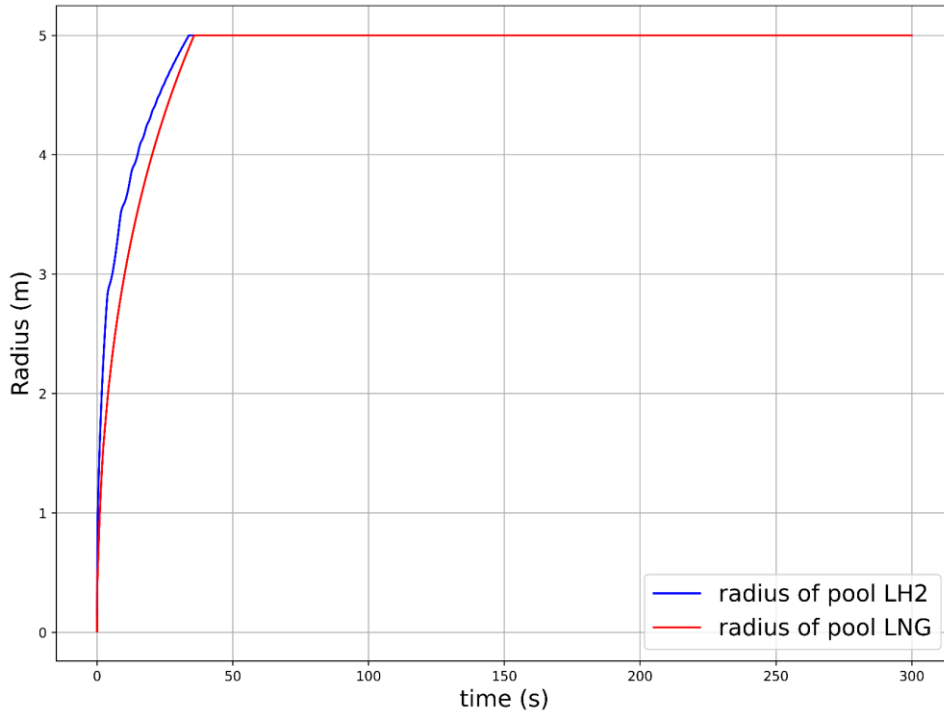


Figure 4.23 Spreading pool in confined space bounded at $r = 5\text{m}$ (Concrete).

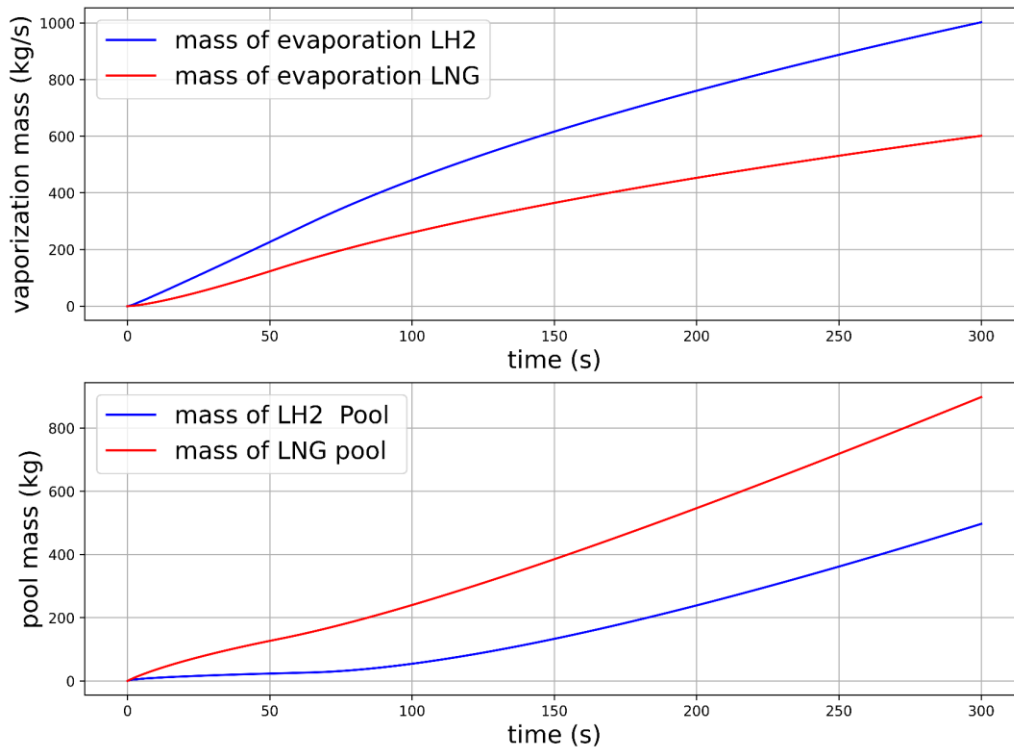


Figure 4.24 The vaporization and pool mass on confined space bounded at $r=5\text{m}$ (concrete).

4 Liquid hydrogen spreading and evaporation

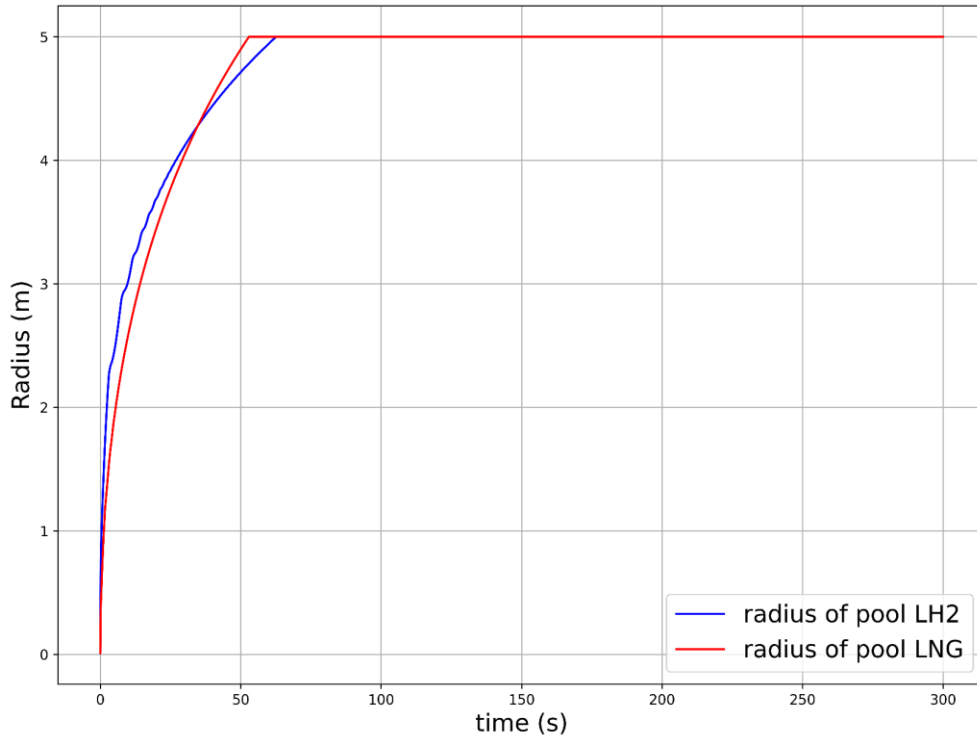


Figure 4.25 Spreading pool in confined space bounded at $r = 5\text{ m}$ (Soil).

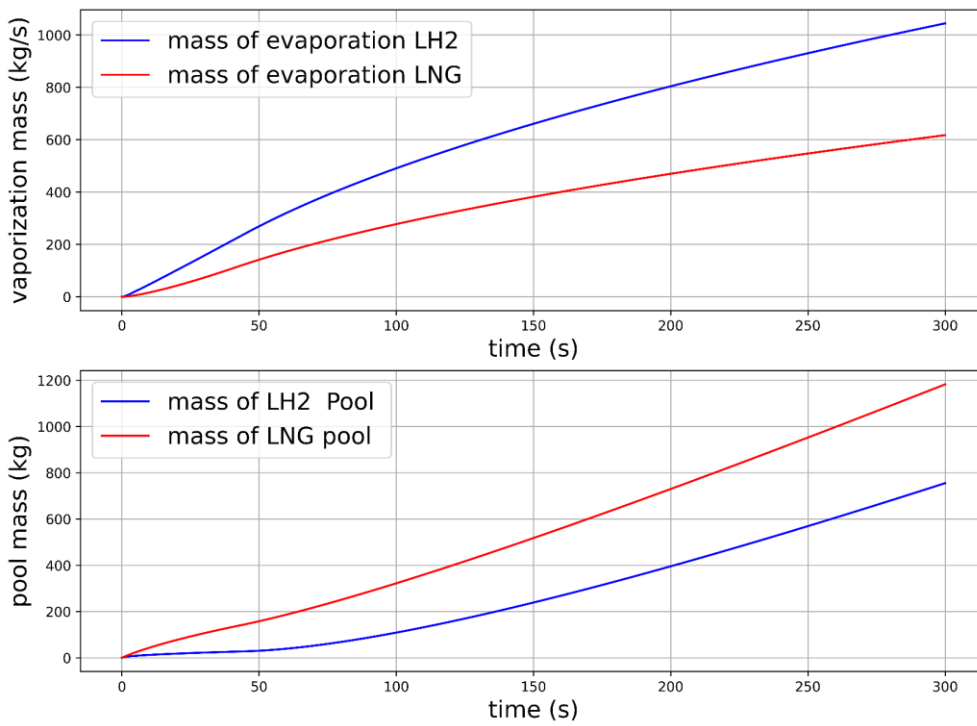


Figure 4.26 The vaporization and pool mass on confined space bounded at $r=5\text{ m}$ (Soil).

4.2.13 Lower spill rates

In this work, cases 1 and 7 of Table 4.2 in section 4.1.11 are selected for the simulation. The experimental data are taken from the work of Nguyen et al. [1]. The behavior of liquid nitrogen is compared with LNG and liquid hydrogen. Figure 4.27 and Figure 4.28 show that the GASP model is in good agreement with experimental data. The pool mass of liquid hydrogen is significantly less than LNG and liquid nitrogen pool mass, as illustrated in Figure 4.27, implying that most of the amount of spilled liquid hydrogen vaporized vigorously. Figure 4.28 indicates the vaporization velocity, i.e., the vaporized volume per unit area, versus time. The vaporization mass diagram is not plotted due to the availability of experimental data of vaporization velocity. As demonstrated in Figure 4.28, liquid hydrogen's vaporization velocity is considerably more than two other cryogenic liquids. The LNG vaporization velocity is slightly more than liquid nitrogen. It can be concluded that the vaporization velocity is highly dependent on the density of the liquids.

Figure 4.29 and Figure 4.30 illustrate the pool radius, pool mass, and vaporization velocity for case 7. As shown in the figures, the model is roughly in better agreement with the experimental data than case 1. Thus, it can be concluded that the higher accuracy can be obtained by the model for the higher spill rates.

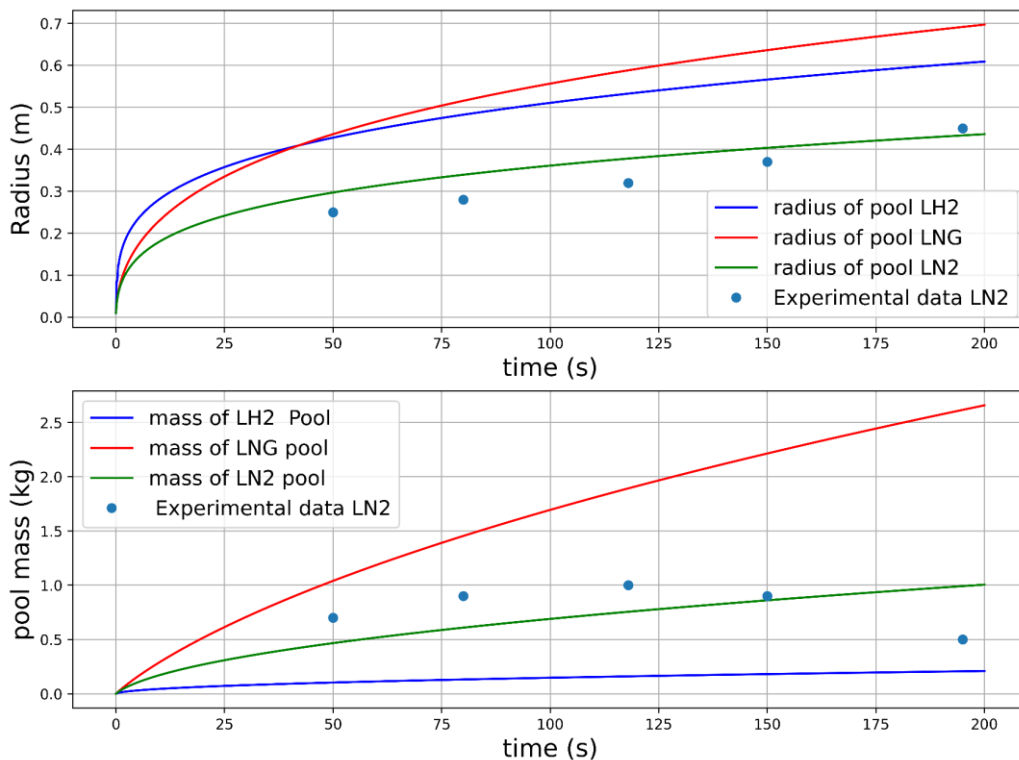


Figure 4.27 Predicted spreading pool radius and mass of LN₂ and LH₂ and LNG with time versus experimental data of LN₂ (case 1).

4 Liquid hydrogen spreading and evaporation

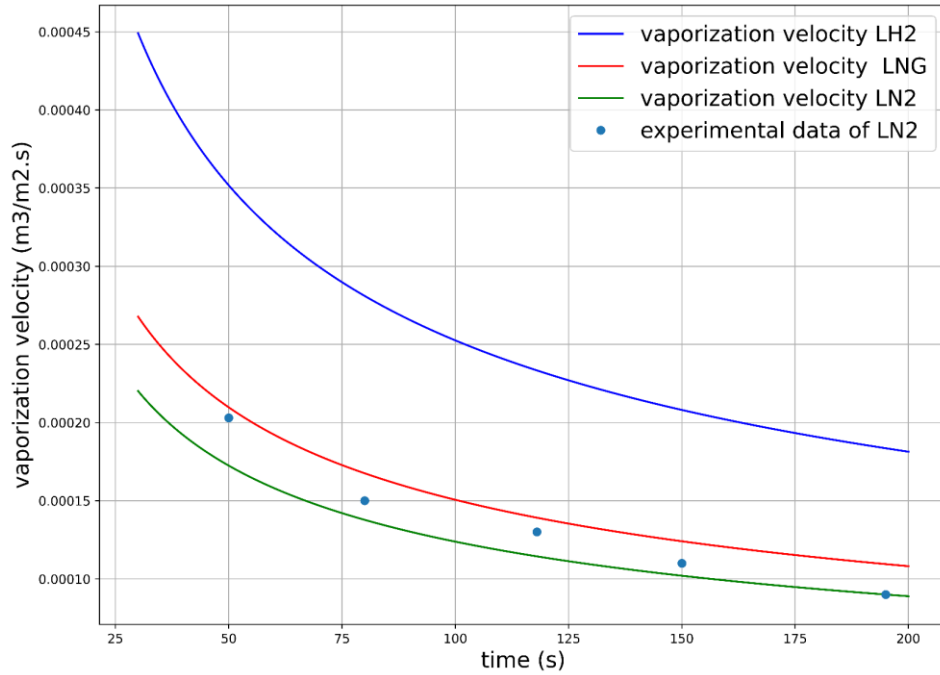


Figure 4.28 Predicted vaporization velocity of LN_2 and LH_2 and LNG with time versus experimental data of LN_2 (case 1).

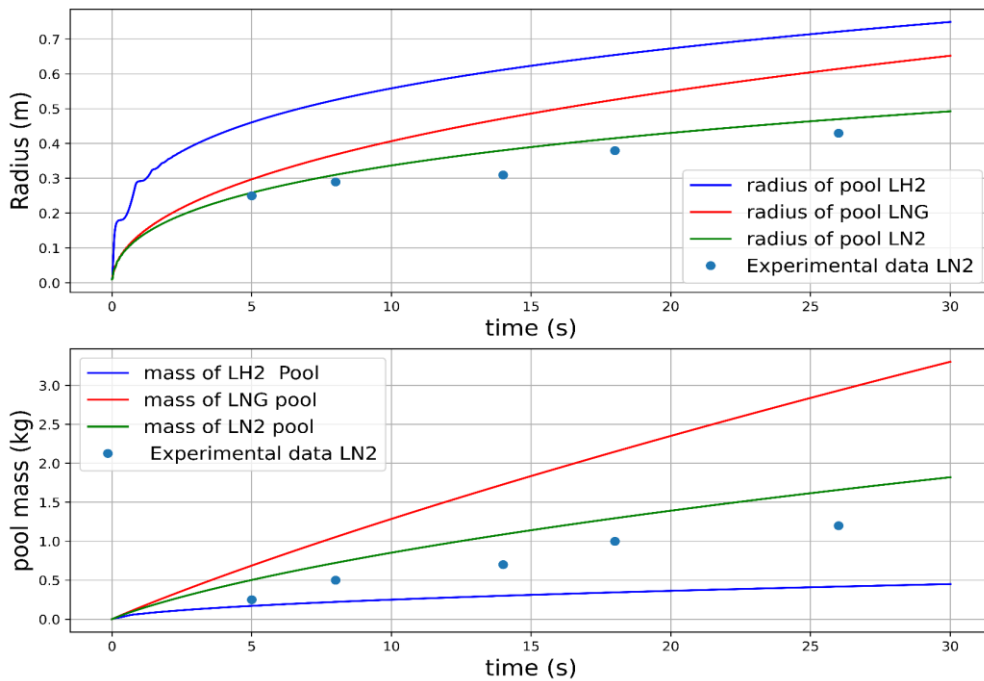


Figure 4.29 Predicted spreading pool radius and mass of LN_2 and LH_2 and LNG with time versus experimental data of LN_2 (case 7)(GASP).

4 Liquid hydrogen spreading and evaporation

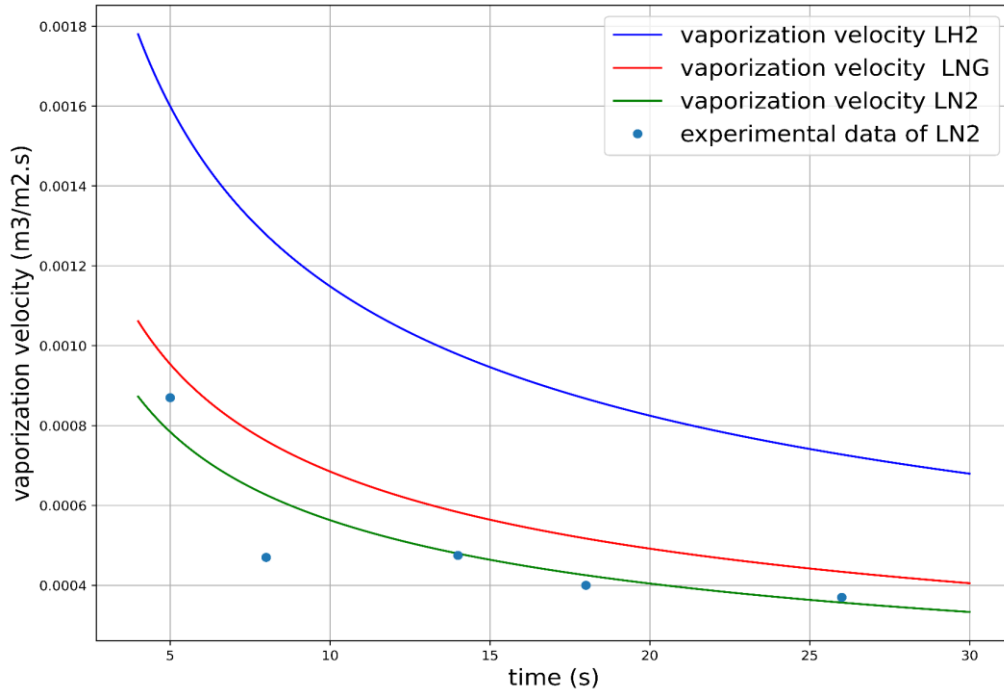


Figure 4.30 Predicted vaporization velocity of LN₂ and LH₂ and LNG with time versus experimental data of LN₂ (case 7).

4.3 Constant Froude Number (CFN) model.

The Constant Froude Number is a modified version of the Briscoe and Shaw model. As mentioned in section 4.1, the relation between gravity and front resistance makes pool to spread. In this model, the symbol ε is mentioned as Froude number unlike B&S model. The only difference of CFN with B&S is driving the vaporization velocity from the pool volume equation. Thus, the algebraic equation (4.2) will be changed to a differential equation as below.

$$\frac{dV}{dt} = \frac{S}{\rho} - W\pi r^2 \quad (4.69)$$

Where W is the vaporization velocity which can be evaluated by equation (4.52) or (4.67), and for releases on concrete equation (4.68) also can be used.

4 Liquid hydrogen spreading and evaporation

4.3.1 Result

As mentioned in section 4.1.11, Cases 1 and 7 of Table 4.2 are selected for the simulation with CFN code. As illustrated in Figure 4.31 and Figure 4.33, roughly the same behavior as the B&S model of liquified gases is achieved for radius and pool mass by the CFN model. As revealed in section 4.1.11, the B&S model was not capable of evaluating the vaporization velocity. By modifying the model, Figure 4.32 and Figure 4.34 have been plotted to indicate the vaporization velocity. Overall, the model is in slightly better agreement with experimental data than the B&S model.

It is worth mentioning that the Froude number for these two cases, same as the B&S model, is approximately 0.003 and 0.06 for cases 1 and 7, respectively. The model is named Constant Froude Number due to being constant for the different spill rates on water. As discussed in Briscoe and Shaw model subchapter 4.1.9, the model must be modified by defining a minimum depth H_{\min} [4] and obtaining the Froude empirically [34]. However, a roughly complete discussion is provided in Chapter 6 of this work for using these models.

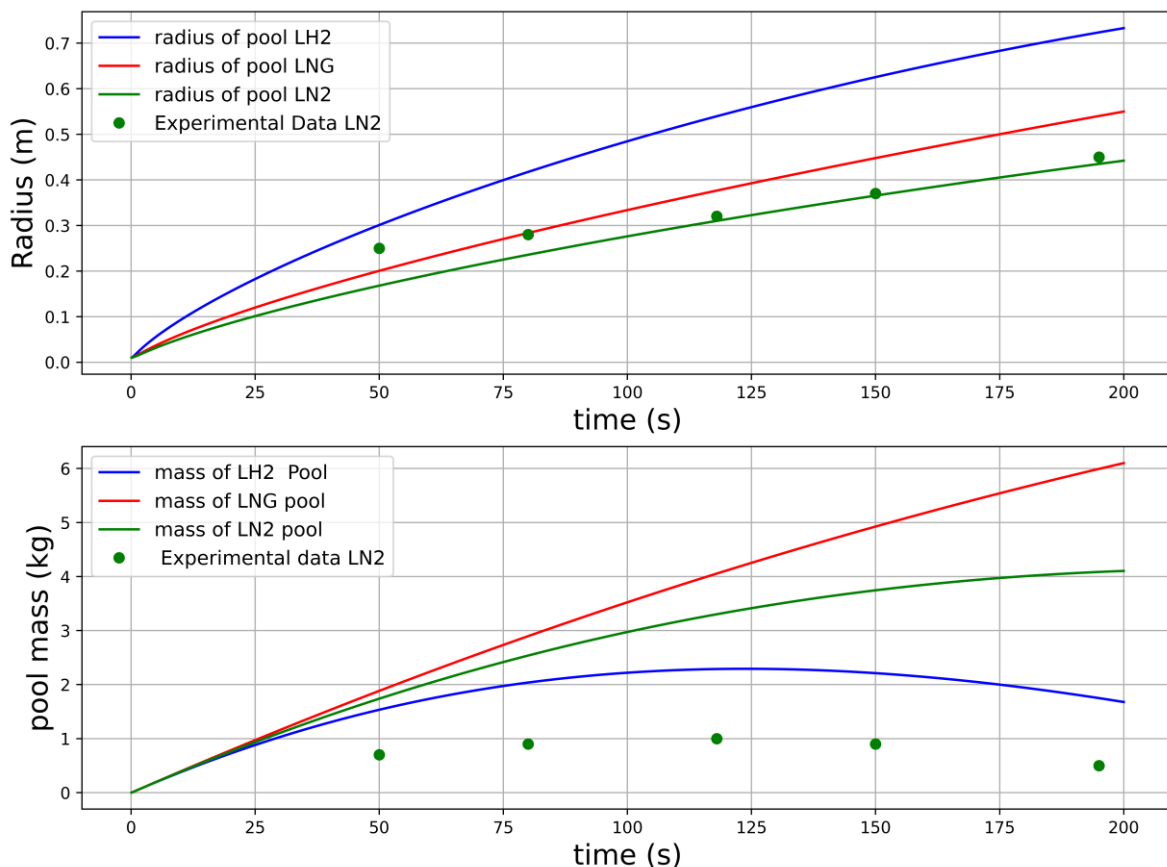


Figure 4.31 Predicted spreading pool radius and mass of LN_2 and LH_2 and LNG with time versus experimental data of LN_2 (case 1)(CFN).

4 Liquid hydrogen spreading and evaporation

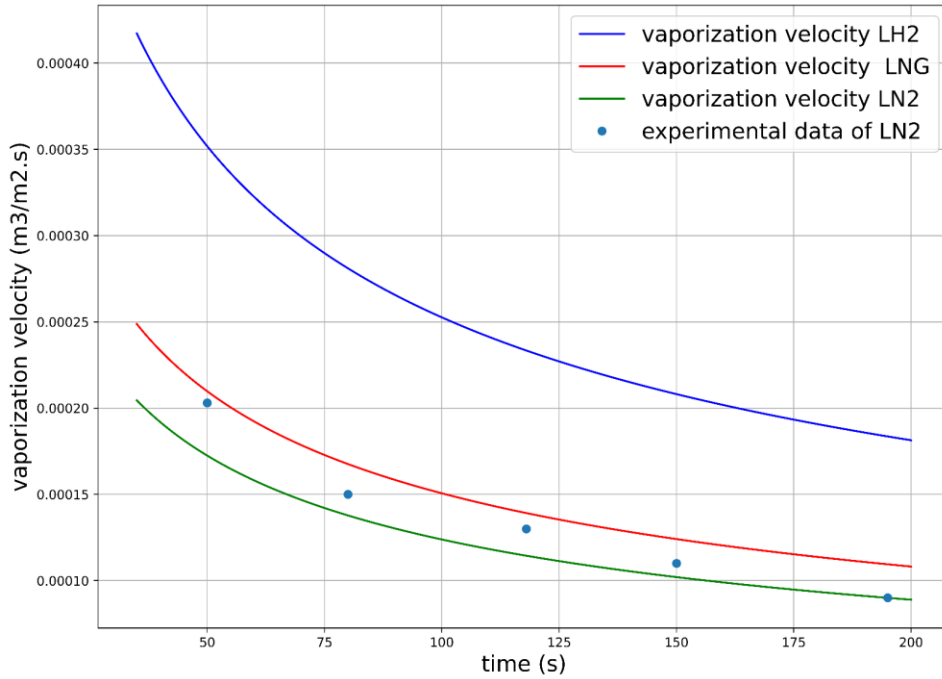


Figure 4.32 Predicted vaporization velocity of LN₂ and LH₂ and LNG with time versus experimental data of LN₂ (case 1)(CFN).

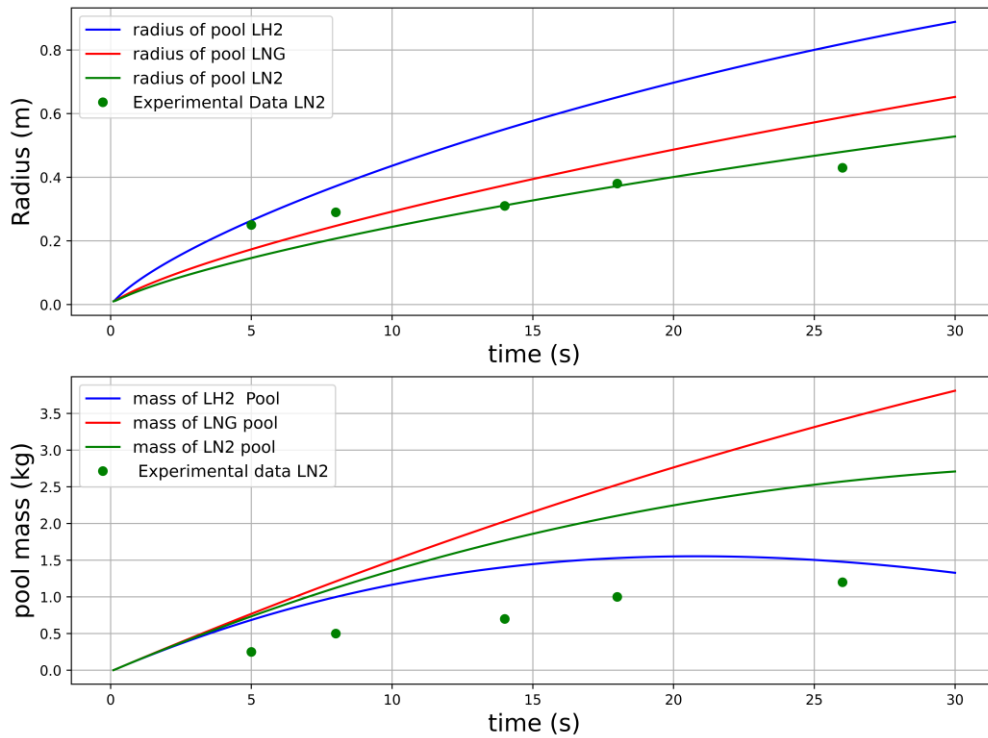


Figure 4.33 Predicted spreading pool radius and mass of LN₂ and LH₂ and LNG with time versus experimental data of LN₂ (case 7)(CFN).

4 Liquid hydrogen spreading and evaporation

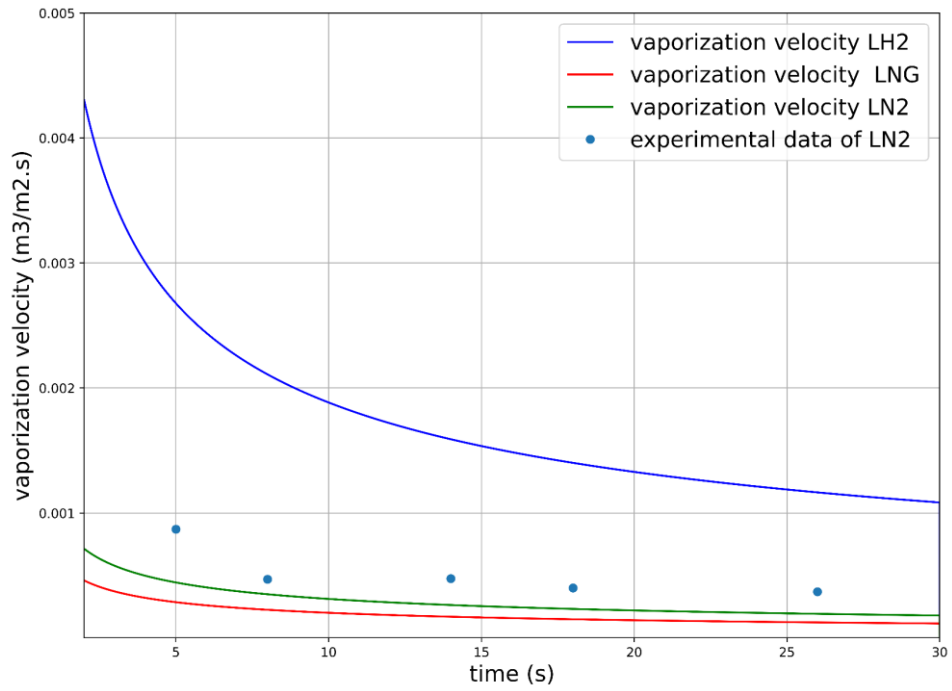


Figure 4.34 Predicted vaporization velocity of LN_2 and LH_2 and LNG with time versus experimental data of LN_2 (case 1)(CFN).

5 Liquid hydrogen spill experiments

In chapter 4, the liquid hydrogen's spreading pool radius, pool mass, mass vaporization, and vaporization velocity have been modeled and compared with liquified natural gas (LNG) and liquid nitrogen behavior. Due to the lack of experimental data for the liquid hydrogen spills, the models were validated against LNG and liquid nitrogen experimental measurement data. The models were in good agreement with the measurement data of experiments. In this chapter, the available experimental data for liquid hydrogen will be reviewed, and the models will only be validated against the available liquid hydrogen's experimental data.

5.1 Literature review

Experiments on liquid hydrogen spills have only contained qualitative observations and are limited in validating models [2]. A summary of several hydrogen spill experiments can be discovered in Venetsanos et al. work [41]. The most commonly applied experimental datasets for validating liquid hydrogen spills are the BAM [42] and NASA [43] experiments. Both involve substantial assumptions and assessments when modeling the experiments owing to uncertainties in the source release processes. The hydrogens spill experiments such as Takeno et al. [44] and Royle and Willoughby [45] are appropriate for validating the mass vaporization and spreading pool radius model, respectively. The newest hydrogen spill experiments are carried out in an indoor and outdoor area by the Norwegian defense research establishment [46] and [47], which both need extraction of data for model validation. These are available hydrogen spill experiments.

5.2 Experiment analysis

Test 6 of Royle and Willoughby's work is the most appropriate experimental data for validation since the discharge nozzle is adjusted vertically downwards 10 mm above the surface [2]. This structure is most expected to be approximated by a radial spread as presumed by the models. The measurement probe structure is demonstrated in Figure 5.1. There were 24 ground-level thermocouples installed in a horizontal line spaced 100 mm separately, starting at a distance of 500 mm from the source, i.e., from 0.5 m to 2.8 m. The tips of the thermocouples were in contact with the surface of the concrete substrate. There were 3 thermocouples inserted in the concrete at depths of 10 mm, 20 mm, and 30 mm to determine the substrate temperature. After All, there were 30 concentration sensors positioned at 5 points in a horizontal line in line with the wind direction in vertical arrays of 6 [2], as shown in Table 5.1.

Table 5.1 Locations of 30 concentration probes [2, 45].

Horizontal distance from release (m)	1.5, 3.0, 4.5, 6.0, 7.5
Vertical locations at each horizontal location (m)	0.25, 0.75, 1.25, 1.75, 2.25, 2.75

5 Liquid hydrogen spill experiments

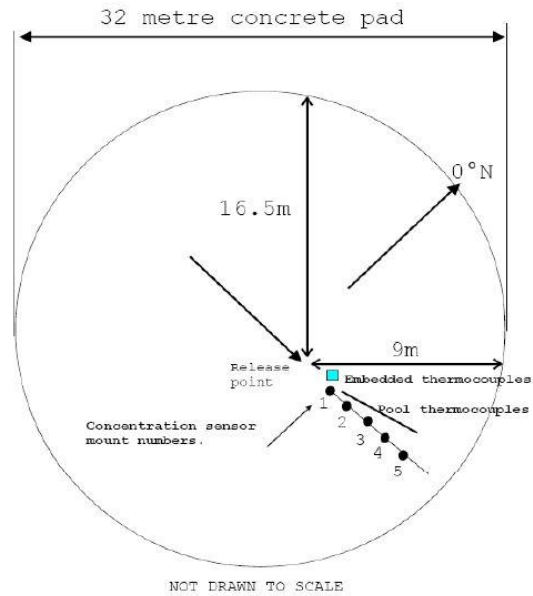


Figure 5.1 Probe layout used in experimental measurements of Test 6 [2, 45].

The spreading rate of the pool, i.e., the radius of the pool as a function of time, is a key parameter in validating the B&S, CFN, and GASP model. This was not directly evaluated throughout the experiments and, therefore, obtained from the ground-level probe data. It was assumed that if the probe temperature dropped below 30 K, then that probe was surrounded by the liquid pool (Take the boiling point of hydrogen equal to 20.4 K).

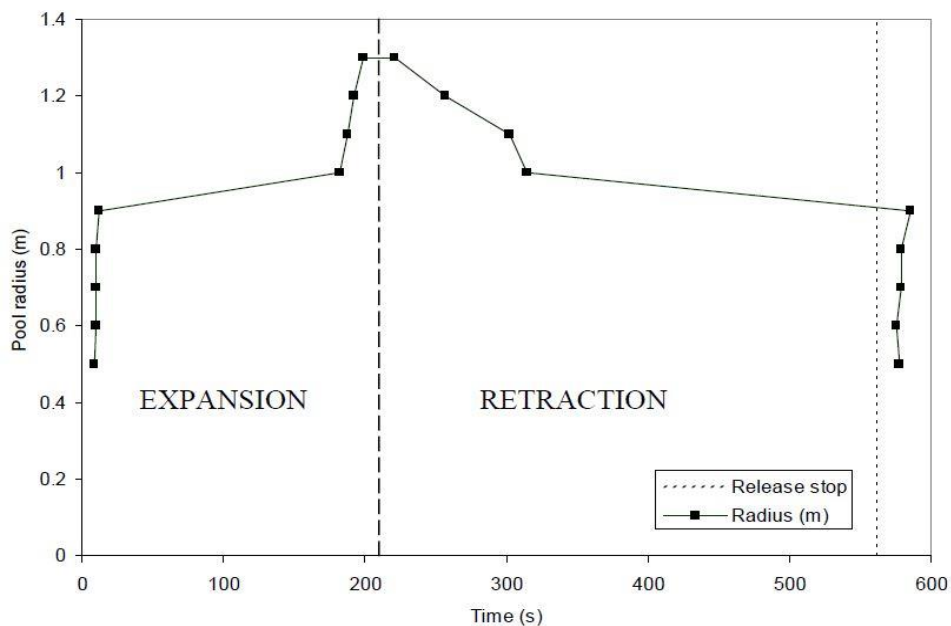


Figure 5.2 Radius of the pool extracted from experimental measurements showing expansion and retraction [2].

5 Liquid hydrogen spill experiments

In Batt's work [2], the pool's radius is extracted from Test 6, as shown in Figure 5.2. It can be observed from Figure 5.2 that for approximately 30s, the pool quickly expands and reach 0.9, and it takes about 150s that the pool spreads from 0.9 to 1.0 meters. After 180 seconds, the pool comes to 1.0 meters. It expands sharply again to reach 1.3 meters in just 20 seconds. It then doesn't extend and remains at this size for a short period before retracting. The pool radius then goes back approximately to 0.93 meters and decreases extremely slow to reach 0.88 m until the discharge stops. It is probable that the stop in spreading and then sudden further expansion is triggered by solid deposition on the ground, which abruptly breaks down, allowing more liquid spread [2]. Thus, the expansion and retraction of the pool should also be considered

5.3 Validation Of models against Royle and Willoughby's work experimental data

In this section, the models described in this work will validate against Royle and Willoughby's work experimental data for the radius of the spreading hydrogen pool.

5.3.1 B&S and CFN model

For validating the models of B&S and CFN, which are basically the same models, as illustrated in Table 5.2, the following nominal inputs have been selected for simulation. As written in Table 5.2, the value of Froude set to 0.0033 after try and error. It worth mentioning that the experimental data are read from Figure 5.2, from Batt's work, and are not the exact values. The values for the ground thermal properties are taken from Table 4.1 in chapter 4. The result will be discussed in the following, and since the result for evaporation rate and volume of the pool are not available, the model will be compared with the GASP model.

Table 5.2 Input into B&S and CFN model

Substrate	Concrete
Heat transfer	PTC
Release type	Continuous
Substance	Liquid hydrogen
Mass flow rate (kgs⁻¹)	0.0707
Duration (s)	561
Initial pool temperature (K)	20.4
Ambient temperature (K)	266
Froude Number	33×10^{-4}

5 Liquid hydrogen spill experiments

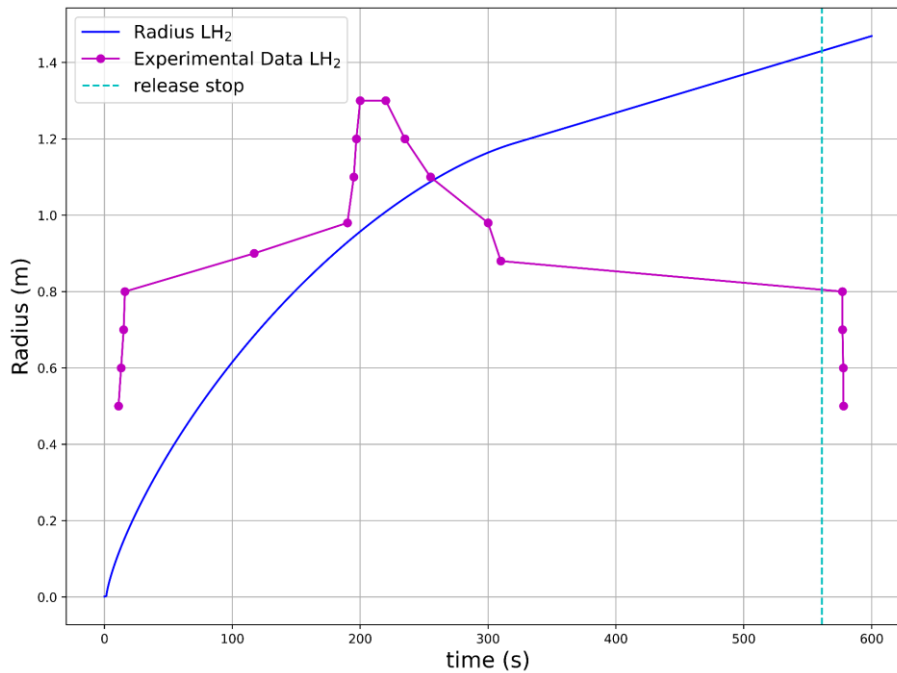


Figure 5.3 Radius of the pool extracted from experimental measurements versus prediction CFN model.

Since the evaporation time after stopping release is required to compare with the GASP model and the same structure of CFN and B&S models, the CFN model was used for modeling. It is owing to that the B&S model uses an algebraic equation for pool mass, and by stopping the release, it will tend to go to zero value instantaneously, while the CFN model uses a differential equation for modeling the pool mass and will decrease slightly with time.

As illustrated in Figure 5.3, the prediction of the models for spreading pool's radius is roughly in good agreement with the measurement data of the experiment for a period of approximately 220s. The pool retraction begins after 220s, and the model's prediction has a different tendency from the experimental data. The pool in the experiment starts to evaporate, and the pool's length starts to drop while the models cannot predict this shift in behavior. The model predicts that the pool continues to spread and reach nearly 1.4m after 561 seconds, while the maximum radius that the pool in the experiment reaches is 1.3m at 200 seconds, which should be taken into consideration because of safety matters.

Figure 5.4 demonstrates the mass vaporization and pool's mass of liquid hydrogen. Since the data for mass vaporization and pool's mass are not available, the obtained results by the model will be kept and compared with the original GASP model result in the following. As it is evident in Figure 5.4, the model predicts that the pool mass will evaporate entirely at approximately 41 seconds after release stops, and the mean vaporization rate is about $0.065 \text{ (kgs}^{-1}\text{)}$.

5 Liquid hydrogen spill experiments

Overall, the model results are appropriate and realistic. However, it will be discussed more next.

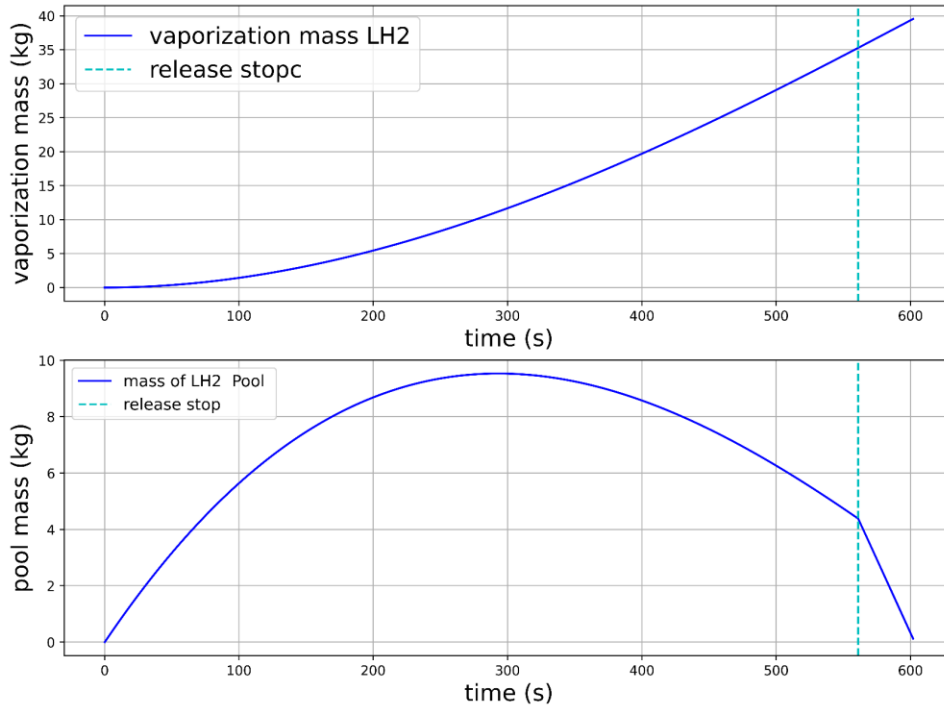


Figure 5.4 Prediction of mass vaporization and pool volume by CFN model.

Table 5.3 inputs to GASP model

Substrate	Concrete
Heat transfer	PTC
Release type	Continuous
Substance	Liquid hydrogen
Mass flow rate (kgs⁻¹)	0.0707
Duration (s)	600
Initial pool temperature (K)	20.4
Ambient temperature (K)	266
Pool roughness (mm)	0.5
Puddle depth (mm)	0.9

5.3.2 GASP model

As illustrated in Table 5.3, the above nominal inputs have been selected for simulation for validating the GASP model against the experimental data. The pool roughness and puddle depth values are taken from Batt's work. Batt's work gave a formula for calculating the puddle depth and suggested specifying the puddle depth based on a correlation associated with the substrate and the volume of released liquid V_* (continuous or instantaneous). The formula has the form below.

$$\begin{aligned} h_p &= 0.001074 \times V_*^{0.3393} \quad (\text{flat surface}) \\ h_p &= 0.003041 \times V_*^{0.3393} \quad (\text{normal surface}) \end{aligned} \quad (4.70)$$

The values for the ground thermal properties are taken from Table 4.1 in chapter 4.

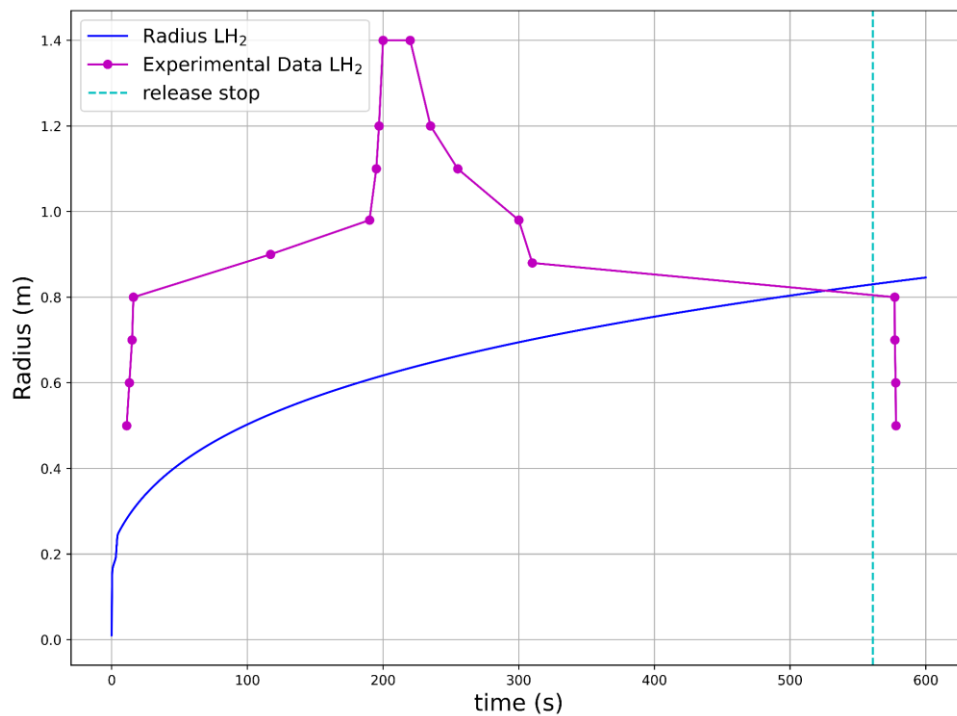


Figure 5.5 Radius of the pool extracted from experimental measurements versus prediction of GASP model.

5 Liquid hydrogen spill experiments

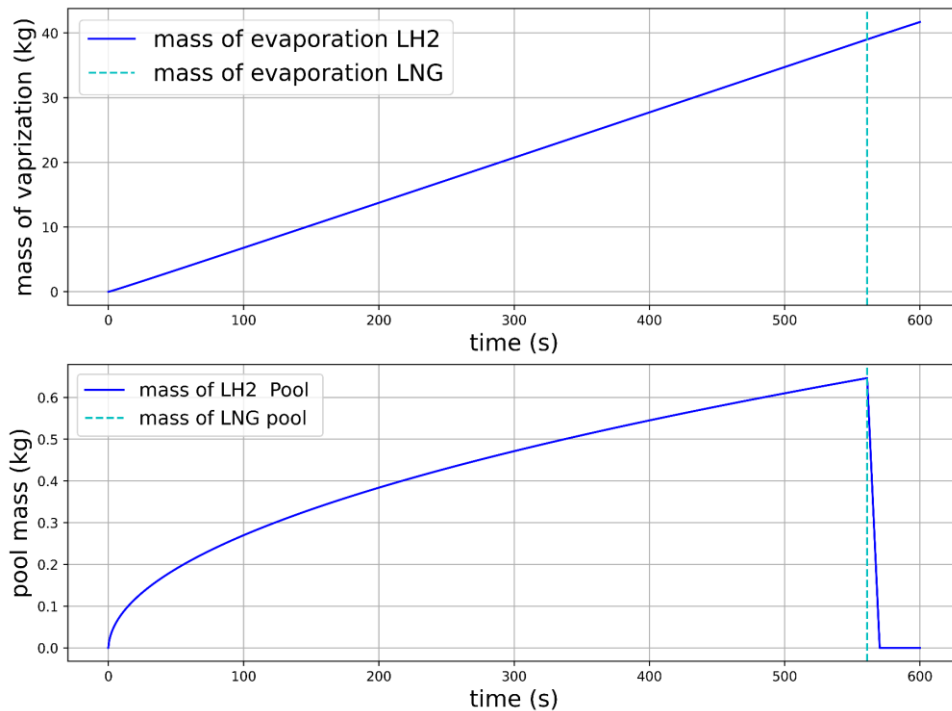


Figure 5.6 Prediction of mass vaporization and pool volume by GASP model.

A comparison of the experimental data against the estimation of the pool spreading is demonstrated in Figure 5.5. As examined previously, the experimental measurements reveal that the pool radius rises up and then retracts throughout the release. The GASP model outcome is of the appropriate order of magnitude and presents a comparably fast preliminary growth in radius, although not to the measured size by the experiment. This agreement is possibly perfect as the GASP model does not consider the condensation of the surrounding air and ice formation observed in the experiments [2]. The model calculates that the pool persists to grow at a decreasing rate but does not predict the expansion and retraction by the liquid hydrogen pool. The final pool size measured by GASP is approximately 0.85 m and illustrates excellent agreement with the experimental measurements, which reveal that the pool edge keeps between 0.8 and 0.9 m by the ending of release.

Figure 5.6 shows the mass vaporization and pool's mass of liquid hydrogen. Since the experimental data for mass vaporization and pool's mass are not accessible, the result obtained by the model will be kept and discussed further in the following. As shown in Figure 5.6, the model predicts that the pool mass will have evaporated in approximately 15 seconds after release stops, and The mean vaporization rate is nearly $0.07 \text{ (kgs}^{-1}\text{)}$.

Overall, these findings show that the GASP model provides an appropriate and realistic result for liquid hydrogen spills.

5 Liquid hydrogen spill experiments

Table 5.4 input into Original GASP model [2].

<i>Substrate</i>	Concrete
<i>Heat transfer</i>	Perfect thermal contact
<i>Puddle depth (mm)</i>	5.0
<i>Release type</i>	Continuous
<i>Pool roughness (m)</i>	0.5
<i>Substance</i>	Hydrogen
<i>Mass flow rate (kgs⁻¹)</i>	0.0707
<i>Aperture diameter (m)</i>	0.025
<i>Duration (s)</i>	561
<i>Initial pool temperature (K)</i>	20.4
<i>Ambient temperature (K)</i>	266
<i>Wind speed (ms⁻¹)</i>	3
<i>Surface roughness (mm)</i>	0.5

5.3.3 Original GASP model

The original GASP model is currently being used by Health and Safety Executive (HSE) for modeling pool spreading [2]. GASP model was established by ESR Technology [48] for modeling the spread of pools from hazardous spills and comprises processes applicable for modeling cryogenic liquids such as heat transfer and vaporization. It is one of HSE's approved models for this type of release [2]. Version 4.0.2 of the GASP model was utilized for all of the computations stated by Batt's work. As illustrated in Table 5.4, the nominal model parameter was selected to enter the original GASP model by Batt's work. As seen from the table, the original GASP model needs the wind speed for simulation, while the GASP model used by this work is simplified to simulate without wind speed.

Table 5.5 Results of the model's simulation for Test 6 of Royle and Willoughby's work.

Parameters \ Models	Original GASP [2]	Simplified GASP	B&S and CFN
Mean vaporization rate (kgs ⁻¹)	0.07	0.07	0.065
Final radius (m)	0.89	0.85	1.4
Release duration (s)	561	561	561
Time to evaporate after release stops (s)	15.2	15	41
Maximum pool mass (kg)	-	0.9	9

5 Liquid hydrogen spill experiments

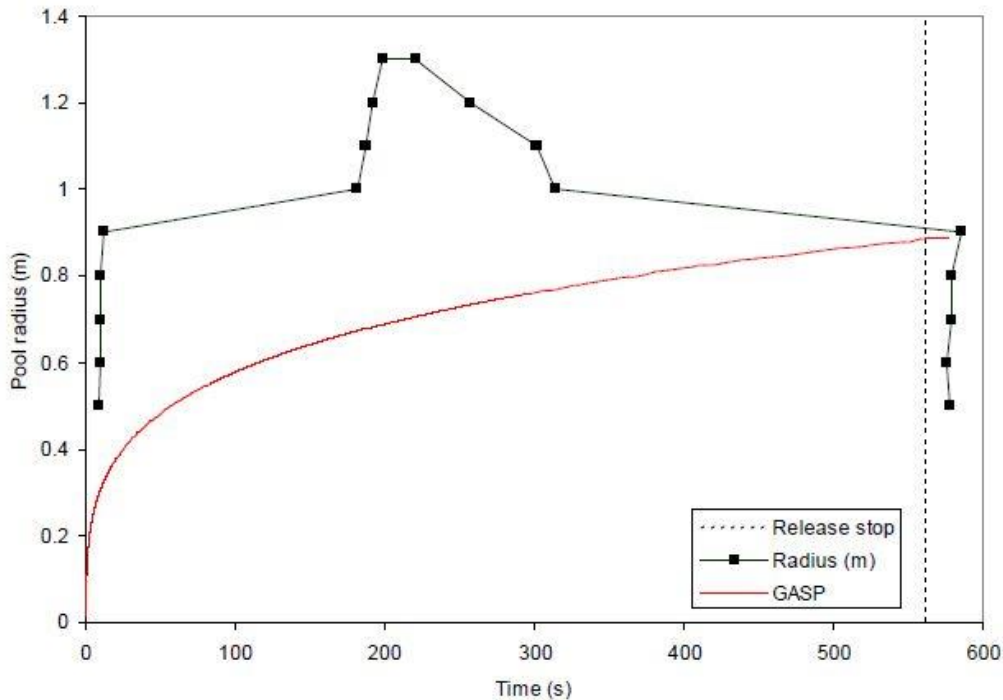


Figure 5.7 Radius of the pool extracted from experimental measurements versus prediction by Original GASP model [2].

Figure 5.7 illustrates the radius of the pool predicted by the original GASP model. As shown in Figure 5.5, the simplified GASP model used by this study gives more or less the same result for the pool's radius, while the B&S and CFN models demonstrate different behavior. The result obtained by the simplified GASP model is due to the domination of both conduction and gravity on spreading.

Table 5.5 provides information about the simulation result of the models. The experimental data calculates that the entire pool will have disappeared in nearly 17 s. The original GASP prediction of 15.2 s is in satisfactory agreement with this value. As it is evident in Table 5.5, the results from B&S and CFN models have roughly reasonable deviations from the Original GASP model, which HSE applies for the simulation of hazardous cryogenic spills. The simplified GASP model predicts nearly the same result as the original GASP model with minor deviations approximately equal to 0.03-0.04. It is worth mentioning that the B&S and CFN models predict the final radius of 1.4 m while it was observed in the experiment that the pool's radius approximately reaches 1.3 in a short period of 200s, which may be beneficial for safety reasons.

Overall, all the models which are investigated in this study show a good sense of prediction. So they can be utilized for liquid hydrogen spills.

5.4 Validation Of models against work of Takeno et al. experimental data

In chapter 4, the liquid hydrogen spreading and evaporation was examined, and its behavior was compared with the actions of LNG and liquid nitrogen. As studied in chapter 4, the experimental data of liquid nitrogen evaporation was used to validate the models. In this section, the validation of models will be investigated against the vaporization rates of non-spreading pools of liquid hydrogen using the data of Takeno et al. [44]. The mass vaporization and heat flux to liquid hydrogen and liquid oxygen pool was measured by Takeno et al. on concrete and sand.

Similar to the work of Batt, the results for the concretes case were used to provide data for validation in this work. The results calculated by the models applied in this work are compared to the result of the original GASP model used by Batt. The inputs utilized by the work of Batt are shown in Table 5.6. So, the same information was used in this study. Since the Original GASP model can predict spurious results if the wind speed is set to zero, and the experiment was in a deep glass vessel [2], Batt considered assessing the wind speed equal to 0.1 m/s^2 , while the simplified model of GASP doesn't need the wind speed as discussed before.

Table 5.6 Input into Original GASP for Takeno et al.[2]

	<i>Liquid hydrogen</i>
<i>Substrate</i>	Concrete
<i>Heat transfer</i>	Perfect thermal contact
<i>Bund radius (m)</i>	0.05
<i>Release type</i>	Instantaneous
<i>Substance</i>	Hydrogen
<i>Pool Radius</i>	0.05
<i>Pool roughness (m)</i>	0
<i>Depth (m)</i>	0.127
<i>Initial pool temperature (K)</i>	19
<i>Ambient temperature (K)</i>	288.15
<i>Wind speed (ms^{-1})</i>	0.1
<i>Surface roughness (m)</i>	0

5.4.1 Original GASP model

Figure 5.8 illustrated the original GASP predictions of mass vaporized for vaporization of liquid hydrogen for the Takeno et al. experiments. The points on the graphs represent the experimental data of Takeno et al.; the solid lines represent results production directly from the original GASP model. Generally, for liquid hydrogen, the results seem to show good

5 Liquid hydrogen spill experiments

agreement. GASP calculates that extra mass is vaporized at earlier periods. Hence, the predicted total time for the pool to vaporize is shorter than observed in the experiment.

5.4.2 Models in this study

As mentioned before, the instantaneous spill in Takeno et al. work is for a non-spreading pool. Thus the B&S, CFN, and GASP models were utilized in this study produce the same result as Figure 5.9. As it is evident, the same result as the original GASP model was obtained by the models in this work. However, since the instantaneous spills experiment was performed in a confined space, it can be considered a non-spreading pool. Therefore, equation (4.11) or (4.13) could be used instead of differential equation systems. The equation (4.10) also can be used for heat transfer calculation, as shown in Figure 4.1.

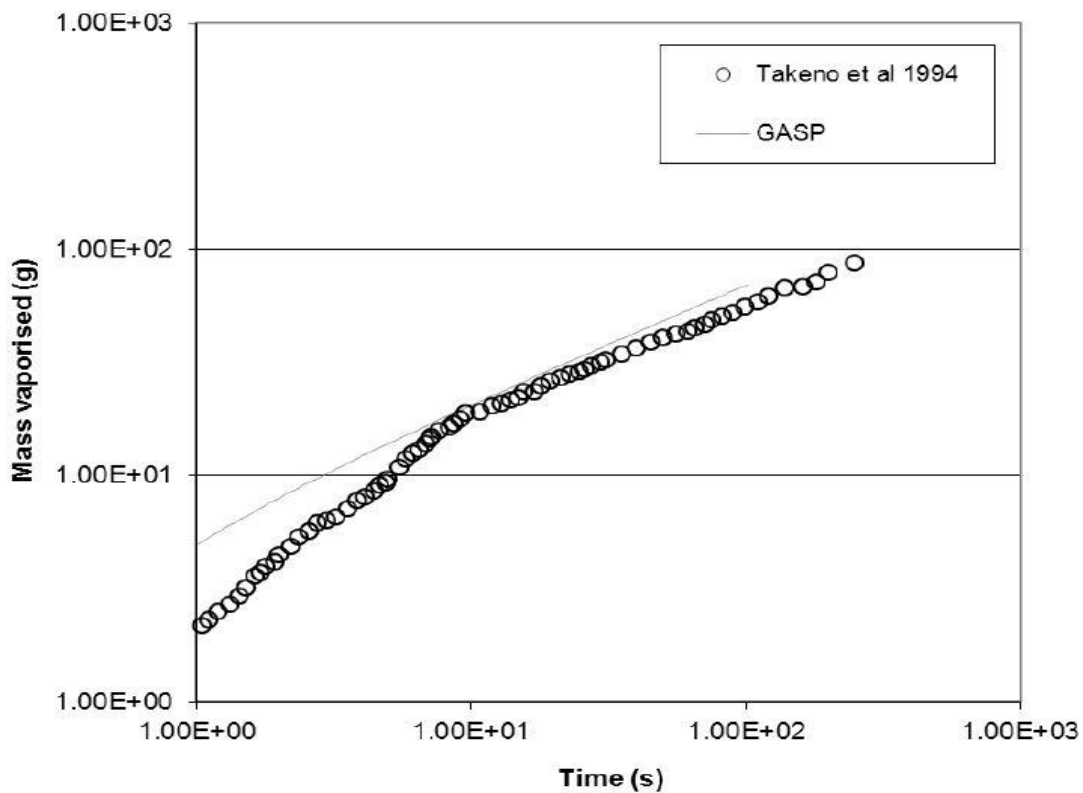


Figure 5.8 GASP predictions of liquid hydrogen mass vaporization for Takeno et al. (1994) experiments [2].

5 Liquid hydrogen spill experiments

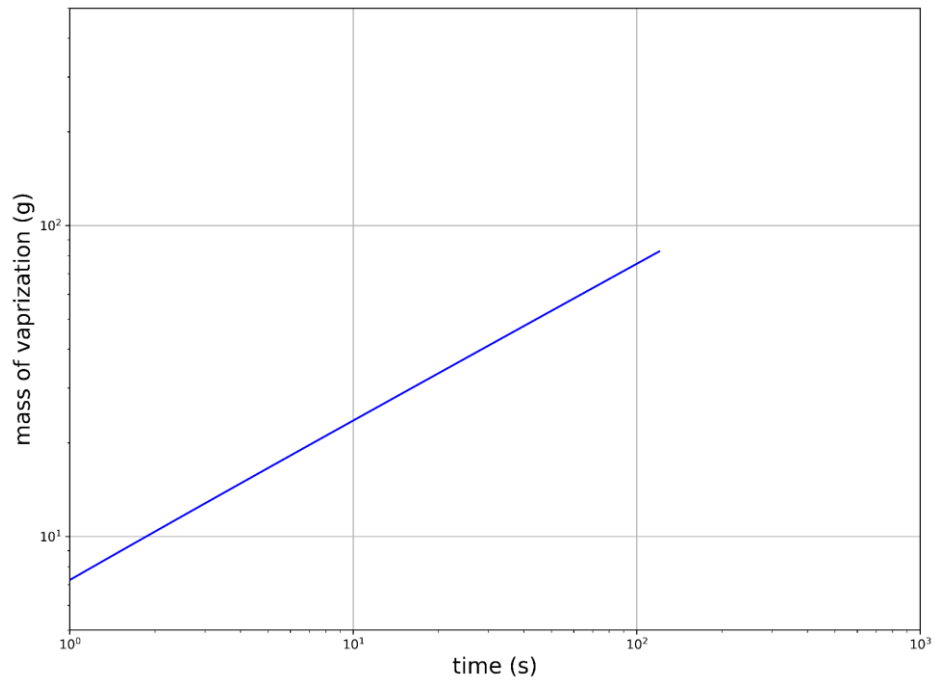


Figure 5.9 Models prediction of liquid hydrogen mass vaporization.

6 Discussion

In this chapter, the characteristics of B&S, CFN, and GASP models will be discussed. Table 6.1 is a summary of the structure of the models, which gives an overview of them.

Webber in Ref. [34] gave a comprehensive description and discussion about the models. It is mentioned clearly that the CFN and B&S models are not appropriate for spills on land. Webber states [34]:

“There has been a history of misunderstanding of the spreading of liquid pools on land, going back well over 30 years. It hinges on the fact that different physical mechanisms control the spread rate of pools on a solid surface, and pools floating on water.”

As a straightforward physical example, Webber considered the examination of a circular pool of immovable size (with liquid neither being distributed nor vaporizing) and then described a moving pool of spreading on water of radius r and depth of h , spreading with front velocity $U = dr/dt$. The pool of density ρ swings some water (of density ρ_w) and with an assumption of that the hydrostatic pressure difference across the front, of instruction $g(\rho_w - \rho)h$ is balanced by a resistance from forcing the water to move out of the way, of order $\rho_w U^2$, then spreading law outcomes will be

$$\frac{dr}{dt} = \varepsilon \sqrt{\frac{g(\rho_w - \rho)h}{\rho_w}} \quad (6.1)$$

The straightforward argument above is extraordinarily successful. It has presented an excellent knowledge of pools spreading on water. But this equation conveys the resistance impact of dislocated water and has undoubtedly no explanation for pools spreading on land. Webber in the following states:

“Unfortunately some earlier models did assume it was true for spreading on land, and this idea, despite its lack of any scientific justification, continues to propagate to this day.”

As can be understood from Webber’s statements, the CFN and B&S are not appropriate for spills on land, but as mentioned before, Nguyen et al. in Ref. [4] suggested using minimum depth as equation (4.15) for helping the model to slow down by restricting the pool depth to a minimum value obtained from viscous effects. Their idea was to model the resistance properly, while for water, it was models by a hydrostatic pressure difference across the front of order $g(\rho_w - \rho)h$. As it is evident in section 4.1.9, this suggestion alone was not enough to model for the realistic result for a very low volumetric rate. Nguyen et al. also didn’t mention about the value of the Froude number explicitly. So, the Froude number for spreading on land should be

Table 6.1 Summary of models

B&S model			
$V = V_i + \dot{V}_c t - \left(\frac{m}{\rho}\right)$	$\frac{dr}{dt} = \sqrt{\varepsilon g \Delta H}$	$\frac{dm}{dt} = \chi k \frac{(T_a - T_B)}{h_{fg}(\sqrt{\pi \alpha t})}$ $\int_0^{r(t)} \frac{2\pi r'}{\sqrt{(t-t')}}$	$\frac{\partial T}{\partial t} = \alpha \frac{\partial^2 T}{\partial z^2}$
CFN model			
$\frac{dV}{dt} = \frac{S}{\rho} - W\pi r^2$	$\frac{dr}{dt} = \sqrt{\varepsilon g \Delta H}$	$m = W\pi r^2$ $W = \frac{T_a - T_B}{\rho h_{fg}}$ $\left[\frac{1}{\pi r^2 (\pi \alpha)^{0.5}} \int_0^{r(t)} \frac{2\pi r' dr'}{(t-t')^{0.5}} + h \right]$	$\frac{\partial T}{\partial t} = \alpha \frac{\partial^2 T}{\partial z^2}$
Original GASP			
$\frac{dV}{dt} = \frac{S}{\rho} - W\pi r^2$	$\frac{dr}{dt} = U \quad (\text{smooth})$ $\frac{dr}{dt} = \Phi_2(\omega) \cdot U \quad (\text{rough})$ $\frac{dU}{dt} = \phi(s) \frac{4g'H}{r} e^{-F}$	$m = W\pi r^2$ $W(T) = \left[\frac{Mp_v}{RT} \right] \left[\frac{u_*}{\rho} \right] \left[\frac{k_v}{\sigma_s} \right] [1 + n]$ $\times G(e^\lambda) x^{-1} \ln((1-x)^{-1})$	$\frac{dT}{dt} = \left(\frac{A_{top}}{C_p \rho V} \right) (Q - \rho WL) + (S/V)(T_s - T)$
Simplified GASP			
$\frac{dV}{dt} = \frac{S}{\rho} - W\pi r^2$	$\frac{dr}{dt} = U \quad (\text{smooth})$ $\frac{dr}{dt} = \Phi_2(\omega) \cdot U \quad (\text{rough})$ $\frac{dU}{dt} = \phi(s) \frac{4g'H}{r} e^{-F}$	$m = W\pi r^2$ $W = \frac{T_a - T_B}{\rho h_{fg}}$ $\left[\frac{1}{\pi r^2 (\pi \alpha)^{0.5}} \int_0^{r(t)} \frac{2\pi r' dr'}{(t-t')^{0.5}} + h \right]$	$\frac{dT}{dt} = \left(\frac{A_{top}}{C_p \rho V} \right) (Q - \rho WL) + (S/V)(T_s - T)$

modified and obtained empirically. Consequently, the CFN and B&S are used by this work to model the cryogenic liquid spill on land, and different values of Froude number and minimum depth are applied to validate the against the experimental data, and the outcome was realistic

6 Discussion

and close to experimental data behavior. The Froude number is tried to determine by and validating the model against the experimental data, but a complete set of experiments is needed to obtain the Froude number, for example, by an empirical correlation. Table 6.2 gives information about the Froude number for different mass flowrate.

Table 6.2 Froude number values for the spill on land.

Mass flowrate (kgs ⁻¹)	Froude number
0.0402	0.003
0.0707	0.0033
0.1642	0.06
3.88	0.12
4.72	0.15

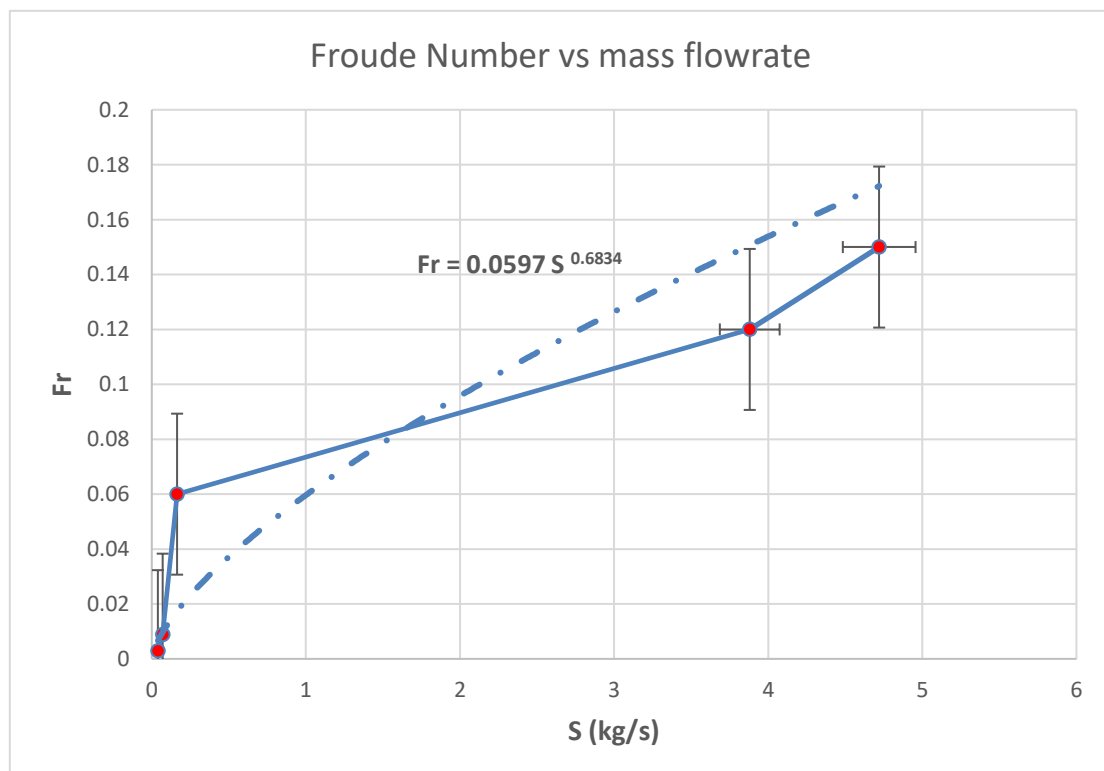


Figure 6.1 Froude number versus mass flowrate.

6 Discussion

It can be seen from Table 6.2 that more values of the Froude number are needed from experimental data. For the range of $0.04 - 4.72 \text{ kgs}^{-1}$, the Froude number can be obtained using Table 6.2 and interpolation for other spill rates in the mentioned range or can be determined by empirical correlation, which is obtained applying these empirical values as shown in Figure 6.1. The equation has a form like below.

$$Fr = 0.0597 S^{0.6834} \quad (6.2)$$

A 5% deviation adjusts the accuracy of the correlation. So, it can be said now, the resistance that is modeled in the GASP model can be modeled in B&S and CFN models by modifying the Froude number.

The GASP model, which is also used in Health and Safety Executive (HSE), is recommended by Webber to use for spreading pools on land. Without modifying any parameters, the result of the GASP model was in good agreement with the experimental data. It was examined in section 5.3.2 that the simplified model also may be used for spills in indoor and outdoor spills.

7 Conclusion

In this study, the available mathematical models for the evaporation of hydrogen during accidental releases were investigated and applied for simulation. For modeling the evaporation of hydrogen, it was required to understand and calculate the heat transfer of liquid hydrogen pool boiling. The spreading of the pool formed by the accidental releases was another requirement for modeling.

For a better understanding of the task in this work, different fundamental mechanisms and processes required for obtaining this study's objective were described in chapter 2 of this study. The contents in chapter 2 have been frequently used in other chapters.

In chapter 3, the heat transfer of liquid hydrogen, same as correlations for calculating the different boiling regimes, were examined. Subsequently, for ambient releases of liquid hydrogen heat fluxes at ONB, CHF and Leidenfrost were estimated 9 W/m², 89627 W/m², and 1596 W/m², respectively, and the corresponding excess temperatures were determined approximately 0.061 K, 2.86 K, and 5.27 K.

Two common boundary conditions (BCs) for heat flux, namely Boiling Regime BR-BCs and Perfect Thermal Contact PTC-BCs, were reviewed in different articles. It was found that various researchers commonly use the PTC-BCs rather than BR-BCs. It was recommended to use PTC-BCs for a spreading pool and BR-BCs for none- spreading. Since our case of study was for spreading pools on lands, it was decided to use PTC-BCs in this work.

In Chapter 4, various integral models have been applied for modeling the spread and vaporization of liquid hydrogen pool.

The B&S model, which was used to model the spread and evaporation of the LNG pool by Briscoe and Shaw, was applied to model the liquid hydrogen's pool spreading and evaporation in this work. It was revealed that this model couldn't be used for spills of cryogenic liquid on land. The model was also controversial for lower mass flow rates and has not been validated. By introducing a minimum edge depth, altering the constant number ε (originally presented Froude number) corresponding to different mass flow rates, and validating against various cryogenic spills, the model demonstrated a roughly accurate result.

The original GASP model wasn't able to simulate without a wind speed value, and the equations were found difficult and complicated to solve numerically due to the large variability of time scales presented by the numerous physical phenomena. Thus, a simplified model of the GASP model was investigated to model the spreading and evaporation of the liquid hydrogen

7 Conclusion

pool in no wind condition. The ability of the model was remarkable and successfully validated against the experimental data.

It was discovered that the CFN model has the same structure as the B&S model with a modification in pool mass or volume equation. In the B&S model, the pool mass equation was an algebraic equation, while in the CFN model, it was proposed to use a differential equation for pool mass. The same modifications as mentioned for the B&S model were applied for the CFN model to model the cryogenic spills on lands. Since the differential equation has a better agreement with the case for this study, it is recommended to use the CFN model instead of B&S model for simulating.

Overall, the GASP model was in better agreement with experimental data of cryogenic and liquid hydrogen spills than the B&S and CFN models. The B&S and CFN models have shown a good deal for spreading pool radius than the GASP model. Despite the proposal of an empirical correlation to determine the Froude number for different mass flowrate, more empirical data is required to obtain more accurate Froude numbers. So, more investigation is expected for CFN and B&S models.

References

- [1] L.-D. Nguyen, M. Kim, and B. Choi, "An experimental investigation of the evaporation of cryogenic-liquid-pool spreading on concrete ground," *Applied Thermal Engineering*, vol. 123, pp. 196-204, 2017/08/01/ 2017, doi: <https://doi.org/10.1016/j.applthermaleng.2017.05.094>.
- [2] R. Batt, *Modelling of Liquid Hydrogen Spills, HSE Research Report, RR985*. 2014.
- [3] K. Verfondern and B. Dienhart, "Pool spreading and vaporization of liquid hydrogen," *International Journal of Hydrogen Energy*, vol. 32, no. 2, pp. 256-267, 2007/02/01/ 2007, doi: <https://doi.org/10.1016/j.ijhydene.2006.01.016>.
- [4] L.-D. Nguyen, M. Kim, B. Choi, and K. Chung, "Validation of numerical models for cryogenic-liquid pool spreading and vaporization on solid ground," *International Journal of Heat and Mass Transfer*, vol. 128, pp. 817-824, 2019/01/01/ 2019, doi: <https://doi.org/10.1016/j.ijheatmasstransfer.2018.09.055>.
- [5] F. Briscoe and P. Shaw, "Spread and evaporation of liquid," *Progress in Energy and Combustion Science*, vol. 6, no. 2, pp. 127-140, 1980/01/01/ 1980, doi: [https://doi.org/10.1016/0360-1285\(80\)90002-7](https://doi.org/10.1016/0360-1285(80)90002-7).
- [6] D. Webber and P. Brighton, *An integral model for spreading, vaporising pools*. Safety and Reliability Directorate, United Kingdom Atomic Energy Authority, 1987.
- [7] D. Webber, *A model for pool spreading and vaporisation and its implementation in the computer code GASP*. Safety and Reliability Directorate, 1990.
- [8] M. Afzali. Modeling of spreading and Evaporation [Online] Available: <https://github.com/afzmojtaba/Modeling-of-Spreading-and-Evaporation.git>
- [9] L. Wang, Y. Li, F. Zhang, F. Xie, and Y. Ma, "Correlations for calculating heat transfer of hydrogen pool boiling," *International Journal of Hydrogen Energy*, vol. 41, no. 38, pp. 17118-17131, 2016/10/15/ 2016, doi: <https://doi.org/10.1016/j.ijhydene.2016.06.254>.
- [10] F. P. INCROPERA, D. P. DEWITT, T. L. BERGMAN, and A. S. LAVINE, *Fundamentals of Heat and Mass Transfer*, 6th ed. John Wiley & Sons Inc, 2007.
- [11] B. Rehm, D. Consultant, A. Haghshenas, A. S. Paknejad, and J. Schubert, "CHAPTER TWO - Situational Problems in MPD," in *Managed Pressure Drilling*, B. Rehm, J. Schubert, A. Haghshenas, A. S. Paknejad, and J. Hughes Eds.: Gulf Publishing Company, 2008, pp. 39-80.
- [12] U. Roy and P. K. Roy, "Chapter 7 - Advances in heat intensification techniques in shell and tube heat exchanger," in *Advanced Analytic and Control Techniques for Thermal Systems with Heat Exchangers*, L. Pekař Ed.: Academic Press, 2020, pp. 197-207.
- [13] D. Camuffo, "Chapter 8 - Dry Deposition of Airborne Particulate Matter: Mechanisms and Effects," in *Microclimate for Cultural Heritage (Second Edition)*, D. Camuffo Ed. Boston: Elsevier, 2014, pp. 283-346.

References

- [14] D. D. Ratnayaka, M. J. Brandt, and K. M. Johnson, "CHAPTER 12 - Hydraulics," in *Water Supply (Sixth Edition)*, D. D. Ratnayaka, M. J. Brandt, and K. M. Johnson Eds. Boston: Butterworth-Heinemann, 2009, pp. 463-498.
- [15] J. Oetjen, H. Schüttrumpf, and M. Engel, "Chapter 27 - Experimental models of coarse-clast transport by tsunamis," in *Geological Records of Tsunamis and Other Extreme Waves*, M. Engel, J. Pilarczyk, S. M. May, D. Brill, and E. Garrett Eds.: Elsevier, 2020, pp. 585-615.
- [16] A. O. Akan, "2 - Energy and momentum principles," in *Open Channel Hydraulics*, A. O. Akan Ed. Oxford: Butterworth-Heinemann, 2006, pp. 24-66.
- [17] K. J. Coeling, J. A. Clark, H. Merte, and E. R. Lady, "Incipient boiling of cryogenic liquids," 1967.
- [18] E. Brentari, *Boiling heat transfer for oxygen, nitrogen, hydrogen, and helium*. US National Bureau of Standards, 1965.
- [19] S. S. Kutateladze, *Heat transfer in condensation and boiling*. US Atomic Energy Commission, Technical Information Service, 1959.
- [20] S. Garcia, "Boiling in liquid hydrogen under gravity compensated with a magnetic field," 2012.
- [21] P. B. Whalley, "Boiling, condensation, and gas-liquid flow," 1987.
- [22] Y. Shirai *et al.*, "Boiling heat transfer from a horizontal flat plate in a pool of liquid hydrogen," *Cryogenics*, vol. 50, no. 6, pp. 410-416, 2010/06/01/ 2010, doi: <https://doi.org/10.1016/j.cryogenics.2010.04.001>.
- [23] V. P. Carey, *Liquid-vapor phase-change phenomena: an introduction to the thermophysics of vaporization and condensation processes in heat transfer equipment*. CRC Press, 2018.
- [24] L. Bewilogua, R. Knöner, and H. Vinzelberg, "Heat transfer in cryogenic liquids under pressure," *Cryogenics*, vol. 15, no. 3, pp. 121-125, 1975/03/01/ 1975, doi: [https://doi.org/10.1016/0011-2275\(75\)90178-2](https://doi.org/10.1016/0011-2275(75)90178-2).
- [25] V. V. Klimenko, "Film boiling on a horizontal plate — new correlation," *International Journal of Heat and Mass Transfer*, vol. 24, no. 1, pp. 69-79, 1981/01/01/ 1981, doi: [https://doi.org/10.1016/0017-9310\(81\)90094-6](https://doi.org/10.1016/0017-9310(81)90094-6).
- [26] P. J. Berenson, "Film-boiling heat transfer from a horizontal surface," 1961.
- [27] H. Merte, "Incipient and steady boiling of liquid nitrogen and liquid hydrogen under reduced gravity," 1970.
- [28] L.-D. Nguyen, M. Kim, B. Choi, K. Chung, K. Do, and T. Kim, "An evaluation of vaporization models for a cryogenic liquid spreading on a solid ground," *International Journal of Heat and Mass Transfer*, vol. 146, p. 118848, 2020/01/01/ 2020, doi: <https://doi.org/10.1016/j.ijheatmasstransfer.2019.118848>.
- [29] O. Basha, T. Olewski, L. Véchet, M. Castier, and S. Mannan, "Modeling of pool spreading of LNG on land," *Journal of Loss Prevention in the Process Industries*, vol. 30, pp. 307-314, 2014/07/01/ 2014, doi: <https://doi.org/10.1016/j.jlp.2014.04.012>.

References

- [30] P. K. Raj, "Models for cryogenic liquid spill behavior on land and water," *Journal of Hazardous Materials*, vol. 5, no. 1, pp. 111-130, 1981/10/01/ 1981, doi: [https://doi.org/10.1016/0304-3894\(81\)85009-1](https://doi.org/10.1016/0304-3894(81)85009-1).
- [31] A. M. Thyer, "A review of data on spreading and vaporisation of cryogenic liquid spills," *Journal of Hazardous Materials*, vol. 99, no. 1, pp. 31-40, 2003/04/04/ 2003, doi: [https://doi.org/10.1016/S0304-3894\(02\)00355-2](https://doi.org/10.1016/S0304-3894(02)00355-2).
- [32] P. P. Raj and A. S. Kalelkar, "Assessment models in support of the hazard assessment handbook," LITTLE (ARTHUR D) INC CAMBRIDGE MA, 1974.
- [33] H. Carslaw and J. Jaeger, "Conduction of heat in solids, Clarendon," ed: Oxford, 1959.
- [34] D. M. Webber, "On models of spreading pools," *Journal of Loss Prevention in the Process Industries*, vol. 25, no. 6, pp. 923-926, 2012/11/01/ 2012, doi: <https://doi.org/10.1016/j.jlp.2012.05.003>.
- [35] J. Moorhouse and R. Carpenter, "Factors affecting vapour evolution rates from liquefied gas spills," *North western Branch Papers, Institution of Chemical Engineers*, vol. 1, pp. 4.1-18, 1986.
- [36] D. M. Webber, "Source terms," *Journal of Loss Prevention in the Process Industries*, vol. 4, no. 1, pp. 5-15, 1991/01/01/ 1991, doi: [https://doi.org/10.1016/0950-4230\(91\)80002-C](https://doi.org/10.1016/0950-4230(91)80002-C).
- [37] C. Van den Bosch and R. Weterings, "Methods for the calculation of physical effects," *Committee for the Prevention of Disasters, CPR E*, vol. 14, 2005.
- [38] P. Brighton, "Evaporation from a plane liquid surface into a turbulent boundary layer," *Journal of Fluid Mechanics*, vol. 159, pp. 323-345, 1985.
- [39] P. Brighton, *Evaporation from a plane liquid surface into a turbulent boundary layer*. UKAEA Safety and Reliability Directorate, 1987.
- [40] O. G. Sutton, "Wind structure and evaporation in a turbulent atmosphere," *Proceedings of the Royal Society of London. Series A, Containing Papers of a Mathematical and Physical Character*, vol. 146, no. 858, pp. 701-722, 1934.
- [41] A. G. Venetsanos, E. Papanikolaou, and J. G. Bartzis, "The ADREA-HF CFD code for consequence assessment of hydrogen applications," *International Journal of Hydrogen Energy*, vol. 35, no. 8, pp. 3908-3918, 2010/04/01/ 2010, doi: <https://doi.org/10.1016/j.ijhydene.2010.01.002>.
- [42] L. Marinescu-Pasoi and B. Sturm, "Messung der Ausbreitung einer Wasserstoff-und Propangaswolke in bebautem Gelände and Gasspezifische Ausbreitungsversuche," *Battelle Ingenieurtechnik GmbH, Reports R-68.202 and R-68.264*, 1994.
- [43] J. Chirivella and R. Witcofski, "Experimental results from fast 1500 gallon LH2 spills," in *Am Inst Chem Eng Symp Ser*, 1986, vol. 82, no. 251, pp. 120-140.
- [44] K. Takeno, T. Ichinose, Y. Hyodo, and H. Nakamura, "Evaporation rates of liquid hydrogen and liquid oxygen spilled onto the ground," *Journal of Loss Prevention in the Process Industries*, vol. 7, no. 5, pp. 425-431, 1994/01/01/ 1994, doi: [https://doi.org/10.1016/0950-4230\(94\)80061-8](https://doi.org/10.1016/0950-4230(94)80061-8).

References

- [45] M. Royle and D. Willoughby, "Releases of unignited liquid hydrogen: Prepared by the Health and Safety Laboratory for the Health and Safety Executive 2014," 2009.
- [46] "Data Report: Closed room and ventilation mast studies, LIQUID HYDROGEN SAFETY," 01, Rev. 1, 2020.
- [47] "Data Report: Outdoor leakage studies, LIQUID HYDROGEN SAFETY," 853182, Rev. 1, 2020.
- [48] "ESR Technology, (Engineering, Safety & Risk)."
<https://www.esrtechnology.com/index.php/software/gasp> (accessed 21.03, 2021).

Appendices

Appendix A Python code for natural convection boiling

```

# -*- coding: utf-8 -*-
"""
Created on Fri Mar  5 19:09:15 2021

@author: afzmo
"""
# -*- coding: utf-8 -*-
"""
Created on Thu Mar  4 15:25:14 2021

@author: afzmo
"""
import numpy as np

Ts = 0.01 # [s]
T_start = 1 # [s]
T_stop = 10 # [s]
N_sim = int((T_stop - T_start)/Ts) + 2
#####
Nu = np.linspace(0, 1000, 1000)
n = (1/3)
C = (0.16)
Pr_Gr = (Nu / C)**(1/n)
k = 0.0125
g = 9.81
v = 3.52*1e-7
Pr = 13.32
B = 2.83
q_ONB = 1e4
dT_ONB = (q_ONB / (6309))**(-2.52)
a=6309
b=2.52
rho_l = 71
rho_v = 1.005
sigma = 3.004e-3
lc = (sigma) / (g*(rho_l - rho_v))**0.5
h_fg = 451

cp = 6666
cpv = 14310
#####
T_k_array = np.zeros(N_sim)
q_array = np.zeros(N_sim)

#####
q=1
#####
for i in range(0, N_sim):

    T_k = i*Ts

    q = (C*k*((g*B*T_k*Pr/(v**2))**n))*T_k

    T_k_array[i] = T_k
    q_array[i] = q
    #q = q_1

import matplotlib.pyplot as plt
plt.close('all') # Closes all figures before plotting
plt.figure(figsize=(12, 9))
plt.xscale('log')
plt.yscale('log')
plt.plot(T_k_array, q_array, 'r--')
#plt.plot(Pr_Gr, Nu, 'r--')
plt.annotate("Nu = C$(Gr.Pr)^n$ ",(1e9, 10), fontsize= "xx-large")
#plt.annotate("----QHF", (2, 6e4))
#plt.annotate("----Leidenfrost", (2.7, 2.37e2))
plt.legend(('Natural convection heat transfer of LH2', 'pool'), fontsize= "xx-large")
#plt.legend(('Nu vs Gr.Pr', 'pool'), fontsize= "xx-Large")
plt.xlabel('\u0394T [K]', fontsize= "xx-large")
plt.ylabel('q [W/m2]', fontsize= "xx-large")
#plt.xlabel('Gr.Pr', fontsize= "xx-Large")
#plt.ylabel('Nu', fontsize= "xx-Large")
plt.grid()
plt.savefig('Natural_convection.png', dpi=700, bbox_inches='tight')

```

Appendix B Python Code Nu versus Pr,Gr

```

# -*- coding: utf-8 -*-
"""
Created on Thu Mar  4 15:25:14 2021

@author: afzmo
"""
import numpy as np

Ts = 0.01 # [s]
T_start = 1 # [s]
T_stop = 10 # [s]
N_sim = int((T_stop - T_start)/Ts) + 2
#%%
Nu = np.linspace (0 , 1000, 1000 )
n = (1/3)
C = (0.16)
Pr_Gr = (Nu / C)**(1/n)
k = 0.0125
g = 9.81
v = 3.52*1e-7
Pr = 13.32
B = 2.83
q_ONB = 1e4
dT_ONB = ( q_ONB / (6309))**(-2.52)
a=6309
b=2.52
rho_l = 71
rho_v = 1.005
sigma = 3.004e-3
lc = ( (sigma) / (g*(rho_l - rho_v)) )**0.5
h_fg = 451
cp = 6666
cpv = 14310
#%%
T_k_array = np.zeros(N_sim)
q_array = np.zeros(N_sim)

#%%
q=1

#%%
for i in range(0, N_sim):

    T_k = i*Ts

    q = (C*k*((g*B*T_k*Pr/(v**2))**n))*T_k

    T_k_array[i] = T_k
    q_array[i] = q
    #q = q_1

import matplotlib.pyplot as plt
plt.close('all') # Closes all figures before plotting
plt.figure(figsize=(12, 9))
plt.xscale('log')
plt.yscale('log')
plt.plot (Pr_Gr , Nu, 'r--')
plt.annotate("Nu = C$(Gr.Pr)^n$ " ,(1e9, 10), fontsize= "xx-large")
plt.legend(("Nu vs Gr.Pr", 'pool'), fontsize= "xx-large")
plt.xlabel('Gr.Pr', fontsize= "xx-large")
plt.ylabel('Nu', fontsize= "xx-large")
plt.grid()
plt.savefig('Natural_convection.png', dpi=700, bbox_inches='tight')

```

Appendix C Python code nucleate boiling

```

1  # -*- coding: utf-8 -*-
2  """
3  Created on Thu Mar  4 18:29:43 2021
4
5  @author: afzmo
6  """
7  # -*- coding: utf-8 -*-
8  """
9  Created on Thu Mar  4 15:25:14 2021
10
11 @author: afzmo
12 """
13 import numpy as np
14
15 Ts = 7e-1 # [s]
16 T_start = 1 # [s]
17 T_stop = 10 # [s]
18 N_sim = int((T_stop - T_start)/Ts) + 2
19 """
20
21
22 k = 0.0125 #thermal conductivity of LH2
23 g = 9.81
24 v = 3.52*1e-7 #kinemtaic viscosity of LH2
25 Pr = 13.32
26 B = 2.83 #coefficent of thermal exapnsion
27 q_ONB = 1e4
28 dT_ONB = ( q_ONB / (6309))**(-2.52)
29 a=6309
30 b=2.52
31 rho_l = 74.252
32 rho_v = 0.4
33 sigma = 3.004e-3
34 lc = ( (sigma) / (g*(rho_l - rho_v)) )**0.5
35 h_fg = 451
36
37 cp = 0.6666
38 cpv = 14310
39 P = 100000
40 M=25*1e-6
41 Kutateladze =( 5.66*1e-10 * ( (k)*(cp**1.5)*(rho_l**1.28)*(P**1.75))/
42 (M**0.625)*(sigma**0.9)*(h_fg**1.5)*(rho_v**1.5) )
43
44 Clarke1 = ( (1/(M*h_fg))*(sigma / (g*(rho_l-rho_v)) )**0.5)
45 Clarke2 = (3.25*1e5*((cp/(h_fg*Pr**1.8))*(120)**1.8)**2.89 )
46
47 print (Kutateladze)
48 print (Clarke1, Clarke2)
49 """
50 T_k_array = np.zeros(N_sim)
51 q_wang_array = np.zeros(N_sim)
52 q_Kutateladze_array = np.zeros(N_sim)
53 q_clarke_array = np.zeros(N_sim)
54 """
55
56 q_wang = 1e3
57 q_Kutateladze = 1e3
58 q_clarke = 1e3
59
60
61
62 T = [1.05, 1.15, 1.25, 1.35, 1.45, 1.55, 1.65, 1.75, 1.85,1.95,
63 1, 1.1, 1.2, 1.3, 1.4, 1.5, 1.6, 1.7, 1.8, 1.9,
64 2, 2.1, 2.2, 2.3, 2.4, 2.5, 2.6, 2.7, 2.8, 2.9,
65 3,4,5,6,7,8,9,10,11]
66 Qe = [6000, 5000, 4000, 3000, 2000, 1500, 1400, 1300, 1200, 1100,
67 9500, 9800, 11000, 17000, 18000, 22000, 24000, 26000, 29000, 30000,
68 3.5e4, 4e4, 4.5e4, 5e4, 5.5e4, 6e4, 7e4, 8e4, 9e4,1e5,
69 1e5,1e5,1e5,1e5,1e5,1e5,1e5,1e5,1e5]

```

```

70  """
71  for i in range(0, N_sim):
72
73      T_k = i*Ts
74
75
76      q_wang = a* (T_k**b)
77      q_Kutateladze = Kutateladze * (T_k**2.5)
78      q_clarke = (Clarke2 /Clarke1 ) *(T_k**2.89)
79
80      T_k_array[i] = T_k
81      q_wang_array[i] = q_wang
82      q_Kutateladze_array[i] =q_Kutateladze
83      q_clarke_array[i] = q_clarke
84
85
86  import matplotlib.pyplot as plt
87  plt.close('all') # Closes all figures before plotting
88  plt.figure(figsize=(12, 9))
89  plt.xscale('log')
90  plt.yscale('log')
91  plt.plot (T_k_array , q_wang_array, 'r')
92  plt.plot (T_k_array , q_Kutateladze_array, 'b')
93  plt.plot (T_k_array ,q_clarke_array, 'g')
94  plt.plot (T , Qe, 'o')
95
96  plt.legend(('Wang', 'Kutateladze corr.', 'Clarke', 'experiment [10]'), fontsiz
97  plt.xlabel('\u0394T[K]', fontsize= "xx-large")
98  plt.ylabel('q [W/m2]', fontsize= "xx-large")
99  plt.grid()
100 plt.savefig('Nucleate.png', dpi=500, bbox_inches='tight')
101

```

Appendix D Python code of LH₂ boiling curve comparison with different correlations

```

1  #-*- coding: utf-8 -*-
2  """
3  Created on Sun Jan 31 13:29:40 2021
4
5  @author: afzmo
6  """
7  import numpy as np
8
9  Ts = 0.01 # [s]
10 T_start = 1e-2 # [s]
11 T_stop = 1e3 # [s]
12 N_sim = int((T_stop - T_start)/Ts) + 2
13 #####
14 Nu = np.linspace(0, 1000, 10000)
15 n = (1/3)
16 C = (0.16)
17 Pr_Gr = (Nu / C)**(1/n)
18
19 g = 9.81
20 v = 3.52*1e-7
21 Pr = 13.32
22 B = 2.83
23 q_ONB = 1.92e4
24 dT_ONB = (q_ONB / (6309))**(-2.52)
25 print('TONB = ', dT_ONB)
26 a=6309
27 b=2.52
28 rho_l = 72
29 rho_v = 0.874
30 sigma = 3.004e-3
31 lc = (sigma) / (g*(rho_l - rho_v))**0.5
32 h_fg = 451e3
33 h_fg2 = 451
34 cp = 0.6666
35 cpv = 14310
36
37 Ck = 0.16
38 CL = 0.09
39 CL16 = 0.16
40 k = 0.0125 #thermal conductivity of LH2
41
42 B = 2.83 #coefficient of thermal expansion
43 P = 100000
44 M=25*1e-6
45 Q_CHF = Ck * h_fg * rho_v * ((g*sigma*(rho_l-rho_v))/(rho_v**2))**0.25
46 dT_CHF = (Q_CHF / a)**(1/b)
47 q_L = CL * rho_v * h_fg * ((g*sigma*(rho_l-rho_v))/(rho_l - rho_v)**2)**(1/
48 dT_L = q_L/(k* 0.425 * ((g*B* (lc**3)*Pr) * (h_fg+0.4 *cpv) / (v**2)*cpv)
49
50 P=101325
51 M=25*1e-6
52 Kutateladze =( 5.66*1e-10 * ( (k)*(cp**1.5)*(rho_l**1.28)*(P**1.75))/
53 (M**0.625)*(sigma**0.9)*(h_fg2**1.5)*(rho_v**1.5) )
54
55 Clarke1 = ( (1/(M*h_fg2))*(sigma / (g*(rho_l-rho_v)))**0.5)
56 Clarke2 = (3.25*1e5*((cp/(h_fg2*Pr**1.8))*(159)**1.8)**2.89 )
57
58 print('\u0394T_CHF = ',dT_CHF)
59 print('q_CHF = ',Q_CHF)
60 print('q_L = ',q_L)
61 print('dT_L = ',dT_L)
62
63 #####
64 T_k_array = np.zeros(N_sim)
65 q_array = np.zeros(N_sim)
66 q_wang_array = np.zeros(N_sim)
67 q_Kutateladze_array = np.zeros(N_sim)
68 q_clarke_array = np.zeros(N_sim)
69 q_C16_array_array = np.zeros(N_sim)
70 #####

```

```

71 q=1
72 q_wang = 1
73 q_clarke = 1|
74 q_Kutateladze = 1
75 q_4 = 1
76 #####
77 for i in range(0, N_sim):
78
79     T_k = i*Ts
80     if (T_k >= T_start and T_k < dT_ONB):
81
82         q = (C*k*((g*B*T_k*Pr/(v**2))**n))*T_k
83         q_wang = (C*k*((g*B*T_k*Pr/(v**2))**n))*T_k
84         q_Kutateladze = (C*k*((g*B*T_k*Pr/(v**2))**n))*T_k
85         q_clarke = (C*k*((g*B*T_k*Pr/(v**2))**n))*T_k
86
87
88     elif (T_k >= dT_ONB and T_k < dT_CHF):
89
90         q = a* (T_k**b)
91         q_wang = a* (T_k**b)
92         q_Kutateladze = Kutateladze * (T_k**2.5)
93         q_clarke = (Clarke2 /Clarke1 ) *(T_k**2.89)
94
95
96     elif (T_k >= dT_CHF and T_k < dT_L):
97
98         q = Q_CHF - ( (T_k - dT_CHF)/(dT_L-dT_CHF)*(Q_CHF - q_L) )
99         q_wang = Q_CHF - ( (T_k - dT_CHF)/(dT_L-dT_CHF)*(Q_CHF - q_L) )
100        q_Kutateladze = Q_CHF - ( (T_k - dT_CHF)/(dT_L-dT_CHF)*(Q_CHF - q_L) )
101        q_clarke = Q_CHF - ( (T_k - dT_CHF)/(dT_L-dT_CHF)*(Q_CHF - q_L) )
102
103
104     elif (T_k >= dT_L and T_k < 3e3):
105
106
107         h_gfp = h_fg + 0.4 * cpv * T_k
108
109         q = ( k* 0.425 * ( ((g*B*T_k*(1c**3)*Pr) * h_gfp /
110             (v**2)*cpv*T_k)**0.25) * T_k)
111         q_wang = ( k* 0.425 * ( ((g*B*T_k*(1c**3)*Pr) * h_gfp /
112             (v**2)*cpv*T_k)**0.25) * T_k)
113         q_Kutateladze = ( k* 0.425 * ( ((g*B*T_k*(1c**3)*Pr) * h_gfp /
114             (v**2)*cpv*T_k)**0.25) * T_k)
115         q_clarke = ( k* 0.425 * ( ((g*B*T_k*(1c**3)*Pr) * h_gfp /
116             (v**2)*cpv*T_k)**0.25) * T_k)
117
118         T_k_array[i] = T_k
119         q_array[i] = q
120         #q = q_1
121
122         q_wang_array[i] = q_wang
123         q_Kutateladze_array[i] = q_Kutateladze
124         q_clarke_array[i] = q_clarke
125
126 import matplotlib.pyplot as plt
127 plt.close('all') # Closes all figures before plotting
128 plt.figure(figsize=(12, 9))
129 plt.xscale('log')
130 plt.yscale('log')
131 plt.plot(T_k_array , q_array, 'b--')
132 plt.plot(T_k_array , q_Kutateladze_array, 'g--')
133 plt.plot(T_k_array , q_clarke_array, 'r--')
134 #plt.plot(T_k_array , q_nat_array, 'b')
135 #plt.plot(T_k_array , q_nuc_array, 'b')
136 #plt.plot(T_k_array , q_tran_array, 'g')
137 #plt.plot(T_k_array , q_film_array, 'y')
138 plt.annotate("-----T.ONB", (0.045, 6), fontsize="xx-large")
139 plt.annotate("-----CHF", (2, 8.5e4),fontsize="xx-large")
140 plt.annotate("-----Leidenfrost", (3, 8e2),fontsize="xx-large")
141 plt.legend(('Wang et al ', 'Kutateladze', 'Clarke'),fontsize="xx-large")
142 plt.xlabel('\u0394T[K]', fontsize="xx-large")
143 plt.ylabel('q [W/m2]', fontsize="xx-large")
144 plt.grid()
145 plt.savefig('plot.png', dpi=700, bbox_inches='tight')

```

Appendix E Python code of LH₂ boiling curve suggested by this work

```

1  # -*- coding: utf-8 -*-
2  """
3  Created on Sun Jan 31 13:29:40 2021
4
5  @author: afzmo
6  """
7  import numpy as np
8
9  Ts = 0.01 # [s]
10 T_start = 1e-2 # [s]
11 T_stop = 1e3 # [s]
12 N_sim = int((T_stop - T_start)/Ts) + 2
13
14 Nu = np.linspace(0, 1000, 10000)
15 n = (1/3)
16 C = (0.16)
17 Pr_Gr = (Nu / C)**(1/n)
18 k = 0.0125
19 g = 9.81
20 v = 3.52*1e-7
21 Pr = 13.32
22 B = 2.83
23 q_ONB = 1.92e4
24 dT_ONB = ( q_ONB / (6309) )**(-2.52)
25 print ('TONB = ', dT_ONB)
26 a=6309
27 b=2.52
28 rho_l = 74.252
29 rho_v = 1.005
30 sigma = 3.004e-3
31 lc = ( (sigma) / (g*(rho_l - rho_v)) )**0.5
32 h_fg = 461*1e3
33 cp = 0.6666
34 cpv = 14310
35 Ck = 0.16
36
37 CL = 0.09
38 Q_CHF = Ck * h_fg * rho_v * ((g*sigma*(rho_l-rho_v))
39                               /(rho_v**2))**0.25
40 dT_CHF = (Q_CHF / a)**(1/b)
41 q_L = CL * rho_v * h_fg * ((g*sigma*(rho_l-rho_v))/
42                             (rho_l - rho_v)**2)**(1/4)
43 dT_L = q_L/( k* 0.425 * ( ((g*B* (lc**3)*Pr) * (h_fg+0.4 *cpv) /
44                           (v**2)*cpv)**0.25) )**(3/2)
45
46 print ('\u0394T_CHF = ',dT_CHF)
47 print ('q_CHF = ',Q_CHF)
48 print ('q_L = ',q_L)
49 print ('dT_L = ',dT_L)
50
51
52
53
54
55
56
57
58
59
60
61
62
63
64
65
66
67
68
69
70

```

```

76     q = Q_CHF - ( (T_k - dT_CHF)/(dT_L-dT_CHF)*(Q_CHF - q_L) )
77
78     elif (T_k >= dT_L and T_k < 3e3):
79
80         h_gfp = h_fg + 0.4 * cpv * T_k
81
82         q = ( k* 0.425 * ( ((g*B*T_k* (lc**3)*Pr) * h_gfp /
83                       (v**2)*cpv*T_k)**0.25) * T_k)
84     T_k_array[i] = T_k
85     q_array[i] = q
86     q_nat_array[i] = q_nat
87     q_nuc_array[i] = q_nuc
88     q_tran_array[i] = q_tran
89     q_film_array[i] = q_film
90
91 import matplotlib.pyplot as plt
92 plt.close('all') # Closes all figures before plotting
93 plt.figure(figsize=(12, 9))
94 plt.xscale('log')
95 plt.yscale('log')
96 plt.plot (T_k_array , q_array, 'r')
97 #plt.plot (T_k_array , q_nat_array, 'b')
98 #plt.plot (T_k_array , q_nuc_array, 'b')
99 #plt.plot (T_k_array , q_tran_array, 'g')
100 #plt.plot (T_k_array , q_film_array, 'y')
101 plt.annotate("-----T.ONB", (0.045, 6), fontsize= "xx-large")
102 plt.annotate("-----CHF", (2, 8.5e4),fontsize="xx-large")
103 plt.annotate("-----Leidenfrost", (4, 1e3),fontsize="xx-large")
104 plt.legend(('Boiling curve of liquid hydrogen pool proposed by this work ',
105 plt.xlabel('\u0394T[K]', fontsize= "xx-large")
106 plt.ylabel('q [W/m2]', fontsize= "xx-large")
107 plt.grid()
108 plt.savefig('plot.png', dpi=700, bbox_inches='tight')
109
110

```

Appendix F Python code of Perfect Thermal Contact Boundary Condition (PTC-BC)

```

1  #-*- coding: utf-8 -*-
2  """
3  Created on Thu Mar 25 17:53:33 2021
4
5  @author: afzmo
6  """
7  import numpy as np
8  from math import pi, log
9  alpha = 9e-7 # soil (average)
10
11  Ts = 0.01 # [s]
12  T_start = 1e-2 # [s]
13  T_stop = 1e3 # [s]
14  N_sim = int((T_stop - T_start)/Ts) + 2
15  ts = 0.01 # [s]
16  t_start = 1e-2 # [s]
17  t_stop = 1e3 # [s]
18  t_sim = int((t_stop - t_start)/Ts) + 2
19  #%%
20  Nu = np.linspace (0 , 1000, 10000 )
21
22  Ta=298
23  TB = 20.4
24  n = (1/3)
25  C = (0.16)
26  Pr_Gr = (Nu / C)**(1/n)
27  k = 0.0125
28  kg=1.2
29  g = 9.81
30  v = 3.52*1e-7
31  Pr = 13.32
32  B = 2.83
33  q_ONB = 1.92e4
34  dT_ONB = ( q_ONB / (6309))**(-2.52)
35  print ('TONB = ', dT_ONB)
36  a=6309
37  b=2.52
38
39  rho_l = 74.252
40  rho_v = 1.005
41  sigma = 3.004e-3
42  lc = ( (sigma) / (g*(rho_l - rho_v)) )**0.5
43  h_fg = 461*1e3
44  cp = 0.6666
45  cpv = 14310
46  Ck = 0.16
47  CL = 0.09
48  Q_CHF = Ck * h_fg * rho_v * ((g*sigma*(rho_l-rho_v))
49  / (rho_v**2))**0.25
50  dT_CHF = (Q_CHF / a)**(1/b)
51  q_L = CL * rho_v * h_fg * ((g*sigma*(rho_l-rho_v))/
52  (rho_l - rho_v)**2)**(1/4)
53  dT_L = q_L / ( k* 0.425 * ( ((g*B* (lc**3)*Pr) * (h_fg+0.4 *cpv) /
54  (v**2)*cpv)**0.25))**(3/2)
55
56  print ('\u0394T_CHF = ',dT_CHF)
57  print ('q_CHF = ',Q_CHF)
58  print ('q_L = ',q_L)
59  print ('dT_L = ',dT_L)
60  #%%
61  T_k_array = np.zeros(N_sim)
62  q_array = np.zeros(N_sim)
63  qstar_array = np.zeros(N_sim)
64
65  q_nat_array = np.ones(N_sim)
66  q_nuc_array = np.ones(N_sim)
67  q_tran_array = np.ones(N_sim)
68  q_film_array = np.ones(N_sim)
69  t_array = np.zeros(N_sim)
70  t1 = np.zeros(N_sim)
71  t2 = np.zeros(N_sim)
72  t3 = np.zeros(N_sim)
73  t4 = np.zeros(N_sim)
74  tf = np.zeros(N_sim)
75  t_array = np.zeros(N_sim)

```

```

75 tstar = np.zeros(N_sim)
76 TPP_ = np.zeros(N_sim)
77
78 #####
79 q_nat = 1
80 q=1
81 q_nuc = 1
82 q_tran = 1
83 q_film = 1
84 t = 0
85 t1[0] = 0
86 t2[0] = 0
87 t3 [0]= 0
88 t4 [0]= 0
89 tf[0] = 0
90 tstar[0] = 0
91
92 TPP = 0
93 #####
94 for i in range(0, N_sim-1):
95
96     T_k = i*Ts
97
98
99
100     if (T_k >= T_start and T_k < dT_ONB):
101
102         q = (C*k*((g*B*T_k*Pr/(v**2))**n))*T_k
103         q_nat = (C*k*((g*B*T_k*Pr/(v**2))**n))*T_k
104
105         t = ((kg*(TB-Ta)/(q*(pi*alpha)**0.5))**2)
106
107         tf[i] = (kg*(T_k)/(q_nat*(pi*alpha)**0.5))**2
108
109         TPP = T_k - Ta
110     elif (T_k >= dT_ONB and T_k < dT_CHF):
111

```

```

112         q = a* (T_k**b)
113
114         t = ((kg*(TB-Ta)/(q*(pi*alpha)**0.5))**2)
115
116
117         q_nuc = a* (T_k**b)
118         tf [i]= (kg*(T_k)/(q*(pi*alpha)**0.5))**2
119
120         TPP = T_k - Ta
121     elif (T_k >= dT_CHF and T_k < dT_L):
122
123         q = Q_CHF - ( (T_k - dT_CHF)/(dT_L-dT_CHF)*(Q_CHF - q_L) )
124
125
126         t = ((kg*(TB-Ta)/(q*(pi*alpha)**0.5))**2)+ t4[i]
127
128         q_tran = Q_CHF - ( (T_k - dT_CHF)/(dT_L-dT_CHF)*(Q_CHF - q_L) )
129
130         TPP = T_k - Ta
131
132     elif (T_k >= dT_L and T_k < 3e3):
133
134         h_gfp = h_fg + 0.4 * cpv * T_k
135
136         q = ( k* 0.425 * ( ((g*B*T_k* (1c**3)*Pr) * h_gfp /
137                        (v**2)*cpv*T_k)**0.25) * T_k)
138         q_film = ( k* 0.425 * ( ((g*B*T_k* (1c**3)*Pr) * h_gfp /
139                        (v**2)*cpv*T_k)**0.25) * T_k)
140
141         #t4= ((kg*(T_k-Ta)/(q*(pi*alpha)**0.5))**2)
142
143         t = ((kg*(TB-Ta)/(q*(pi*alpha)**0.5))**2)
144         #t1[i]= (kg*(T_k)/(q*(pi*alpha)**0.5))**2
145
146         tf [i] = (kg*(T_k)/(q*(pi*alpha)**0.5))**2
147
148         TPP = T_k - Ta

```

```
#plt.plot (T_k_array , q_film_array, 'y')
#plt.annotate("-----T.ONB", (0.045, 6), fontsize= "xx-large")
#plt.annotate("-----CHF", (2, 8.5e4),fontsize="xx-large")
#plt.annotate("-----Leidenfrost", (4, 1e3),fontsize="xx-large")
#plt.legend(('Boiling curve of liquid hydrogen pool proposed by this work ', 'pool'),f
#plt.xlabel('\u00394T[K]', fontsize= "xx-large")
plt.xlabel('t(s)', fontsize= "xx-large")

plt.legend(labels=('Perfect Thermal contact BC', ''),fontsize= "xx-large")
plt.ylabel('q [W/m2]', fontsize= "xx-large")
plt.grid()
plt.savefig('nso.png', dpi=700, bbox_inches='tight')
```

Appendix F List of figures

Figure 2.1 Heat transfer mechanism to the pool and mass evaporation 16

Figure 2.2 Typical boiling curve of water at 1 atm [10]. 19

Figure 3.1 Calculated natural convection heat transfer for Nu and Gr.Pr relation. 25

Figure 3.2 Natural convection regime of hydrogen, based on eq (3.1-3.3) 26

Figure 3.3 Comparison of different correlation with experimental data in nucleate boiling with ambient pressure 27

Figure 3.4 Comparison of different correlation with experimental data in nucleate boiling in $(P/P_c) = 0.23$ 28

Figure 3.5 The boiling curve of hydrogen with the comparison of different correlations for the nucleate regime. 32

Figure 3.6 The boiling curve of hydrogen proposed by this work $C_L = 0.09$ 32

Figure 3.7 Heat flux versus time (PTC-BR). 33

Figure 3.8 The heat flux versus temperature difference and time BR-BC [28]. 34

Figure 4.1 The heat transfer by conduction from the ground (concrete). 41

Figure 4.2 The spreading radius and the pool volume of LNG and liquid hydrogen pool by 1000 m³ of an instantaneous spill (B&S). 42

Figure 4.3 Mass evaporation of 1000 m³ instantaneous spill of LNG and Hydrogen (B&S). 43

Figure 4.4 The spreading radius and the pool volume of LNG and liquid hydrogen pool by 1000 m³ of an instantaneous spill bounded at r =50m (B&S) 44

Figure 4.5 Mass evaporation of 1000 m³ instantaneous spill of LNG and Hydrogen bounded at r = 50m (B&S). 44

Figure 4.6 The spreading radius and the pool volume of LNG and liquid hydrogen by a continuous spill of 10 m³/s (B&S). 45

Figure 4.7 Mass evaporation by 10 m³/s continuous spills of LNG and Hydrogen (B&S). 46

Figure 4.8 The spreading radius and the pool volume of LNG and liquid hydrogen pool by 10 m³ /s of a continuous spill bounded at r =50m (B&S) 47

Figure 4.9 Mass evaporation of 10 m³ /s continuous spill of LNG and Hydrogen bounded at r = 50m (B&S). 47

Figure 4.10 The spreading radius and the pool volume of LNG and liquid hydrogen pool by 0.07 kg /s of a continuous spill (B&S). 48

Figure 4.11 Mass evaporation of 0.07 kg /s continuous spill of LNG and Hydrogen (B&S). 49

Figure 4.12 The spreading radius and the pool volume of LNG and liquid hydrogen pool by 0.07 kg /s of a continuous spill with $\epsilon =1.34$ and applying equation (4.15) (B&S). 50

Figure 4.13 The spreading radius and the pool volume of LNG and liquid hydrogen pool by 0.07 kg /s of a continuous spill with $\epsilon =0.015$ (B&S) 51

Figure 4.14 Mass evaporation of 0.07 kg /s continuous spill of LNG and Hydrogen with $\epsilon =0.015$ (B&S). 51

Figure 4.15 The spreading pool's radius versus time (Concrete) (B&S).52

Figure 4.16 The spreading pool's radius versus time (Soil) (B&S).53

Figure 4.17 Predicted spreading pool radius and mass of LN₂ and LH₂ and LNG with time versus experimental data of LN₂ (case 1) (B&S).....54

Figure 4.18 Predicted spreading pool radius and mass of LN₂ and LH₂ and LNG with time versus experimental data of LN₂ (case 7) (B&S).....55

Figure 4.19 The spreading pool's radius versus time (Concrete).....68

Figure 4.20 The spreading pool's radius versus time (Soil).....69

Figure 4.21 The vaporization and pool mass (soil).....69

Figure 4.22 The vaporization and pool mass (concrete).....70

Figure 4.23 Spreading pool in confined space bounded at r = 5m (Concrete).71

Figure 4.24 The vaporization and pool mass on confined space bounded at r=5m (concrete).71

Figure 4.25 Spreading pool in confined space bounded at r = 5m (Soil).72

Figure 4.26 The vaporization and pool mass on confined space bounded at r=5m (Soil).....72

Figure 4.27 Predicted spreading pool radius and mass of LN₂ and LH₂ and LNG with time versus experimental data of LN₂ (case 1).73

Figure 4.28 Predicted vaporization velocity of LN₂ and LH₂ and LNG with time versus experimental data of LN₂ (case 1).....74

Figure 4.29 Predicted spreading pool radius and mass of LN₂ and LH₂ and LNG with time versus experimental data of LN₂ (case 7)(GASP).74

Figure 4.30 Predicted vaporization velocity of LN₂ and LH₂ and LNG with time versus experimental data of LN₂ (case 7).....75

Figure 4.31 Predicted spreading pool radius and mass of LN₂ and LH₂ and LNG with time versus experimental data of LN₂ (case 1)(CFN).....76

Figure 4.32 Predicted vaporization velocity of LN₂ and LH₂ and LNG with time versus experimental data of LN₂ (case 1)(CFN).77

Figure 4.33 Predicted spreading pool radius and mass of LN₂ and LH₂ and LNG with time versus experimental data of LN₂ (case 7)(CFN).....77

Figure 4.34 Predicted vaporization velocity of LN₂ and LH₂ and LNG with time versus experimental data of LN₂ (case 1)(CFN).78

Figure 5.1 Probe layout used in experimental measurements of Test 6 [2, 45].....80

Figure 5.2 Radius of the pool extracted from experimental measurements showing expansion and retraction [2].....80

Figure 5.3 Radius of the pool extracted from experimental measurements versus prediction CFN model.....82

Figure 5.4 Prediction of mass vaporization and pool volume by CFN model.....83

Appendices

Figure 5.5 Radius of the pool extracted from experimental measurements versus prediction of GASP model.	84
Figure 5.6 Prediction of mass vaporization and pool volume by GASP model.	85
Figure 5.7 Radius of the pool extracted from experimental measurements versus prediction by Original GASP model [2].	87
Figure 5.8 GASP predictions of liquid hydrogen mass vaporization for Takeno et al. (1994) experiments [2].	89
Figure 5.9 Models prediction of liquid hydrogen mass vaporization.	90
Figure 6.1 Froude number versus mass flowrate.	93

Appendix H List of tables

Table 3.1 The critical values of hydrogen boiling curve.31

Table 4.1 Thermal properties of concrete and soil [5].....52

Table 4.2 Nominal spill rates of liquid nitrogen [1].53

Table 5.1 Locations of 30 concentration probes [2, 45].79

Table 5.2 Input into B&S and CFN model81

Table 5.3 inputs to GASP model83

Table 5.4 input into Original GASP model [2].....86

Table 5.5 Results of the model's simulation for Test 6 of Royle and Willoughby's work.86

Table 5.6 Input into Original GASP for Takeno et al.[2]88

Table 6.1 Summary of models92

Table 6.2 Froude number values for the spill on land.93

Appendix I Task description



Faculty of Technology, Natural Sciences and Maritime Sciences, Campus Porsgrunn

FMH606 Master's Thesis

Title: Modelling of evaporation of hydrogen during accidental releases

USN supervisor: André V. Gaathaug, Knut Vågsæther, Per Morten Hansen

External partner: H2Maritime, MoZEES

Task background:

Hydrogen is a possible carbon-free energy carrier as fuel for transportation; however, there is a need for research and development of technology to handle and produce larger amounts of hydrogen for heavy-duty transportation. For instance, in maritime applications, large amounts of hydrogen need to be transported and refueled during bunkering.

Models for hydrogen systems for production or refueling are both used for optimization and control purposes. This project will develop models for liquid and gaseous hydrogen flow in typical systems for maritime applications. Both thermodynamic states and flow variables need to be solved in these models.

This project is part of two larger national research projects using hydrogen for transport: MoZEES (mozees.no) and H2Maritime.

More information regarding these projects can be found here: <https://ife.no/wp-content/uploads/2019/04/2019-04-26-Hydrogen-i-Transport-%C3%98ystein-Ulleberg-IFE.pdf>

In 2019/2020, a set of experiments on the release of liquid hydrogen was carried out at Spadeadam in the UK: https://www.vegvesen.no/fag/trafikk/ferje/utviklingskontrakt-hydrogen/testing/attachment/2847318?ts=16e02d99038&download=true&fast_title=Liquid+hydrogen+safety+experiments+2019+%28PDF%29

These experiments also contained measurements of the temperature on the ground and inside the metal floor so that heat transfer can be estimated.

Task description:

- Literature review on the release of liquefied gases
- Create a model for the vaporization of hydrogen during accidental release on the ground or inside a room
- Use experimental data for model development

Student category: PT, EET

Is the task suitable for online students (not present at the campus)? Yes

Practical arrangements: -

Supervision:

As a general rule, the student is entitled to 15-20 hours of supervision. This includes necessary time for the supervisor to prepare for supervision meetings (reading material to be discussed, etc).

Signatures:

Supervisor (date and signature): 06.05.21 

Student (write clearly in all capitalized letters): **MOJTABA AFZALI**

Student (date and signature):
05.MAY.2021 